2002

Stress Analysis of Tapered Sandwich Panels with Isotropic or Laminated Composite Facings

Huyue Zhao

STRESS ANALYSIS OF TAPERED SANDWICH PANELS WITH ISOTROPIC OR LAMINATED COMPOSITE FACINGS

By

Huyue Zhao

B.S. Huazhong University of Science and Technology, 1996

M.S. Huazhong University of Science and Technology, 2000

A THESIS

Submitted in Partial Fulfillment of the

Requirements for the Degree of

Master of Science

(in Mechanical Engineering)

The Graduate School

The University of Maine

December, 2002

Advisory Committee:

Senthil Vel, Assistant Professor of Mechanical Engineering, Co-Advisor

Vincent Caccese, Associate Professor of Mechanical Engineering, Co-Advisor

Donald A. Grant, R.C. Hill Professor of Mechanical Engineering

Michael "Mick" Peterson, Assistant Professor of Mechanical Engineering

LIBRARY RIGHTS STATEMENT

In presenting this thesis in partial fulfillment of the requirements for an advanced degree at The University of Maine, I agree that the Library shall make it freely available for inspection. I further agree that permission for "fair use" copying of this thesis for scholarly purposes may be granted by the Librarian. It is understood that any copying or publication of this thesis for financial gain shall not be allowed without my written permission.

Signature: 

Date: 08/30/02

STRESS ANALYSIS OF TAPERED SANDWICH PANELS WITH ISOTROPIC OR LAMINATED COMPOSITE FACINGS

By Huyue Zhao

Thesis Co-Advisors: Dr. Senthil Vel and Dr. Vincent Caccese

An Abstract of the Thesis Presented
in Partial Fulfillment of the Requirements for the
Degree of Master of Science
(in Mechanical Engineering)
December, 2002

Structural sandwich construction is used in many air and space vehicles, cargo containers, boats and ships. Connection of the sandwich construction component to a framework or substructure is a critical issue in the detail design for sandwich construction. The tapered connection where the facings are drawn together at the support is one of the most efficient types of connections in composite sandwich construction.

We present a tapered sandwich theory that is simple to use, yet accurately predicts the stresses and deflection of both symmetric and non-symmetric tapered sections. In this investigation we assume that the facings are relatively thin and therefore in a state of plane stress. The core is assumed to be inextensible in the thickness direction and carry only transverse shear stress. Since the facings are tapered, the plane stress conditions for each facing are established in a local coordinate system with axes oriented parallel and

normal to the facing to obtain the reduced stiffness for the tapered laminae. The force and moment resultants are obtained by integrating the stresses in the facings and core.

The resulting resultants are related to the reference surface strains and curvatures through the familiar [A], [B] and [D] matrices. The deflections are computed using an energy method approach. The shear and peeling stresses at the interface between the core and the facings, which may cause delamination at the interface, are computed by integrating the three-dimensional equilibrium equations along a straight path that is perpendicular to the facings.

We also have systematically derived a total of 12 elastic stiffnesses that couple the force and moment resultants to the transverse shear deformation. Six of the twelve elastic couplings are due to the tapered sandwich construction itself, irrespective of whether the facings are isotropic or anisotropic, whereas the remaining six elastic couplings are present only for anisotropic laminated facings. Their influence on the behavior of tapered sandwich beams of the stiffnesses is investigated. Analytical models have shown that the behavior of the tapered section is counterintuitive and that, for a tapered cantilever sandwich beam with fixed dimensions at the clamped edge, there is an optimum taper angle where the tip deflection is a minimum. This decrease in deformation with increasing taper angle is due to the participation of the facings in resisting transverse shear loads. Results from the tapered sandwich theory show very good comparison with finite element models for several case studies. The theory enhances our understanding of tapered sandwich beams and clarifies the causes of premature failure encountered at the interfaces between the core and facings.

TABLE OF CONTENTS

LIST OF TABLES

LIST OF FIGURES

Chapter 1

INTRODUCTION

This chapter presents an introduction to the research conducted on tapered sandwich composite structures. In the first part, the motivation for this study is given followed by a review of the literature on sandwich composites. An overview of this thesis, including its contributions and approach, are summarized in Section 1.3.

1.1. Motivation

Sandwich construction is one of the most functional forms of composite structures developed by the composite industry. It is widely employed in aircraft and space vehicles, ships, boats, cargo containers and residential construction (Vinson, 1999). Honeycomb sandwich panels revolutionized the aerospace industry over 40 years ago, making aircraft lighter, stronger and faster and allowing them to carry more weight and improve fuel efficiency. Every aircraft in production today with two or more engines utilizes some honeycomb sandwich (Bitzer, 1992). In the Boeing 747, the fuselage shell, floors, side panels, overhead bins and ceiling are of sandwich construction. A major portion of the space shuttle is made of honeycomb-core sandwich construction with composite facings. The U.S. Navy uses honeycomb-sandwich bulkheads to reduce the weight of ships above the waterline. Fiberglass sandwich construction with foam core is widely used in the construction of recreational boat hulls. Sandwich composite construction offers great potential for large civil infrastructure projects such as industrial buildings and vehicular bridges (Karbhari, 1997). Sandwich-cladding panels composed of

metallic facings and a lightweight insulating core are being increasingly used for roof cladding due to their outstanding thermal performance (Davies, 1997).

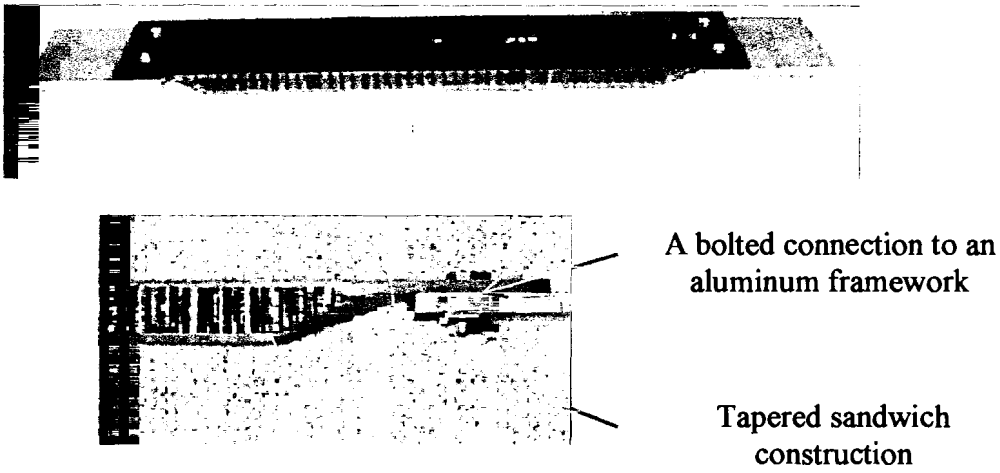

Figure 1.1 Photograph of tapered sandwich construction and a connection to a framework (Caccese, 1998)

Sandwich construction provides several key benefits over conventional structures, such as very high bending stiffness, low weight, cost effectiveness and durability. A typical sandwich beam or panel usually consists of honeycomb, polymer foams or low-density wood cores sandwiched between isotropic or laminated anisotropic facings. When laminate composite facings are used, they may be designed to have quasi-isotropic or anisotropic properties. The facings are designed to carry primarily the bending stresses while the core resists the shear loads (analogous to the web of an I-beam) and increases the stiffness of the structure by holding the facings apart. The major advantage of this structural type is the very large stiffness-to-weight ratio and high bending strength. With proper design the sandwich increases the flexural rigidity while adding very little weight. Sandwich composite structures are easier to manufacture than laminated skin panels with bonded or mechanically fastened stiffeners.

In some applications, such as in the design of aerospace vehicles, it is necessary to use variable-thickness sandwich construction, either locally or globally, for functional and/or aerodynamic reasons. The tapered connection where the facings are drawn together at the support is one of the most functionally efficient types of connections in composite sandwich construction. Use of a tapered connection in sandwich structural components typically leads to a substantial reduction in construction depth. This type of connection, as shown in Figure 1.1, was studied experimentally and analytically by Caccese and Gauthier (1998a, 1998b) for its potential use in the aeroshell structure of the NASA X-38. The tapering of the core can also be used to improve the load transfer mechanism between a sandwich laminate and a monolithic laminated skin panel. In the Boeing's Model 360 helicopter, the frame and longeron spars are attached to a sandwich-to-laminate tapered member (Llorente, 1989).

In general, experience has shown that the tapered region is the weak link in tapered sandwich structures. Tensile tests indicate that the initial damage occurs at the root of the taper in the form of delamination at the interface between the core and the facings (Kuczma and Vizzini, 1999). In order to design and use tapered sandwich composite construction in practical applications, it is essential to accurately compute the stresses and deflections. Reliable estimates of the stresses, including the shear and peeling stresses at the interface between the core and the facings, in conjunction with a good failure theory, are needed to predict the maximum load carrying capacity of a tapered sandwich structure. One way to approach the problem is to treat the tapered sandwich structure as a three-dimensional anisotropic elastic composite continuum and utilize the three dimensional equations of equilibrium and associated point wise boundary

conditions to compute the stresses and deflections. However, solving a three-dimensional boundary value problem is tedious and time consuming. Therefore, there is a need to develop a simplified theory that is easy to use and able to capture the salient features of the displacement and stress fields in tapered sandwich structures.

1.2. Literature Review

1.2.1. Sandwich Structures with Uniform Thickness

A great deal of research has been conducted on the analysis of sandwich members of uniform depth. Considering the vast number of papers on the topic of sandwich construction, the following review is meant to be a brief overview of the literature and it is by no means complete.

The first research paper concerning sandwich construction was due to Marguerre, and it dealt with in-plane compressive loads (Marguerre, 1944). Libove and Batdorf (1948) published a general small deflection theory for sandwich plates. Hoff (1950) derived the differential equations and boundary conditions for the bending and buckling of sandwich plates using the principle of virtual displacements. In all cases studied, the materials were isotropic and the edges were free or simply supported. Bijlaard (1951) approached the subject of sandwich optimization by considering plates with given weight per unit surface area, and computing the ratio of the elastic moduli of core and faces, which lead to a maximum buckling load (Bijlaard, 1951). He carried out the optimization for a given ratio between thickness of core and face. In 1952, Flugge published a paper on the structural optimization of sandwich panels (Flugge, 1952).

Ericksen of U.S Forest Products Laboratory (USFPL) issued a report in 1956 accounting for the effects of shear deformation on deflections of the sandwich panels with isotropic core and facings. He presented general expressions for the strains in a sandwich panel with orthotropic facings and core. Eringen (1952) used the theorem of minimum potential energy to obtain four partial differential equations for the bending and buckling of rectangular sandwich plates with isotropic cores and faces under various loading and edge conditions. The early theoretical work on the behavior of rectangular sandwich panels subjected to lateral loads was restricted to uniform loads and simply support edge conditions. During the early post-World-War-II period, the USFPL was the primary group in the development of analysis and design methods for sandwich structures.

By the mid 1960s, efforts in sandwich construction research had spread widely. In 1966, Plantema published his famous, and the first, book on sandwich structures (Plantema, 1966). In 1969, this was followed by the book by H.G. Allen (Allen, 1969). In 1989, Ha provided an overview of finite elements applied to sandwich plates (Ha, 1989). Noor and Burton (1995) also reviewed the computational models for sandwich panels and shells. The review by Noor, Burton, and Bert (1996) provides over 800 references discussed in the review and another 559 references as a supplemental bibliography.

1.2.2. Tapered Sandwich Structures

Although there are hundreds of papers related to sandwich composites of uniform thickness, only a handful of them deal with tapered sandwich construction. When dealing with homogeneous beams of variable thickness, it is usually assumed that the constant-

thickness moment-curvature relationships of beam theory are still valid, provided we use the bending rigidity based on the local thickness. Huang and Aspaugh (1974) used a constant-thickness sandwich theory, with stiffnesses that varied in accordance with the local thickness, to study sandwich beams of variable thickness. It has been shown that this approach can lead to significant errors since the membrane stresses in the facings have a transverse shear component which alters the transverse shear load in the core and hence the transverse shear deformation (Libove and Lu, 1989; Lu and Libove, 1991). Lu (1994) has analyzed symmetric tapered sandwich beams consisting of laminated fiber-reinforced anisotropic facings and honeycomb core. Paydar and Libove (1986, 1988) analyzed the general bending of sandwich plates of variable thickness with isotropic facings. In order to design and use tapered sandwich composite construction in practical applications, it is essential to accurately compute the stresses and deflections. Peled and Frostig (1994) have rigorously developed a theory for tapered sandwich beams with transversely flexible core. Their analysis accounts for higher-order effects in the form of nonlinear displacements fields through the thickness of the sandwich beam which are pronounced in the vicinity of concentrated loads or supports as well as at the ends of tapered transition zones.

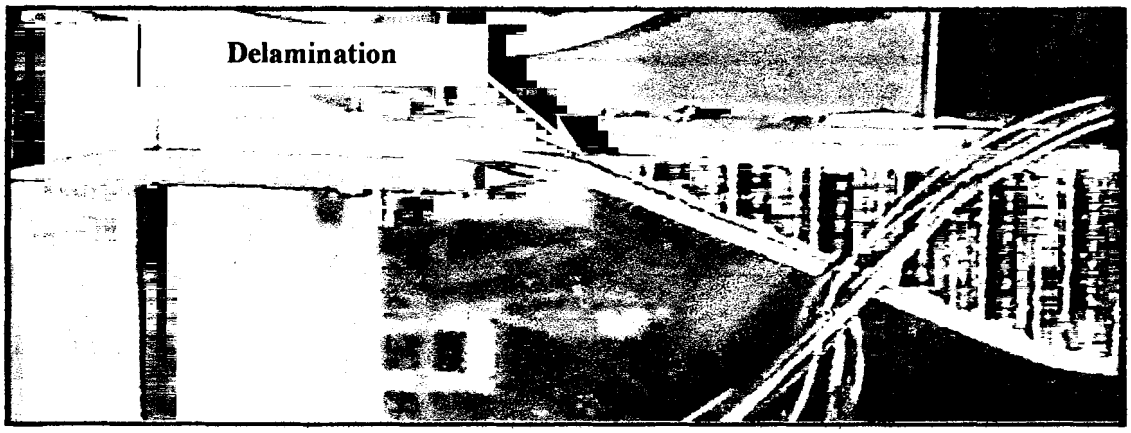

Figure 1.2 High interlaminar stresses cause delamination in experiment (Caccese and Malm, 1999)

Kuczma and Vizzini (1999) have investigated the failure modes and load distributions in tapered sandwich-to-laminate specimens under tensile, compressive and bending loads and the experimental data were correlated with three-dimensional finite element models. In general, experiments have shown that initial damage in tapered sandwich connections occurs at the root of the taper resulting in delamination of the facings from the core, as shown in Figure 1.2 (Caccese and Malm, 1999).

1.3. Overview of Thesis

1.3.1. Contribution

The significance of this thesis is in the development of a new tapered sandwich theory that is simple to use, yet accurately predicts the stresses and deflection of both symmetric and non-symmetric tapered sections. Results from the tapered sandwich theory show very good comparison with plane strain finite element models for several case studies. The significant contributions of this thesis are as follows:

1. The analysis of laminated composite materials has been developed since the 1960s and it is now well established and widely used. There are many books devoted to the analysis of laminated and sandwich composite structures (Jones, 1998; Hyer, 1997;

Herakovich, 1997; Gibson, 1994; Whitney, 1987; Vinson, 1999; Reddy, 1997). Thus, the analysis and design methodology is well known and the notation has been standardized. For example, the elastic stiffness matrices of a laminated or sandwich composite structure are denoted by $[A]$, $[B]$ and $[D]$, which are the extensional stiffness, bending-extension coupling stiffness and bending stiffness matrices, respectively. Commercial computer codes that have been developed for the analysis and design of composite structures also employ the standardized notation. However, the analysis of tapered sandwich panels has not yet been cast in this standard notation. In this thesis, we have developed a tapered sandwich theory in which the force and moment resultants are related to the reference surface strains and curvatures through the familiar $[A]$, $[B]$ and $[D]$ matrices. This facilitates implementation in the standard finite element codes.

2. Unlike sandwich panels of uniform thickness, tapered sandwich structures exhibit bending-shear and extension-shear elastic couplings. For example, the bending-shear coupling implies that a bending moment will cause shear deformation of the core in a tapered sandwich beam. This is because the longitudinal force in the plane of facing, caused by the bending moment, has a vertical component that alters the shear force in the core. Although, the bending-shear coupling effect in tapered sandwich beams is well known (Paydar and Libove, 1988, Libove and Lu, 1989), there are additional elastic couplings in tapered sandwich beams. In our tapered sandwich formulation, we have systematically derived a total of 12 elastic stiffnesses that couple the force and moment resultants to the transverse shear deformation. Six of the twelve elastic couplings are due to the tapered sandwich construction itself, irrespective of whether

the facings are isotropic or anisotropic, whereas the remaining six elastic couplings are present only for anisotropic laminated facings.

3. Stresses and displacements from the tapered sandwich theory show good comparison with plane strain finite element models for several case studies. The cases include symmetric and unsymmetric tapered sandwich beams composed of either isotropic or laminated anisotropic facings.
4. It is important to quantify the shear and peeling stresses at the interface between the core and the facings since excessive interfacial stresses could cause delamination followed by debonding of the facings. By integrating the three-dimensional equilibrium equations, we are able to obtain the transverse shear and peeling stresses at the interfaces that compare well with results from plane strain finite element analysis.

1.3.2. Approach

In this investigation, we assume that the facings are relatively thin and therefore in a state of plane stress. The core is assumed to be inextensible in the thickness direction and carry only transverse shear stress. Since the facings are tapered, the plane stress conditions for each facing are established in a local coordinate system with axes oriented parallel and normal to the facing to obtain the reduced stiffness for the tapered laminae. The force and moment resultants are obtained by integrating the stresses in the facings and core. The resultants are related to the reference surface strains and curvatures through the familiar $[A]$, $[B]$ and $[D]$ matrices. The deflections are computed using an energy method approach. The shear and peeling stresses at the interface between the core and the

facings is computed by integrating the three-dimensional equilibrium equations along a straight path that is perpendicular to the facings.

1.3.3. Outline

The analysis of sandwich composite beams and plates of uniform thickness are briefly reviewed in Chapter 2. Chapter 3 deals with the analysis of tapered sandwich panels composed of isotropic facings and the theory is extended to laminated anisotropic facings in Chapter 4. The displacements and stresses from the tapered sandwich theory are compared with plane strain finite element analyses for several cases in Chapter 5. Chapter 6 is the conclusion of this thesis.

Chapter 2

BACKGROUND ON ANALYSIS OF SANDWICH PLATES OF CONSTANT THICKNESS

This chapter provides a brief overview of sandwich members of uniform thickness. The mechanics of sandwich structures presented here is well known and can be found in the books by Whitney (1987) and Vinson (1999). This chapter is included so that one may fully understand and appreciate the subsequent analysis of tapered sandwich members and to delineate the differences between tapered sandwich members and sandwich members of constant depth.

2.1. Problem Formulation

The analytical development of a sandwich composite with constant depth starts with the general depiction of a sandwich beam as shown in Figure 2.1. It is assumed that

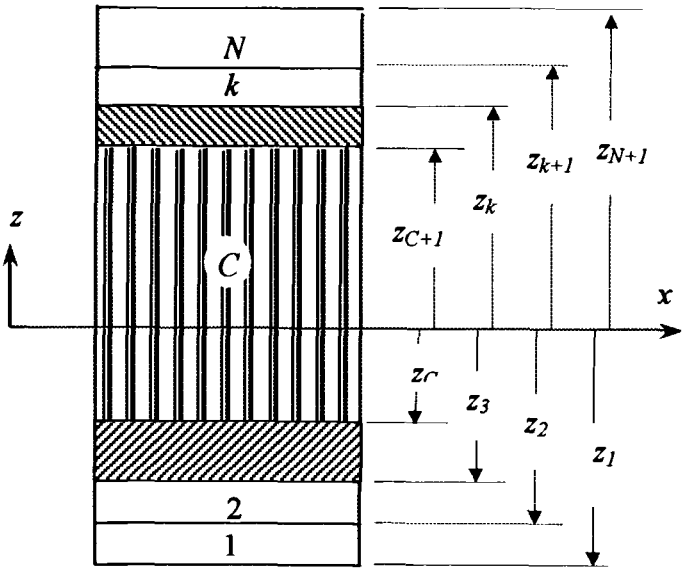

Figure 2.1 Layer numbering for a sandwich structure with constant thickness

the thickness of the core is constant and the laminated facings are relatively thin compared to the core and therefore behave as membranes. The primary function of the core is to stabilize the facings and resist the shear load. The coordinate system is placed at the center of the core.

The laminated facings consist of orthotropic laminae and each lamina has a distinct fiber orientation θ_k relative to the x-axis. The sandwich member is composed of N distinct layers numbered from bottom to top as shown in Figure 2.1. The core is denoted as layer number C and the bottom and top facings are composed of C -1 and N - C distinct laminae, respectively. The z-coordinates of the bottom and top surfaces of the kth layer are designated as z_k and z_{k+1}, respectively.

2.2. Analytical Model

Since the facings are relatively thin compared to the core, we assume that the facings are in a state of plane stress:

$$\sigma_{zz} = \tau_{xz} = \tau_{yz} = 0. \tag{2.1}$$

The plane stress reduced constitutive relations for an orthotropic lamina in the material coordinate system are

$$\begin{bmatrix} \sigma_{11} \\ \sigma_{22} \\ \tau_{12} \end{bmatrix} = \begin{bmatrix} Q_{11} & Q_{12} & 0 \\ Q_{12} & Q_{22} & 0 \\ 0 & 0 & Q_{66} \end{bmatrix} \begin{bmatrix} \varepsilon_{11} \\ \varepsilon_{22} \\ \gamma_{12} \end{bmatrix}, \tag{2.2}$$

where Q_{ij} are the reduced stiffnesses for an orthotropic material in the principal material coordinate system (Hyer, 1998). The reduced stiffnesses are defined in terms of the engineering constants as follows

$$Q_{11} = \frac{E_1}{1-\nu_{12}\nu_{21}}, \quad Q_{12} = \frac{\nu_{12}E_2}{1-\nu_{12}\nu_{21}},$$
$$Q_{22} = \frac{E_2}{1-\nu_{12}\nu_{21}}, \quad Q_{66} = G_{12},$$

where E, ν and G denote the Young's modulus, Poisson's ratio and shear modulus respectively. The principal material direction of the k^{th} lamina is oriented at angle θ_k with respect to the x-coordinate direction. The plane stress reduced constitutive relations for an orthotropic lamina in the (x, y, z) coordinate system are

$$\begin{bmatrix} \sigma_{xx} \\ \sigma_{yy} \\ \tau_{xy} \end{bmatrix} = \begin{bmatrix} \overline{Q}_{11} & \overline{Q}_{12} & \overline{Q}_{16} \\ \overline{Q}_{12} & \overline{Q}_{22} & \overline{Q}_{26} \\ \overline{Q}_{16} & \overline{Q}_{26} & \overline{Q}_{66} \end{bmatrix} \begin{bmatrix} \varepsilon_{xx} \\ \varepsilon_{yy} \\ \gamma_{xy} \end{bmatrix}, \tag{2.3}$$

where the reduced stiffness $\overline{Q}_{ij}$ components for the laminae in terms of the engineering constants are

$$\begin{aligned}
\overline{Q}_{11} &= Q_{11}m^4 + 2m^2n^2(Q_{12} + 2Q_{66}) + Q_{22}n^4, \\
\overline{Q}_{12} &= m^2n^2(Q_{11} + Q_{22} - 4Q_{66}) + Q_{12}(m^4 + n^4), \\
\overline{Q}_{16} &= mn[Q_{11}m^2 - Q_{22}n^2 - (Q_{12} + 2Q_{66})(m^2 - n^2)], \\
\overline{Q}_{22} &= Q_{11}n^4 + 2m^2n^2(Q_{12} + 2Q_{66}) + Q_{22}m^4, \\
\overline{Q}_{26} &= mn[Q_{11}n^2 - Q_{22}m^2 + (Q_{12} + 2Q_{66})(m^2 - n^2)], \\
\overline{Q}_{66} &= m^2n^2(Q_{11} + Q_{22} - 2Q_{12}) + Q_{66}(m^2 - n^2)^2,
\end{aligned} \tag{2.4}$$

where $m = cos\ \theta_k$ and $n = sin\ \theta_k$.

We assume that the strains in the facings are linear functions of the thickness coordinate. The strains in the facing ε_{xx}, ε_{yy} and γ_{xy} are taken to be linear functions of the z-coordinate as follows:

$$\begin{aligned}
\varepsilon_{xx} &= \varepsilon^0_{xx}(x) + z\kappa^0_{xx}(x), \\
\varepsilon_{yy} &= \varepsilon^0_{yy}(x) + z\kappa^0_{yy}(x), \\
\gamma_{xy} &= \gamma^0_{xy}(x) + z\kappa^0_{xy}(x).
\end{aligned} \tag{2.5}$$

where ε^0_{xx}, ε^0_{yy}, and ε^0_{xy} are strain in the reference surface, and κ^0_{xx}, κ^0_{yy} and κ^0_{xy} are bending curvature in the reference surface.

The core is made of an orthotropic material and its primary function is to space and stabilize the facings and transfer shear between them. The in-plane stresses σ_{xx}, σ_{yy} and τ_{xy} of the core are assumed to be negligible compared to that in the facings. The transverse shear stresses τ_{xz} and τ_{yz} in the core are assumed to be constant throughout the thickness and they are related to the core shear strains by

$$\begin{aligned} \tau_{xz} &= G^c_{xz}\gamma^c_{xz}, \\ \tau_{yz} &= G^c_{yz}\gamma^c_{yz}, \end{aligned} \tag{2.6}$$

where G^c_{xz} and G^c_{yz} are the transverse shear moduli, and γ^c_{xz} and γ^c_{yz} are the transverse shear strains of the core. The stress resultants are defined as

$$\begin{aligned} [N_x, N_y, N_{xy}] &= \int_{z_1(x)}^{z_N(x)} [\sigma_{xx}, \sigma_{yy}, \tau_{xy}]\, dz, \\ [M_x, M_y, M_{xy}] &= \int_{z_1(x)}^{z_N(x)} z[\sigma_{xx}, \sigma_{yy}, \tau_{xy}]\, dz, \\ [Q_x, Q_y] &= \int_{z_1(x)}^{z_N(x)} [\tau_{xz}, \tau_{yz}]\, dz, \end{aligned} \tag{2.7}$$

where the quantities N_x, N_y and N_{xy} are the in-plane force resultants, Q_x and Q_y are the transverse shear load resultants and M_x, M_y and M_{xy} are the moment resultants, as depicted in Figure 2.2.

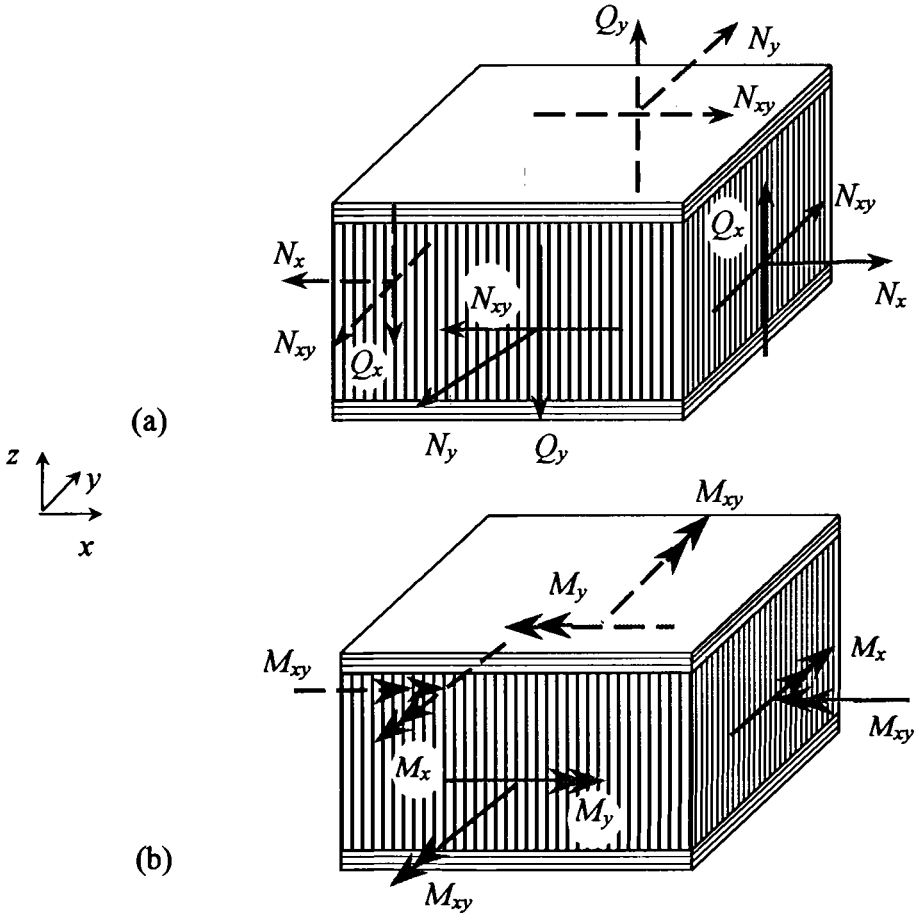

Figure 2.2 Force and moment resultants for a sandwich panel with constant thickness (a) force resultants (b) moment resultants

Substitution of the facing stresses from (2.3) and the core stresses from (2.6) into (2.7) leads to the following matrix equation for the resultant forces and moments in terms of the core shear strains and reference surface strains and curvatures,

$$\begin{Bmatrix} N_x \\ N_y \\ N_{xy} \\ M_x \\ M_y \\ M_{xy} \end{Bmatrix} = \begin{bmatrix} A_{11} & A_{12} & A_{16} & B_{11} & B_{12} & B_{16} \\ A_{12} & A_{22} & A_{26} & B_{12} & B_{22} & B_{26} \\ A_{16} & A_{26} & A_{66} & B_{16} & B_{26} & B_{66} \\ B_{11} & B_{12} & B_{16} & D_{11} & D_{12} & D_{16} \\ B_{12} & B_{22} & B_{26} & D_{12} & D_{22} & D_{26} \\ B_{16} & B_{26} & B_{66} & D_{16} & D_{26} & D_{66} \end{bmatrix} \begin{Bmatrix} \varepsilon_{xx}^0 \\ \varepsilon_{yy}^0 \\ \gamma_{xy}^0 \\ \kappa_{xx}^0 \\ \kappa_{yy}^0 \\ \kappa_{xy}^0 \end{Bmatrix},$$

$$\begin{bmatrix} Q_y \\ Q_x \end{bmatrix} = \begin{Bmatrix} A_{44} & 0 \\ 0 & A_{55} \end{Bmatrix} \begin{Bmatrix} \gamma_{yz}^c \\ \gamma_{xz}^c \end{Bmatrix}. \qquad (2.8)$$

where A_{ij} are the extensional and shear rigidities, D_{ij} are the bending rigidities and B_{ij} are the bending-extension rigidities defined by

$$\left[A_{ij}(x), B_{ij}(x), D_{ij}(x)\right] = \sum_{\substack{k=1 \\ k \neq c}}^{N} \int_{z_k(x)}^{z_{k+1}(x)} Q_{ij}^{(k)} \left[1, z, z^2\right] dz; i, j = 1,2,6$$

$$\left[A_{44}(x), A_{55}(x)\right] = \left[G_{yz}^{c}, G_{xz}^{c}\right](z_{C+1} - z_C). \tag{2.9}$$

The most important feature of Equation (2.8) is the elastic coupling that exists between extension and bending. The rigidities B_{ij} relate the bending moments M's to the reference surface strains ε^0's, and the resultant forces N's to the reference surface curvatures κ^0's. Therefore, *the matrix [B_{ij}] is known as the bending-extension coupling matrix*. An examination of equation (2.9) reveals that bending-extension coupling vanishes for sandwich plates that are symmetric about the middle surface (Whitney, 1999).

Chapter 3

ANALYTICAL MODEL OF ISOTROPIC FACINGS

A new tapered sandwich theory that accurately predicts the stresses and deflection of both symmetric and non-symmetric tapered sections of sandwich composites with isotropic facings is presented. We have obtained explicit expressions for 6 elastic rigidities that couple the reference surface strains and curvatures to the transverse shear forces. The physical interpretations of the elastic couplings are given in this chapter. The elastic couplings are intrinsic to tapered sandwich members and they are identically zero for sandwich members of uniform depth as one would expect. The interface shear and peeling stresses between the core and the facings are computed by integrating the three-dimensional equilibrium equations in a direction perpendicular to the facing surfaces. For sandwich members that are highly tapered, the bending and extension rigidities can be negative. We give physical explanations for the negative rigidities and discuss its ramifications on the response of tapered sandwich members.

3.1. Problem Formulation

The analytical development of tapered composite members starts with the general depiction of a tapered sandwich beam as shown in Figure 3.1. We use a rectangular Cartesian coordinate system, denoted by x-y-z in Figure 3.1(a), to describe the deformation of a tapered sandwich beam with isotropic facings. The thickness is assumed to vary linearly along the span (x-direction). It is assumed that the facings are relatively thin compared to the core and therefore behave as membranes. The core is assumed to be

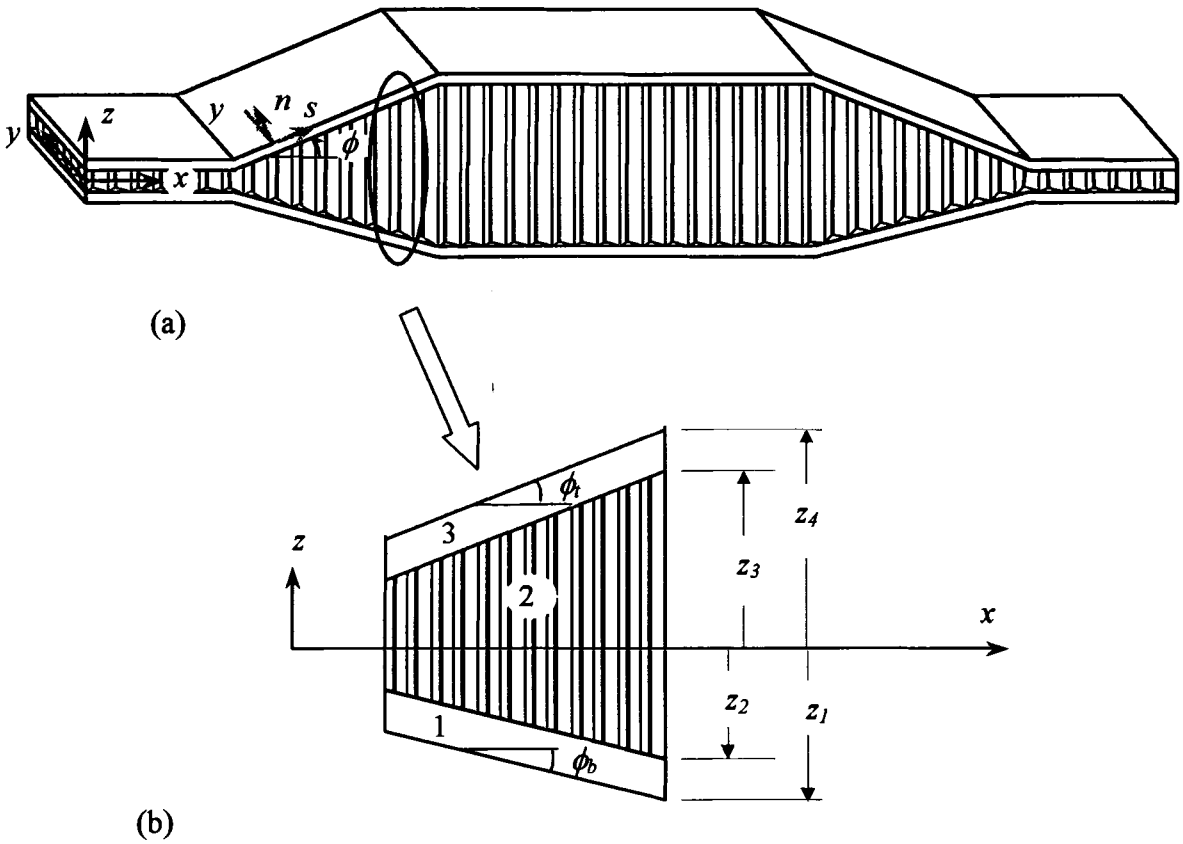

Figure 3.1 Coordinate system and layer numbering for a tapered section

inextensible in the thickness direction and to carry only transverse shear stresses. Since the facings are tapered, it is advantageous to use a local coordinate system, denoted by *s*-*y*-*n* in Figure 3.1(a), such that the *s*- and *n*-axes are parallel and normal to the facing, respectively. The taper angle of the facing, ϕ, is taken as positive counter-clockwise with respect to the *x*-axis.

The tapered beam is assumed to be composed of three distinct layers numbered from bottom to top as shown in Figure 3.1(b). The core is denoted as layer number 2, the bottom facing as layer number 1 and top facing as layer number 3. The *z*-coordinate of the bottom surface of layer number k is designated z_k with the top surface of the layer being z_{k+1}. In general, the z_k's are functions of the *x*-coordinate since the sandwich

member is tapered. The taper angle of the top and bottom facings are $\phi = \phi_t$ and $\phi = \phi_b$, respectively. The sandwich member is said to be *symmetric* if $\phi_t = -\phi_b$ and the material properties and thickness of the facings are identical. If the laminate is not symmetric, it is referred to as an *unsymmetric* laminate.

3.2. Analytical Model

Since the facings are relatively thin compared to the core, we assume that the facings are in a state of plane stress. This is a reasonable assumption since the stress components in the plane of the facing are generally much larger than the stress components perpendicular to the plane. For tapered sandwich structures, the plane stress conditions are

$$\sigma_{nn} = \tau_{sn} = \tau_{yn} = 0, \tag{3.1}$$

where the normal stress components are denoted by σ and the shear stress components by τ. The facings are made of an isotropic material, such as aluminum. The stress-strain relations for an isotropic facing in the (s, y, n) coordinate system are,

$$\begin{bmatrix} \sigma_{ss} \\ \sigma_{yy} \\ \sigma_{nn} \\ \tau_{yn} \\ \tau_{sn} \\ \tau_{sy} \end{bmatrix} = \begin{bmatrix} C_{11} & C_{12} & C_{13} & 0 & 0 & 0 \\ C_{12} & C_{22} & C_{23} & 0 & 0 & 0 \\ C_{13} & C_{23} & C_{33} & 0 & 0 & 0 \\ 0 & 0 & 0 & C_{44} & 0 & 0 \\ 0 & 0 & 0 & 0 & C_{55} & 0 \\ 0 & 0 & 0 & 0 & 0 & C_{66} \end{bmatrix} \begin{bmatrix} \varepsilon_{ss} \\ \varepsilon_{yy} \\ \varepsilon_{nn} \\ \gamma_{yn} \\ \gamma_{sn} \\ \gamma_{sy} \end{bmatrix}, \tag{3.2}$$

where C_{ij} are the components of the elastic stiffness matrix in contracted notation. The elastic stiffness components for the isotropic facings in terms of the Young's moduli E and Poisson's ratio ν are

$$C_{11} = C_{22} = C_{33} = E(1-\nu)/(1+\nu)(1-2\nu),$$

$$C_{12} = C_{13} = C_{23} = E\nu/(1+\nu)(1-2\nu),$$

$$C_{44} = C_{55} = C_{66} = G = E/2(1+\nu),$$

where G is the shear modulus of the facings .The stresses and strains in the (x, y, z) and (s, y, n) coordinate systems are related as

$$\begin{aligned} \{\sigma\}_{syn} &= [R^+]\{\sigma\}_{xyz}, \\ \{\sigma\}_{xyz} &= [R^-]\{\sigma\}_{syn}, \end{aligned} \tag{3.3}$$

$$\begin{aligned} \{\varepsilon\}_{syn} &= [R^-]^T\{\varepsilon\}_{xyz}, \\ \{\varepsilon\}_{xyz} &= [R^+]^T\{\varepsilon\}_{syn}, \end{aligned} \tag{3.4}$$

where $\{\sigma\}_{xyz} = \{\sigma_{xx}, \sigma_{yy}, \sigma_{zz}, \tau_{yz}, \tau_{xz}, \tau_{xy}\}^T$, $\{\varepsilon\}_{xyz} = \{\varepsilon_{xx}, \varepsilon_{yy}, \varepsilon_{zz}, \gamma_{yz}, \gamma_{xz}, \gamma_{xy}\}^T$, $\{\sigma\}_{syn} = \{\sigma_{ss}, \sigma_{yy}, \sigma_{nn}, \tau_{yn}, \tau_{sn}, \tau_{sy}\}^T$ and $\{\varepsilon\}_{syn} = \{\varepsilon_{ss}, \varepsilon_{yy}, \varepsilon_{nn}, \gamma_{yn}, \gamma_{sn}, \gamma_{sy}\}^T$ are column vectors of stresses and strains in the (x, y, z) and (s, y, n) coordinate systems, respectively. Matrices $[R^+]$ and $[R^-]$ are the transformation matrices defined by

$$[R^+] = \begin{bmatrix} \cos^2\phi & 0 & \sin^2\phi & 0 & 2\cos\phi\sin\phi & 0 \\ 0 & 1 & 0 & 0 & 0 & 0 \\ \sin^2\phi & 0 & \cos^2\phi & 0 & -2\cos\phi\sin\phi & 0 \\ 0 & 0 & 0 & \cos\phi & 0 & -\sin\phi \\ -\cos\phi\sin\phi & 0 & \cos\phi\sin\phi & 0 & \cos^2\phi - \sin^2\phi & 0 \\ 0 & 0 & 0 & \sin\phi & 0 & \cos\phi \end{bmatrix}, \tag{3.5}$$

$$[R^-] = \begin{bmatrix} \cos^2\phi & 0 & \sin^2\phi & 0 & -2\cos\phi\sin\phi & 0 \\ 0 & 1 & 0 & 0 & 0 & 0 \\ \sin^2\phi & 0 & \cos^2\phi & 0 & 2\cos\phi\sin\phi & 0 \\ 0 & 0 & 0 & \cos\phi & 0 & \sin\phi \\ \cos\phi\sin\phi & 0 & -\cos\phi\sin\phi & 0 & \cos^2\phi - \sin^2\phi & 0 \\ 0 & 0 & 0 & -\sin\phi & 0 & \cos\phi \end{bmatrix}. \tag{3.6}$$

As in the case of uniform sandwich beams of constant depth (see Whitney, 1987; Vinson, 1999), an analytical model for tapered members is developed by assuming that the strains in the facings ε_{xx}, ε_{yy} and γ_{xy} are linear functions of the z-coordinate as follows

$$\begin{aligned}
\varepsilon_{xx} &= \varepsilon^0_{xx}(x) + z\kappa^0_{xx}(x), \\
\varepsilon_{yy} &= \varepsilon^0_{yy}(x) + z\kappa^0_{yy}(x), \\
\gamma_{xy} &= \gamma^0_{xy}(x) + z\kappa^0_{xy}(x),
\end{aligned} \tag{3.7}$$

where ε^0_{xx}, ε^0_{yy}, γ^0_{xy} and κ^0_{xx}, κ^0_{yy}, κ^0_{xy} are the strains and curvatures of the reference surfaces $z = 0$. The transverse normal strain ε_{zz}, and the transverse shear strains γ_{xz} and γ_{yz} in the facings are obtained from ε_{xx}, ε_{yy} and γ_{xy} by recognizing that the facings are in a state of plane stress. The stresses in the (s, y, n) coordinate system are obtained through $\{\sigma\}_{syn} = [C]\{\varepsilon\}_{syn} = [C][R]^T\{\varepsilon\}_{xyz}$. The three plane stress equations (3.1) are enforced to obtain ε_{zz}, γ_{xz} and γ_{yz} in terms of ε_{xx}, ε_{yy} and γ_{xy} as

$$\begin{aligned}
\varepsilon_{zz} &= \frac{(1-2\nu-\cos 2\phi)\varepsilon_{xx} - 2\nu\varepsilon_{yy}\cos 2\phi}{1-2\nu+\cos 2\phi}, \\
\gamma_{xz} &= \frac{2(\varepsilon_{xx}+\nu\varepsilon_{yy})\sin 2\phi}{1-2\nu+\cos 2\phi}, \\
\gamma_{yz} &= \gamma_{xy}\tan\phi.
\end{aligned} \tag{3.8}$$

The stress-strain relations in the (x, y, z) coordinate system for a tapered facing lamina, computed using (3.8), $(3.4)_1$, (3.2), $(3.3)_2$, are

$$\begin{bmatrix} \sigma_{xx} \\ \sigma_{yy} \\ \sigma_{zz} \\ \tau_{yz} \\ \tau_{xz} \\ \tau_{xy} \end{bmatrix} = \begin{bmatrix} \tilde{Q}_{11} & \tilde{Q}_{12} & 0 \\ \tilde{Q}_{21} & \tilde{Q}_{22} & 0 \\ \tilde{Q}_{31} & \tilde{Q}_{32} & 0 \\ 0 & 0 & \tilde{Q}_{46} \\ \tilde{Q}_{51} & \tilde{Q}_{52} & 0 \\ 0 & 0 & \tilde{Q}_{66} \end{bmatrix} \begin{Bmatrix} \varepsilon_{xx} \\ \varepsilon_{yy} \\ \gamma_{xy} \end{Bmatrix}, \tag{3.9}$$

where $\tilde{Q}_{ij}$ are the reduced stiffnesses for a tapered isotropic facings, defined as

$$
\begin{aligned}
&\tilde{Q}_{11} = \frac{2E\cos^2\phi}{D}, \tilde{Q}_{12} = \frac{2E\nu\cos^2\phi}{D},\\
&\tilde{Q}_{21} = \frac{2E\nu}{D}, \tilde{Q}_{22} = E + \frac{2E\nu^2}{D},\\
&\tilde{Q}_{31} = \frac{2E\sin^2\phi}{D}, \tilde{Q}_{32} = \frac{2E\nu\sin^2\phi}{D},\\
&\tilde{Q}_{46} = G\tan\phi, \tilde{Q}_{51} = \frac{E\sin 2\phi}{D},\\
&\tilde{Q}_{52} = \frac{E\nu\sin 2\phi}{D}, \tilde{Q}_{66} = G,\\
&D = (1+\nu)(1-2\nu+\cos 2\phi).
\end{aligned}
\tag{3.10}
$$

The core is made of an orthotropic material and its primary function is to space and stabilize the facings and transfers shear between them. The in-plane stresses σ_{xx}, σ_{yy} and τ_{xy} of the core are assumed to be negligible compared to the stresses in the facings. The transverse shear stresses τ_{xz} and τ_{yz} in the core are assumed to be constant throughout the thickness and they are related to the core shear strains by

$$
\begin{aligned}
\tau_{xz}^{(2)} &= G_{xz}^{c}\gamma_{xz}^{c},\\
\tau_{yz}^{(2)} &= G_{yz}^{c}\gamma_{yz}^{c},
\end{aligned}
\tag{3.11}
$$

where G^c_{xz} and G^c_{yz} are the transverse shear moduli of the core, and γ^c_{xz} and γ^c_{yz} are the transverse shear strains of the core. The stress resultants are defined as

$$
\begin{aligned}
\left[N_x, N_y, N_{xy}\right] &= \int_{z_1(x)}^{z_4(x)} \left[\sigma_{xx}, \sigma_{yy}, \tau_{xy}\right] dz,\\
\left[M_x, M_y, M_{xy}\right] &= \int_{z_1(x)}^{z_4(x)} z\left[\sigma_{xx}, \sigma_{yy}, \tau_{xy}\right] dz,\\
\left[Q_x, Q_y\right] &= \int_{z_1(x)}^{z_4(x)} \left[\tau_{xz}, \tau_{yz}\right] dz,
\end{aligned}
\tag{3.12}
$$

where the quantities N_x, N_y and N_{xy} are the in-plane force resultants, Q_x and Q_y are the transverse shear load resultants and M_x, M_y and M_{xy} are the moment resultants, as

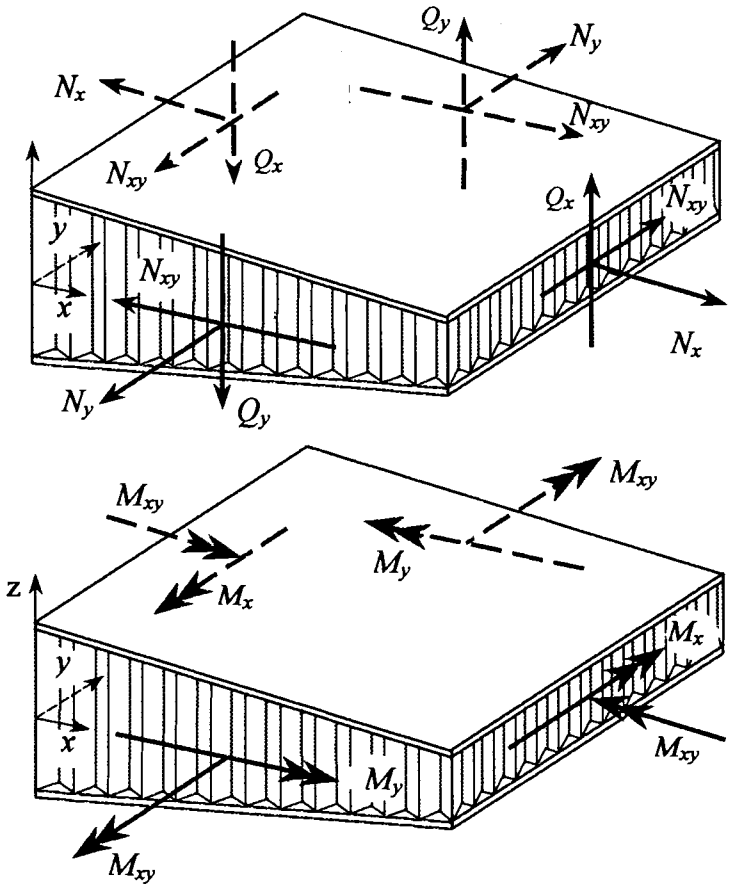

Figure 3.2 Force and moment resultants for a tapered sandwich element
(a) force resultants (b) moment resultants

depicted in Figure 3.2.

Substitution of the stresses in the facings from (3.9) and the core stresses from (3.11) into (3.12) leads to the following matrix equation for the resultant forces and moments in terms of the core shear strains and reference surface strains and curvatures,

$$\begin{Bmatrix} N_x \\ N_y \\ Q_y \\ Q_x \\ N_{xy} \\ M_x \\ M_y \\ M_{xy} \end{Bmatrix} = \begin{bmatrix} A_{11} & A_{12} & 0 & 0 & 0 & B_{11} & B_{12} & 0 \\ A_{21} & A_{22} & 0 & 0 & 0 & B_{21} & B_{22} & 0 \\ 0 & 0 & A_{44} & 0 & A_{46} & 0 & 0 & B_{46} \\ A_{51} & A_{52} & 0 & A_{55} & 0 & B_{51} & B_{52} & 0 \\ 0 & 0 & 0 & 0 & A_{66} & 0 & 0 & B_{66} \\ B_{11} & B_{12} & 0 & 0 & 0 & D_{11} & D_{12} & 0 \\ B_{21} & B_{22} & 0 & 0 & 0 & D_{21} & D_{22} & 0 \\ 0 & 0 & 0 & 0 & B_{66} & 0 & 0 & D_{66} \end{bmatrix} \begin{Bmatrix} \varepsilon_{xx}^0 \\ \varepsilon_{yy}^0 \\ \gamma_{yz}^c \\ \gamma_{xz}^c \\ \gamma_{xy}^0 \\ \kappa_{xx}^0 \\ \kappa_{yy}^0 \\ \kappa_{xy}^0 \end{Bmatrix}, \tag{3.13}$$

where A_{ij} are the extensional and shear rigidities, D_{ij} are the bending rigidities and B_{ij} are the rigidities that couple bending to extension and shear. The rigidities in the *ABD* matrix are defined by

$$\begin{aligned} \left[A_{ij}(x), B_{ij}(x), D_{ij}(x)\right] &= \sum_{k=1,3} \int_{z_k(x)}^{z_{k+1}(x)} \widetilde{Q}_{ij}^k \left[1, z, z^2\right] dz; i, j = 1,2,6 \\ \left[A_{44}(x), A_{55}(x)\right] &= \left[G_{yz}^c, G_{xz}^c\right] (z_3(x) - z_2(x)). \end{aligned} \tag{3.14}$$

The relation (3.14) can be inverted to obtain the following equation, from which the reference strains and core shear strains can be determined if the resultant forces and moments are known:

$$\begin{Bmatrix} \varepsilon_{xx}^0 \\ \varepsilon_{yy}^0 \\ \gamma_{yz}^c \\ \gamma_{xz}^c \\ \gamma_{xy}^0 \\ \kappa_{xx}^0 \\ \kappa_{yy}^0 \\ \kappa_{xy}^0 \end{Bmatrix} = \begin{bmatrix} a_{11} & a_{12} & 0 & 0 & 0 & b_{11} & b_{12} & 0 \\ a_{21} & a_{22} & 0 & 0 & 0 & b_{21} & b_{22} & 0 \\ 0 & 0 & a_{44} & 0 & a_{46} & 0 & 0 & b_{46} \\ a_{51} & a_{52} & 0 & a_{55} & 0 & b_{51} & b_{52} & 0 \\ 0 & 0 & 0 & 0 & a_{66} & 0 & 0 & b_{66} \\ b_{11} & b_{12} & 0 & 0 & 0 & d_{11} & d_{12} & 0 \\ b_{21} & b_{22} & 0 & 0 & 0 & d_{21} & d_{22} & 0 \\ 0 & 0 & 0 & 0 & b_{66} & 0 & 0 & d_{66} \end{bmatrix} \begin{Bmatrix} N_x \\ N_y \\ Q_y \\ Q_x \\ N_{xy} \\ M_x \\ M_y \\ M_{xy} \end{Bmatrix}, \tag{3.15}$$

3.3. Beam Bending and Cylindrical Bending

There are two cases of tapered sandwich plates that can be treated as one-dimensional problems: (1) tapered sandwich beams, and (2) cylindrical bending of tapered sandwich members.

When the width of the sandwich member along the y-axis is much smaller that the length along the x-axis, it is treated as a sandwich beam. For a sandwich beam in bending, the transverse load Q_x and bending moment M_x are assumed to be known, whereas the other loads vanish, i.e., $N_x = N_y = Q_y = N_{xy} = M_y = M_{xy} = 0$. By substituting of the quantity of resultant force into Equation (3.15), the reference surface strains, curvatures and transverse shear strains of the core are

$$\begin{aligned} &\varepsilon_{xx}^0 = b_{11}M_x, \varepsilon_{yy}^0 = b_{21}M_x, \\ &\gamma_{xz}^c = a_{55}Q_x + b_{51}M_x, \\ &\kappa_{xx}^0 = d_{11}M_x, \kappa_{yy}^0 = d_{21}M_x, \\ &\gamma_{yz}^c = 0, \gamma_{xy}^0 = 0, \kappa_{xy}^0 = 0. \end{aligned} \tag{3.16}$$

In cylindrical bending, the tapered sandwich plate is assumed to be a sandwich plate strip that is very long along y-axis and has a finite dimension along x- and z-axes. All derivatives with respect to y are zero and reference surface of the tapered member bends into a cylindrical shape. For cylindrical bending, transverse shear load Q_x and bending moment M_x are assumed to be know and $N_x = Q_y = N_{xy} = M_{xy} = 0$, $\varepsilon_{yy}^0 = \kappa_{yy}^0 = 0$. The reaction forces resultant N_y and moment resultant M_y required to produce cylindrical bending can be determined from the second and seventh rows of matrix equation (3.15)

$$\begin{Bmatrix} N_y \\ M_y \end{Bmatrix} = -\begin{bmatrix} a_{22} & b_{22} \\ b_{22} & d_{22} \end{bmatrix}^{-1} \begin{Bmatrix} b_{21} \\ d_{21} \end{Bmatrix} M_x. \tag{3.17}$$

By substituting of the quantity of resultant force into Equation (3.15), the reference surface strains and transverse shear strains of the core are

$$\begin{aligned}
\varepsilon_{xx}^0 &= \frac{a_{12}(-d_{22}b_{21}+b_{22}d_{21})+b_{11}(a_{22}d_{22}-b_{22}^2)+b_{12}(b_{22}b_{21}+a_{22}d_{21})}{a_{22}d_{22}-b_{22}^2} M_x, \\
\gamma_{xz}^c &= \frac{a_{52}(-d_{22}b_{21}+b_{22}d_{21})+b_{51}(a_{22}d_{22}-b_{22}^2)+b_{52}(b_{22}b_{21}+a_{22}d_{21})}{a_{22}d_{22}-b_{22}^2} M_x + a_{55}Q_x, \\
\kappa_{xx}^0 &= \frac{b_{12}(-d_{22}b_{21}+b_{22}d_{21})+d_{11}(a_{22}d_{22}-b_{22}^2)+d_{12}(b_{22}b_{21}+a_{22}d_{21})}{a_{22}d_{22}-b_{22}^2} M_x, \\
\gamma_{xy}^0 &= 0, \gamma_{yz}^c = 0, \kappa_{xy}^0 = 0, \\
\varepsilon_{yy}^0 &= 0, \kappa_{yy}^0 = 0.
\end{aligned} \tag{3.18}$$

We can obtain the distributions of strains through the thickness of the tapered sandwich section from Equation (3.7) after all the core shear strains and reference surface strains and curvatures have been determined. The stresses in the tapered sandwich member are obtained from the stress-strain relations (3.9) and (3.11). By using the transformation relations (3.3), we can determine the stresses and strains in the local *s-y-n* coordinate system.

3.4. Deflections of Tapered Sandwich Structures

An energy method approach can be used to facilitate the calculation of deflections at some particular key point in the structure. After calculating all the stresses and strains in the structure, a general expression for the strain energies in the bottom facing, top facing and core at any location are respectively:

$$U_{bottom}(x)=\frac{1}{2}\int_{z_1(x)}^{z_2(x)}\left[\sigma_{ss}^{(1)}\varepsilon_{ss}^{(1)}+\sigma_{yy}^{(1)}\varepsilon_{yy}^{(1)}+\tau_{sy}^{(1)}\gamma_{sy}^{(1)}\right]dz,$$

$$U_{top}(x)=\frac{1}{2}\int_{z_3(x)}^{z_4(x)}\left[\sigma_{ss}^{(3)}\varepsilon_{ss}^{(3)}+\sigma_{yy}^{(3)}\varepsilon_{yy}^{(3)}+\tau_{sy}^{(3)}\gamma_{sy}^{(3)}\right]dz, \tag{3.19}$$

$$U_{core}(x)=\frac{1}{2}\int_{z_2(x)}^{z_3(x)}\left[\tau_{xz}^{(2)}\gamma_{xz}^{(2)}+\tau_{yz}^{(2)}\gamma_{yz}^{(2)}\right]dz.$$

The general expression for the total strain energy U_0 is:

$$U_0=\int_0^L\left[U_{bottom}(x)+U_{top}(x)+U_{core}(x)\right]dx, \tag{3.20}$$

Let vertical forces P_i (i = 1,2,3,...) be applied at various locations along the tapered sandwich beam. Using Castigliano's second theorem, the deflection δ_i at the location of concentrated load P_i is

$$\delta_i=\partial U_0/\partial P_i.$$

3.5. Transverse Shear Stresses and Transverse Normal Stresses

An important assumption in the development of our theory for tapered sandwich member is the plane stress conditions σ_{nn} = τ_{sn} = τ_{yn} = 0 for the facings stated earlier in Equation (3.1). Yet these three stress components, although small, are nonzero within the facings and they are usually largest at the interface between the core and the facings. Large interlaminar stresses are known to be the basis of a particular failure mechanism in laminated fiber-reinforced composite materials, namely free-edge delamination and subsequent delamination growth along the length. Some real applications and experiments have shown that these stresses can also cause failure of a tapered sandwich member, such as debonding of the facings from the core, as shown in Figure 1.3.

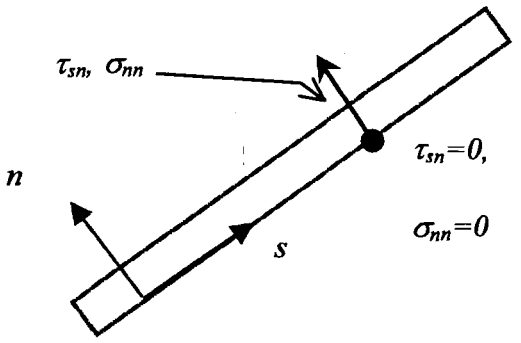

Figure 3.3 Integration path to obtain interface shear and peeling stresses

Therefore, in order to design tapered sandwich members, it is important that we are able to compute the stresses at the interface between the core and facings.

We compute the transverse shear and normal stresses by integrating the 3D equilibrium equations along a straight path that is perpendicular to the facings, as depicted in Figure 3.3. This is done after we have calculated the in-plane stresses σ_{ss}, σ_{yy} and τ_{sy} in the facings. The transverse shear stress τ_{sn} can be obtained by integrating the 3D equilibrium equation given in Equation $(3.21)_1$,

$$\begin{aligned} &\sigma_{ss,s} + \tau_{sy,y} + \tau_{sn,n} = 0, \\ &\tau_{sn}(s,n) = -\int_0^n \left(\sigma_{ss,s} + \tau_{sy,y}\right) dn. \end{aligned} \tag{3.21}$$

Equation $(3.21)_2$ not only allows us to compute the τ_{ns} within the layers but also at the layer interface. Integrating the 3D equilibrium equations, as shown in Equation $(3.22)_1$, leads to the transverse shear stresses τ_{yn} in the *s-y-n* coordinate system

$$\begin{aligned} &\tau_{ys,s} + \sigma_{yy,y} + \tau_{yn,n} = 0, \\ &\tau_{yn}(s,n) = -\int_0^n \left(\tau_{ys,s} + \sigma_{yy,y}\right) dn. \end{aligned} \tag{3.22}$$

The transverse normal ('peeling') stress σ_{nn} is computed by integrating Equation $(3.23)_1$, after τ_{sn} and τ_{yn} have been determined,

$$\tau_{ns,s} + \tau_{ny,y} + \sigma_{nn,n} = 0,$$

$$\sigma_{nn}(s,n) = -\int_0^n (\tau_{ns,s} + \tau_{ny,y})dn. \tag{3.23}$$

The integration constants in Equation $(3.21)_2$, $(3.22)_2$ and $(3.23)_2$ are determined by recognizing that τ_{sn}, τ_{yn} and σ_{nn} vanish on the top and bottom surfaces of the sandwich member.

3.6. Elastic Couplings

Whitney (1987, pp. 299-300) has discussed the structural analysis of constant-thickness sandwich composite structures. The constitutive equation that relates the resultant forces and moments to the reference surface strains and curvatures for a sandwich member of constant thickness is

$$\begin{Bmatrix} N_x \\ N_y \\ N_{xy} \\ M_x \\ M_y \\ M_{xy} \end{Bmatrix} = \begin{bmatrix} A_{11} & A_{12} & A_{16} & B_{11} & B_{12} & B_{16} \\ A_{12} & A_{22} & A_{26} & B_{12} & B_{22} & B_{26} \\ A_{16} & A_{26} & A_{66} & B_{16} & B_{26} & B_{66} \\ B_{11} & B_{12} & B_{16} & D_{11} & D_{12} & D_{16} \\ B_{12} & B_{22} & B_{26} & D_{12} & D_{22} & D_{26} \\ B_{16} & B_{26} & B_{66} & D_{16} & D_{26} & D_{66} \end{bmatrix} \begin{Bmatrix} \varepsilon_{xx}^0 \\ \varepsilon_{yy}^0 \\ \gamma_{xy}^0 \\ \kappa_{xx}^0 \\ \kappa_{yy}^0 \\ \kappa_{xy}^0 \end{Bmatrix},$$

$$\begin{bmatrix} Q_y \\ Q_x \end{bmatrix} = \begin{Bmatrix} A_{44} & 0 \\ 0 & A_{55} \end{Bmatrix} \begin{Bmatrix} \gamma_{yz}^c \\ \gamma_{xz}^c \end{Bmatrix}. \tag{3.24}$$

Notice that the constitutive equation that relates the transverse shear forces Q_y and Q_x to the shear strains γ^c_{yz} and γ^c_{xz} of the core are uncoupled from the in-plane force and moment resultants. An important feature of tapered sandwich members is the elastic couplings between bending and transverse shear, and extension and transverse shear as shown in Equation. (3.13). For a tapered member with isotropic facings, there are 6 new

elastic couplings, namely A_{51}, A_{52}, A_{46}, B_{51}, B_{52} and B_{46}. These elastic couplings vanish for sandwich members with constant depth. In this section, we give physical interpretations of the new elastic coupling coefficients.

3.6.1. Bending – Transverse Shear Coupling B_{51}

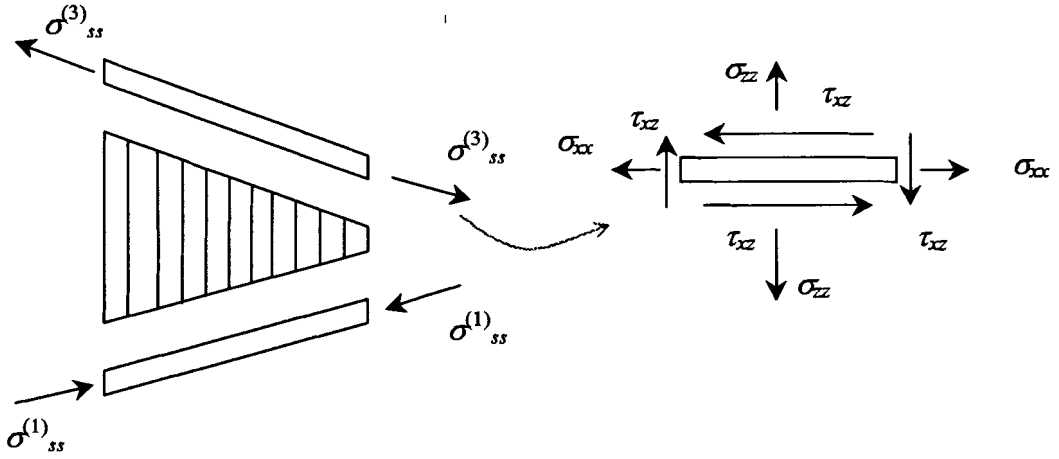

Figure 3.4. Transforming extensional stresses in *s-y-n* coordinate system to *x-y-z* coordinate system

The elastic rigidity B_{51} in Equation (3.13) is bending-shear coupling. To study the effect of B_{51}, consider the following deformation wherein the reference surface strains and curvatures of a tapered sandwich section are $\kappa^0_{xx} > 0$ and $\varepsilon^0_{xx} = \varepsilon^0_{yy} = \gamma^0_{xy} = \kappa^0_{yy} = \kappa^0_{xy} = \gamma^c_{yz} = \gamma^c_{xz} = 0$. Since the core shear strain γ^c_{xz} has been prescribed to be zero, the core shear stress $\tau^c_{xz} = 0$ using $(3.11)_1$. Strain ε_{xx} in the *x*-direction of the facings is computed by Equation (3.7). Strains ε_{ss}, ε_{nn} and γ_{sn} in the *s-y-n* coordinate system are obtained by transforming the strain ε_{xx} to the *s-y-n* coordinate system from Equations (3.8) and $(3.4)_1$. Stresses σ_{ss}, σ_{yy} and $\tau_{sy} = 0$ are obtained using the stress-strain relations in the *s-y-n* coordinate system (3.2). By transforming the stress σ_{ss} to the *x-y-z* coordinate system, we would get the stresses σ_{xx}, σ_{zz} and τ_{xz}, as shown in Figure 3.4. The shear stress

τ_{xz} in the facings act in the same direction and gives rise to a shear force Q_x. In other words, *a transverse shear force Q_x has to be applied in order to obtain the reference surface bending curvature κ^0_{xx}, although the transverse shear strain in the x-z plane is zero*. Therefore we refer to the constant B_{51} as the bending-transverse shear elastic coupling.

The physical meaning of the shear-bending elastic coupling can also be understood through a simple analysis of the forces on a cross-section of a symmetric

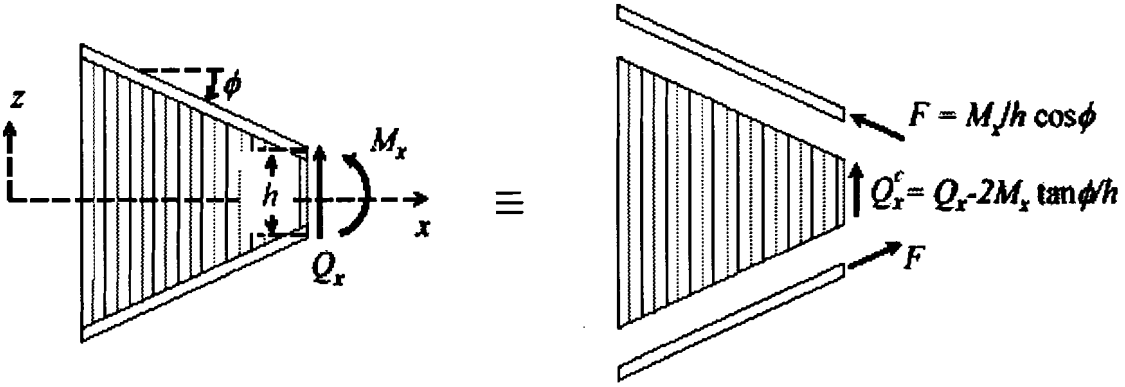

Figure 3.5 Shear-bending coupling in symmetric tapered sandwich

tapered member as shown in Figure 3.5. The forces include the internal moment M_x and shear force Q_x. The assumption is made that normal force due to the bending moment is transmitted through the facings only. A portion of the resultant shear force is transmitted through the facings due to their angle of inclination. The core resists the remainder of the shear force. As can be seen, even if the shear load Q_x is absent, a shear force Q^c_x is induced in the core due to the inclinations of the facings, thus causing transverse shear deformation of the core.

3.6.2. Bending – Transverse Shear Coupling B_{52}

The elastic rigidity B_{52} in Equation (3.13) is a bending-transverse shear coupling caused by the Poisson's effect. To study the effect of B_{52}, consider the following situation wherein at a point on the reference surface of a tapered sandwich section, $\kappa^0_{yy} > 0$ and $\varepsilon^0_{xx} = \varepsilon^0_{yy} = \gamma^0_{xy} = \kappa^0_{xx} = \kappa^0_{xy} = \gamma^c_{yz} = \gamma^c_{xz} = 0$. From Equation (3.7), the facings would have a strain ε_{yy} in the y-direction. Since the facings are inclined, the strain ε_{zz} and γ_{xz} from Equation (3.8) are nonzero due to the plane stress state in the facings. Transforming the strains using Equation $(3.4)_1$ to obtain strains ε_{ss}, ε_{nn} and γ_{sn} in the s-y-n coordinate system and making using of the stress-strain relations Equation (3.2) in the s-y-n coordinate system, we obtain the stresses σ_{ss}, σ_{yy} and $\tau_{sy} = 0$. The stress σ_{ss}, which is essentially a reaction stress component due to the constraint $\varepsilon_{xx} = 0$, gives rise to a transverse shear stress τ_{xz} and transverse shear force Q_x as shown in Figure 3.4.

3.6.3. Extension – Transverse Shear Coupling A_{51}

To study the effect of A_{51}, consider the following situation wherein at every point

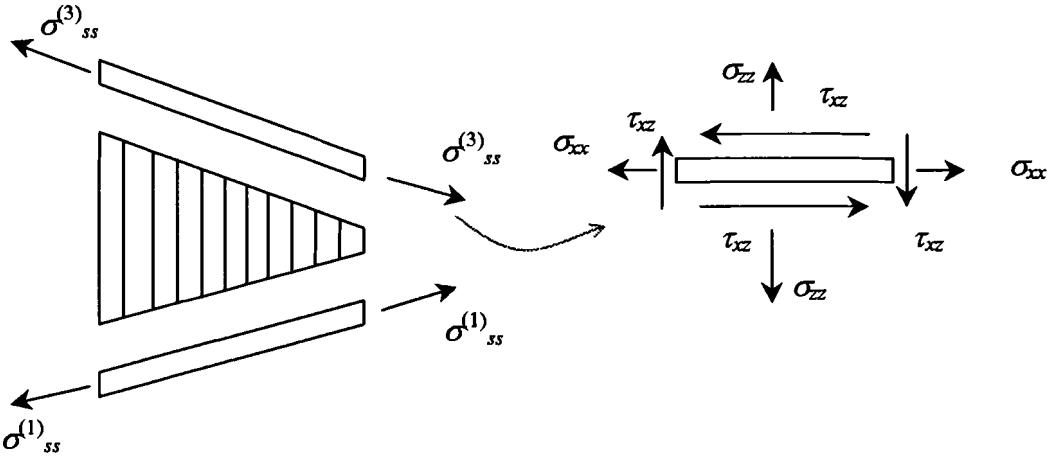

Figure 3.6 Transforming extensional stresses in s-y-n coordinate system to x-y-z coordinate system

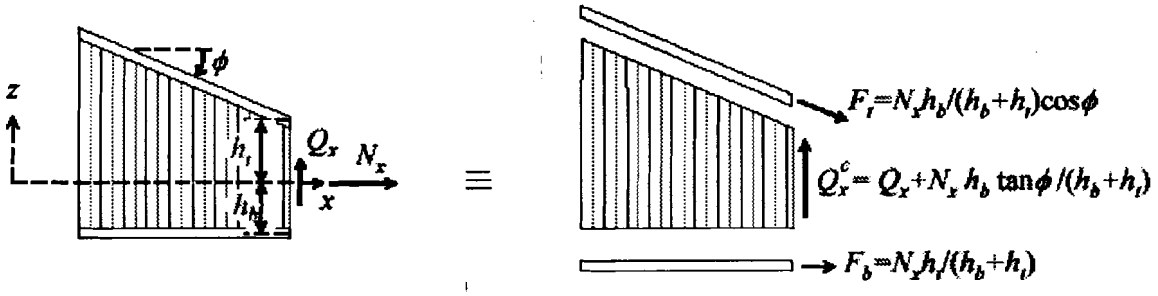

Figure 3.7 Extension- shear coupling in unsymmetric tapered sandwich beams

on the reference surface of a sandwich members, $\varepsilon^0_{xx} > 0$ and $\varepsilon^0_{yy} = \gamma^0_{xy} = \kappa^0_{xx} = \kappa^0_{yy} = \kappa^0_{xy} = \gamma^c_{yz} = \gamma^c_{xz} = 0$. Strain ε_{xx} in the x-direction of the facings causes the stress σ_{xx}, σ_{zz} and τ_{xz} in the facings as shown in Figure 3.6. The transverse shear stress τ_{xz} in the facings contribute to the transverse shear force Q_x. *The presence of the elastic coupling rigidity A_{51} implies that a transverse shear force Q_x is required to produce an extensional strain ε^0_{xx}.* Note that if the tapered sandwich section is symmetric, the directions of transverse shear stress τ_{xz} of top and bottom facing are equal and opposite, and the transverse shear force Q_x is zero. Therefore, *$A_{51}=0$ for symmetric tapered sandwich members*. However, A_{51} is nonzero for unsymmetric sandwich members.

The physical meaning of the extension–transverse shear elastic coupling can also be understood through a simple analysis of the forces on a cross-section of an unsymmetric tapered member shown in Figure 3.7. The forces acting on the section include the stress resultant N_x and transverse shear force Q_x. The assumption is made that the normal force N_x is transmitted through the facing only. A portion of the resultant shear force is transmitted through the facing due to the angle of inclination. The core

resists the remainder of the shear force. As can be seen, the transverse shear force carried by the core Q^c_x is different from the transverse shear force resultant Q_x due to N_x. That is, the stress resultant N_x can cause shear deformation in the core even when Q_x is zero.

3.6.4. Extension – Transverse Shear Coupling A_{52}

The elastic rigidity A_{52} is an extension-transverse shear coupling caused by the Poisson's effect. Consider the following deformation wherein a point on the reference surface of a sandwich member has the following strains and curvatures, $\varepsilon^0_{yy} > 0$ and $\varepsilon^0_{xx} = \gamma^0_{xy} = \kappa^0_{xx} = \kappa^0_{yy} = \kappa^0_{xy} = \gamma^c_{yz} = \gamma^c_{xz} = 0$. As explained in section 3.6.2, the strain ε_{yy} causes a transverse shear stress τ_{xz} in the facings. Therefore, *it is necessary to have Q_x in order to obtain an extensional strain in the y-direction, although there is no shear deformation of the core in the x-z plane*. If the tapered sandwich section is symmetric, the shear stresses τ_{xz} of the both top and bottom facing are equal in magnitude and opposite in direction and therefore $Q_x = 0$. That is, *the elastic coupling $A_{52} = 0$ for symmetric tapered sandwich members*. It can be directly verified that A_{52} in Equation (3.14) zero.

3.6.5. In-plane Shear – Transverse Shear Coupling A_{46}

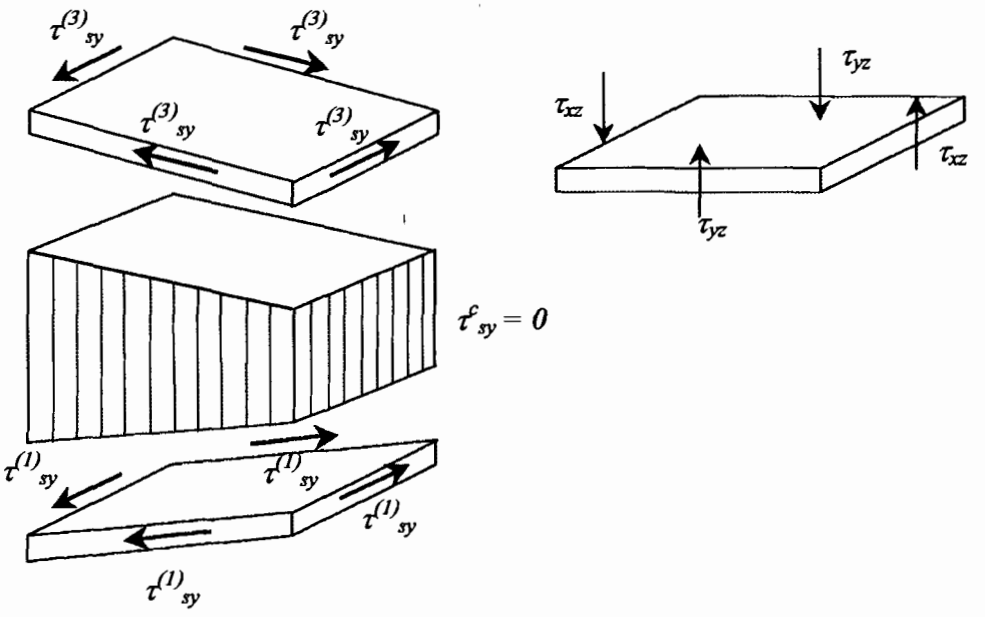

Figure 3.8 Stresses required to produce only γ^{0}_{xy}

The elastic rigidity A_{46} in Equation (3.13) causes coupling between the shear strain in x-y plane and the transverse shear force Q_y. Consider the following situation wherein points on the reference surface of sandwich members have the following strains and curvatures, $\gamma^{0}_{xy} > 0$ and $\varepsilon^{0}_{xx} = \varepsilon^{0}_{yy} = \kappa^{0}_{xx} = \kappa^{0}_{yy} = \kappa^{0}_{xy} = \gamma^{f}_{yz} = \gamma^{f}_{xz} = 0$. From Equation (3.7), the shear strain γ^{0}_{xy} on reference surface causes shear strain γ_{xy} in the facings. Transforming this shear strain γ_{xy} using Equation $(3.4)_1$ leads to shear strains γ_{sy} and γ_{yn} in the s-y-n coordinate system. By using of the stress-strain relations (3.2) in the s-y-n coordinate system, we see that the shear stress τ_{sy} is nonzero as depicted in Figure 3.8. The shear stress τ_{sy} acting on the x-z surfaces of the facings causes a shear stress τ_{yz} and hence Q_y when transformed to the x-y-z coordinate system. *The presence of the elastic*

coupling rigidity A_{46} implies that a transverse shear force Q_y is required to produce an in-plane shear strain γ^0_{xy}.

Note that if the tapered sandwich section is symmetric, the directions of the shear stress τ_{yz} of top and bottom facings are equal in magnitude and opposite in direction, therefore $Q_y = 0$. Therefore, *the elastic coupling $A_{46} = 0$ for symmetric sandwich members.*

3.6.6 Twisting – Transverse Shear Coupling B_{46}

To understand the physical interpretation of B_{46}, consider the following situation wherein the strains and curvatures of a point on the reference surface of a sandwich

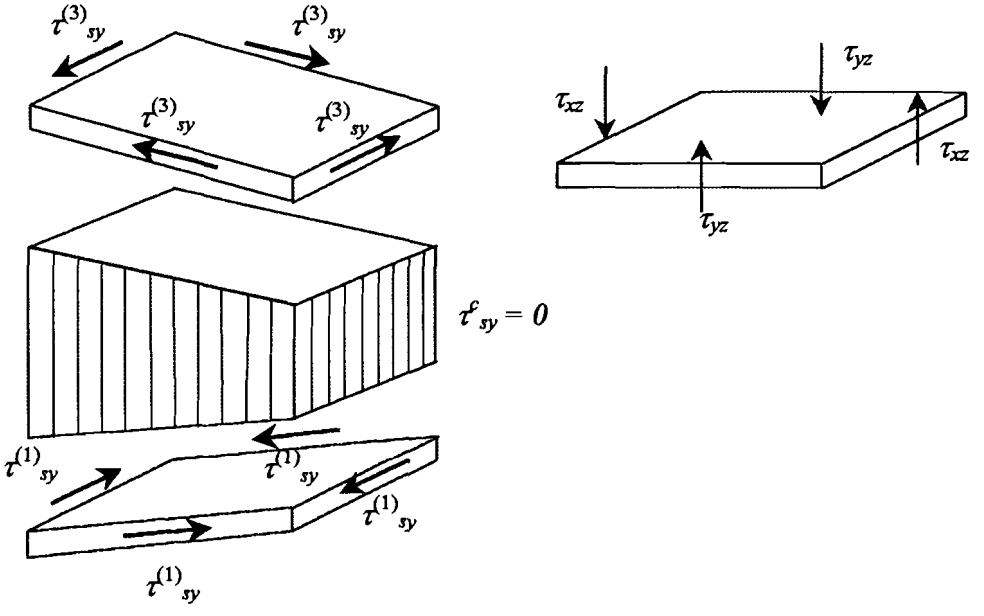

Figure 3.9 Stresses required to produce only κ^0_{xy}

member are $\kappa^0_{xy} > 0$ and $\varepsilon^0_{xx} = \varepsilon^0_{yy} = \gamma^0_{xy} = \kappa^0_{xx} = \kappa^0_{yy} = \gamma^c_{yz} = \gamma^c_{xz} = 0$. From Equation (3.7), the twisting curvature κ^0_{xy} on the reference surface causes shear strain γ_{xy} in both facings. Transforming this shear strain using Equation $(3.4)_1$ and by using the constitutive

equation (3.2), we obtain a shear stress τ_{yz}, and hence a shear force Q_y, that acts on the x-z plane of the facings, as shown in Figure 3.9. *The presence of the elastic coupling rigidity B_{46} implies that a transverse shear force Q_y is required to produce a twisting curvature κ^0_{xy}.* Note that if the facings are parallel to each other, $B_{46} = 0$, which implies that this coupling vanishes.

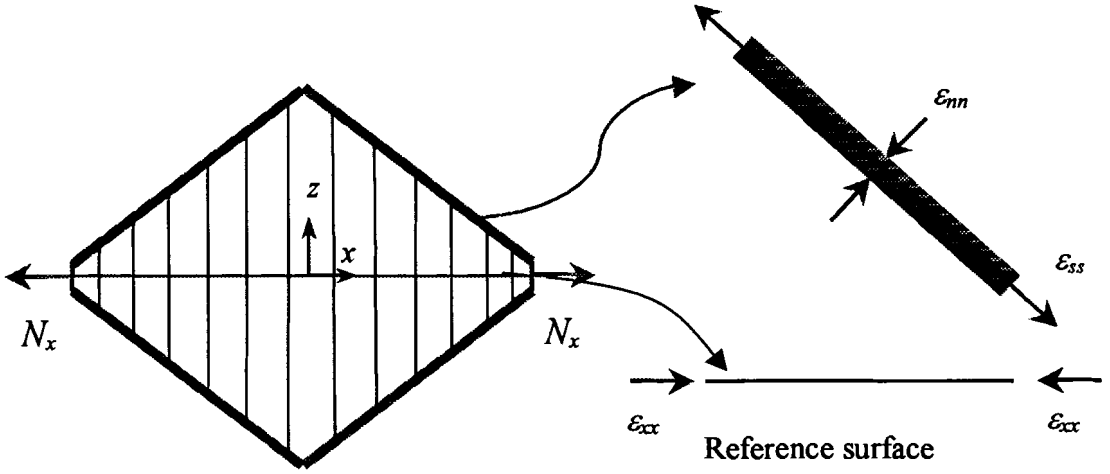

Figure 3.10 Negative extension rigidity for sandwich members with large taper angles

3.7. Negative Rigidity for Steep Taper Angles

It is observed from Equation (3.9), that the reduced elastic stiffness of the facings is negative if the tapered angle ϕ is larger than the critical angle

$$\phi_{cr} = \frac{1}{2}\cos^{-1}(2\nu - 1). \tag{3.25}$$

Since the critical taper angle depends only on the Poisson's ratio of the facing material and $0<\nu<0.5$ for the isotropic facings, ϕ_{cr} lies in the range $45^\circ < \phi_{cr} < 90^\circ$. If the facings are made of aluminum, the critical angle $\phi_{cr} = 54.39^0$. If the taper angle of a symmetric sandwich member is greater than ϕ_{cr}, then both the extension rigidity A_{11} and bending

rigidity D_{11} are negative. Since negative bending and extensional rigidities are rarely encountered in mechanics, we need to explore its physical interpretations and implications on the response of sandwich members with very large taper angles.

For the effects of the negative extension rigidity A_{11}, consider the following situation wherein a point on the reference surface is subjected to the axial load $N_x > 0$, and all other resultant forces and moments are zero. The negative extension rigidity A_{11} implies that the strain in the x-direction is negative, although the axial load is positive. There is a physical explanation for this phenomenon. The axial force is transmitted through the facings only and the core doesn't resist any extension loading due to its negligible extension stiffness. Therefore, the stress σ_{ss} and strain ε_{ss} in the facings are positive. However, since the facings are in a state of plane stress, the normal strain ε_{nn} in the facings is negative due to the Poisson's effect, as shown in Figure 3.10. The negative Poisson's contraction of the facings, in conjunction with the steep taper angle, outweighs the effect of the positive strain ε_{ss} and results in a negative axial strain ε_{xx}. It is important to note that although $\varepsilon_{xx} < 0$, the sandwich member extends in the axial direction since the strain energy is positive.

The explanation for the occurrence of negative bending D_{11} at large taper angles $\phi > \phi_{cr}$ is similar to the reasoning for the negative extension rigidity A_{11}. Consider a tapered member that is subjected to a positive bending moment M_x. The stress σ_{ss} and strain ε_{ss} are positive in the top facing and negative in the bottom facing. Due to the Poisson's effect and the steep taper angle, the corresponding transverse normal strain ε_{nn} and axial strain ε_{xx}, are negative in the top facing and positive in the bottom facing as shown in

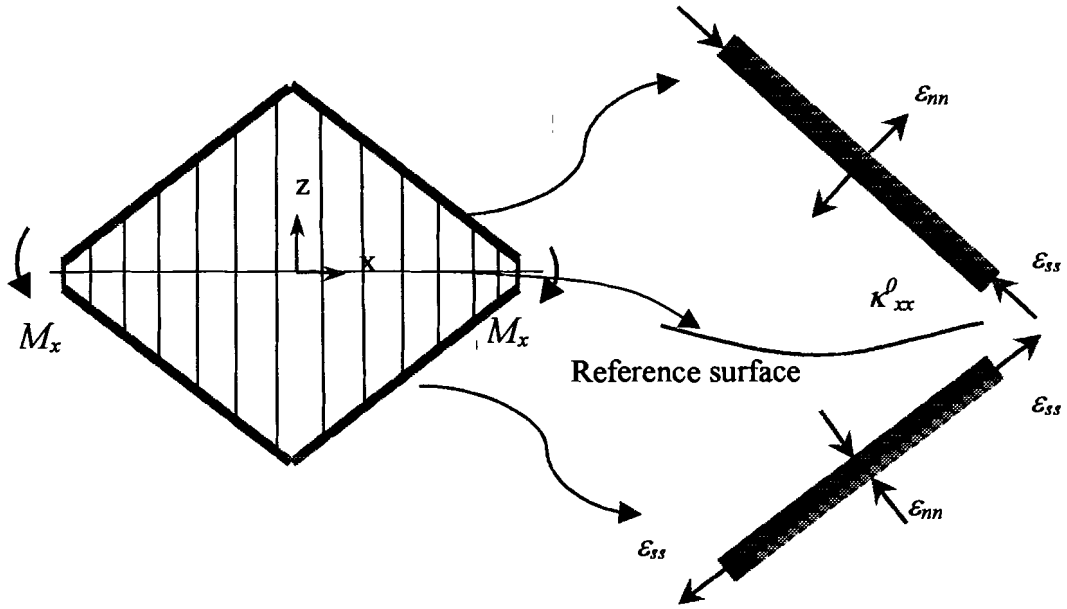

Figure 3.11 Negative bending rigidity for sandwich members with large taper angles

Figure 3.11. Since the reference surface strain $\varepsilon^0_{xx} = 0$, Equation $(3.7)_1$ implies a negative reference surface curvature κ^0_{xx}.

Chapter 4

ANALYTICAL MODEL OF ANISOTROPIC FACINGS

In this chapter, we extend the theory to tapered sandwich members with laminated fiber-reinforced facings. In addition to the 6 elastic couplings described in the previous chapter for isotropic facings, we obtain 6 additional elastic couplings due to the anisotropic facings. The physical interpretations of the elastic couplings are given in this chapter.

4.1. Problem Formulation

The analytical development of a tapered sandwich member with laminated anisotropic facings starts with the general depiction of the geometry as shown in Figure 4.1. We use a rectangular Cartesian coordinate system *x-y-z*. The thickness is assumed to

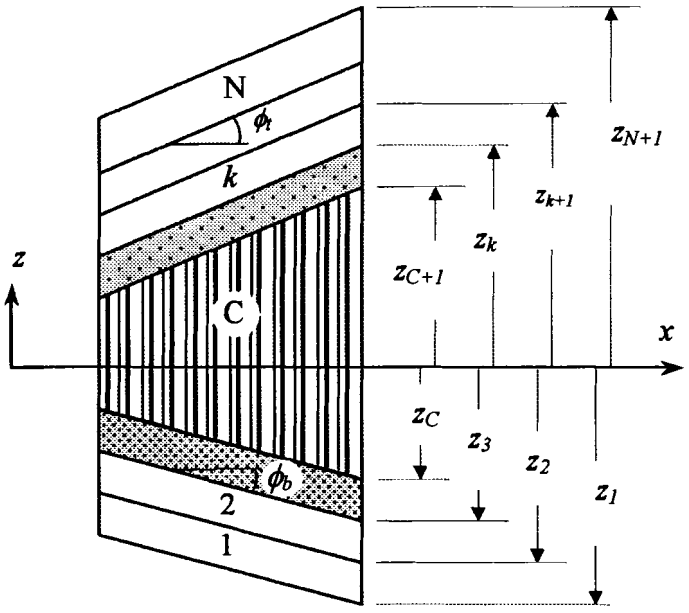

Figure 4.1 Layer numbering for a tapered sandwich structure

vary linearly along the span (x-direction). It is assumed that the facings are relatively thin compared to the core and therefore behave as membranes. The core is assumed to be inextensible in the thickness direction and to carry only transverse shear stresses. Since the facings are tapered, it is advantageous to use a local coordinate system, denoted by s-y-n, such that the s- and n-axes are parallel and normal to the facing, respectively. The taper angle of the facing, ϕ, is taken as positive counter-clockwise with respect to the x-axis. The facing laminae are orthotropic and each lamina has a distinct fiber orientation θ_k relative to the s-axis. The tapered member is composed of N distinct layers numbered from bottom to top as shown in Figure 4.1. The core is denoted as layer number C and the bottom and top facings are composed of C -1 and N - C distinct laminae, respectively. The z-coordinate of the bottom surface of the kth layer is designated z_k with the top surface of the layer being z_{k+1}. In general, the z_k's are functions of the x-coordinate since the sandwich beam is tapered. The taper angle of the top and bottom facings are $\phi = \phi_t$ and $\phi = \phi_b$, respectively.

4.2. Analytical Model

Since the facings are relatively thin compared to the core, we assume that the plane stress conditions stated in Equation 3.1 are applicable to the anisotropic laminae of the facings. The stress-strain relations for an orthotropic lamina in the principal material coordinate system are

$$\begin{bmatrix} \sigma_{11} \\ \sigma_{22} \\ \sigma_{33} \\ \tau_{23} \\ \tau_{13} \\ \tau_{11} \end{bmatrix} = \begin{bmatrix} C_{11} & C_{12} & C_{13} & 0 & 0 & 0 \\ C_{12} & C_{22} & C_{23} & 0 & 0 & 0 \\ C_{13} & C_{23} & C_{33} & 0 & 0 & 0 \\ 0 & 0 & 0 & C_{44} & 0 & 0 \\ 0 & 0 & 0 & 0 & C_{55} & 0 \\ 0 & 0 & 0 & 0 & 0 & C_{66} \end{bmatrix} \begin{bmatrix} \varepsilon_{11} \\ \varepsilon_{22} \\ \varepsilon_{33} \\ \gamma_{23} \\ \gamma_{13} \\ \gamma_{11} \end{bmatrix}, \tag{4.1}$$

The elastic stiffnesses C_{ij} in Equation (4.1) for an orthotropic material in terms of the engineering constants are

$$C_{11} = \frac{E_1\left(1-\nu_{23}^2 E_3/E_2\right)}{1-\nu},$$
$$C_{12} = \frac{E_2\left(\nu_{12}+\nu_{13}\nu_{23} E_3/E_2\right)}{1-\nu},$$
$$C_{13} = \frac{E_3\left(\nu_{13}+\nu_{12}\nu_{23}\right)}{1-\nu},$$
$$C_{22} = \frac{E_2\left(1-\nu_{13}^2 E_3/E_1\right)}{1-\nu},$$
$$C_{23} = \frac{E_3\left(\nu_{23}+\nu_{12}\nu_{13} E_2/E_1\right)}{1-\nu},$$
$$C_{33} = \frac{E_3\left(1-\nu_{12}^2 E_2/E_1\right)}{1-\nu},$$
$$C_{44} = G_{23}, C_{55} = G_{13}, C_{66} = G_{12},$$

where

$$\nu = \frac{\nu_{12}^2 E_2 + \nu_{13}^2 E_3 + \nu_{23}^2 E_3 - 2\nu_{12}\nu_{23}\nu_{13} E_3}{E_1}.$$

The principal material direction of the k^{th} lamina is oriented at angle θ_k with respect to the *s*-coordinate direction. The stress-strain relations for an orthotropic lamina in the (*s, y, n*) coordinate system are,

$$\begin{bmatrix} \sigma_{ss} \\ \sigma_{yy} \\ \sigma_{nn} \\ \tau_{yn} \\ \tau_{sn} \\ \tau_{sy} \end{bmatrix} = \begin{bmatrix} \overline{C}_{11} & \overline{C}_{12} & \overline{C}_{13} & 0 & 0 & \overline{C}_{16} \\ \overline{C}_{12} & \overline{C}_{22} & \overline{C}_{23} & 0 & 0 & \overline{C}_{26} \\ \overline{C}_{13} & \overline{C}_{23} & \overline{C}_{33} & 0 & 0 & \overline{C}_{36} \\ 0 & 0 & 0 & \overline{C}_{44} & \overline{C}_{45} & 0 \\ 0 & 0 & 0 & \overline{C}_{45} & \overline{C}_{55} & 0 \\ \overline{C}_{16} & \overline{C}_{26} & \overline{C}_{36} & 0 & 0 & \overline{C}_{66} \end{bmatrix} \begin{bmatrix} \varepsilon_{ss} \\ \varepsilon_{yy} \\ \varepsilon_{nn} \\ \gamma_{yn} \\ \gamma_{sn} \\ \gamma_{sy} \end{bmatrix}, \tag{4.2}$$

where the elastic stiffness components $\overline{C}_{ij}$ in terms of the Young's moduli, Poisson's ratios, shear moduli and the angle θ_k are

$$\begin{aligned}
\overline{C}_{11} &= C_{11}m^4 + 2m^2n^2(C_{12} + 2C_{66}) + C_{22}n^4, \\
\overline{C}_{12} &= m^2n^2(C_{11} + C_{22} - 4C_{66}) + C_{12}(m^4 + n^4), \\
\overline{C}_{13} &= C_{13}m^2 + C_{23}n^2, \\
\overline{C}_{16} &= mn[C_{11}m^2 - C_{22}n^2 - (C_{12} + 2C_{66})(m^2 - n^2)], \\
\overline{C}_{22} &= C_{11}n^4 + 2m^2n^2(C_{12} + 2C_{66}) + C_{22}m^4, \\
\overline{C}_{23} &= C_{13}n^2 + C_{23}m^2, \\
\overline{C}_{26} &= mn[C_{11}n^2 - C_{22}m^2 + (C_{12} + 2C_{66})(m^2 - n^2)], \\
\overline{C}_{33} &= C_{33}, \\
\overline{C}_{36} &= mn(C_{23} - C_{13}), \\
\overline{C}_{44} &= C_{44}m^2 + C_{55}n^2, \\
\overline{C}_{45} &= mn(C_{44} - C_{55}), \\
\overline{C}_{55} &= C_{44}n^2 + C_{55}m^2, \\
\overline{C}_{66} &= m^2n^2(C_{11} + C_{22} - 2C_{12}) + C_{66}(m^2 - n^2)^2,
\end{aligned} \tag{4.3}$$

where $m = cos\theta_k$ and $n = sin\theta_k$. The expressions are also available in books on composite materials (e.g. see Herakovich, 1997, pp. 57-61). The transformation of the stresses and strains between the (x, y, z) and (s, y, n) coordinate systems given in Equation (3.3) and (3.4) remain unchanged.

As before, it is assumed that the strains in the facings are linear functions of the thickness coordinate, as shown in Equation (3.7). Likewise, the transverse normal strain ε_{zz}, and the transverse shear strains γ_{xz} and γ_{yz} in the facings are expressed in terms of ε_{xx},

ε_{yy} and γ_{xy} by recognizing that the facings are in a state of plane stress. The stresses in the (s, y, n) coordinate system are obtained through $\{\sigma\}_{syn} = [C]\{\varepsilon\}_{syn} = [C][R]^T\{\varepsilon\}_{xyz}$. The three plane stress equations (3.1) are enforced to obtain ε_{zz}, γ_{xz} and γ_{yz} in terms of ε_{xx}, ε_{yy} and γ_{xy} as

$$\begin{aligned}
\varepsilon_{zz} &= \frac{\overline{C}_{13}\cos^2\phi - \overline{C}_{33}\sin^2\phi}{D}\varepsilon_{xx} + \frac{\overline{C}_{23}\left(\cos^2\phi - \sin^2\phi\right)}{D}\varepsilon_{yy} + \frac{\overline{C}_{36}\left(\cos^2\phi - \sin^2\phi\right)}{D}\gamma_{xy}, \\
\gamma_{xz} &= -\frac{2\left(\overline{C}_{13} + \overline{C}_{33}\right)\cos\phi\sin\phi}{D}\varepsilon_{xx} - \frac{2\overline{C}_{23}\cos\phi\sin\phi}{D}\varepsilon_{yy} - \frac{2\overline{C}_{36}\sin\phi}{D}\gamma_{xy}, \\
\gamma_{yz} &= \gamma_{xy}\tan\phi,
\end{aligned} \tag{4.4}$$

where,

$$D = \overline{C}_{13}\sin^2\phi - \overline{C}_{33}\cos^2\phi.$$

The stress-strain relations in the (x, y, z) coordinate system for a tapered facing lamina, computed using (4.4), $(3.4)_1$, (4.2), $(3.3)_2$, are

$$\begin{bmatrix} \sigma_{xx} \\ \sigma_{yy} \\ \sigma_{zz} \\ \tau_{yz} \\ \tau_{xz} \\ \tau_{xy} \end{bmatrix} = \begin{bmatrix} \tilde{Q}_{11} & \tilde{Q}_{12} & \tilde{Q}_{16} \\ \tilde{Q}_{21} & \tilde{Q}_{22} & \tilde{Q}_{26} \\ \tilde{Q}_{31} & \tilde{Q}_{32} & \tilde{Q}_{36} \\ \tilde{Q}_{41} & \tilde{Q}_{42} & \tilde{Q}_{46} \\ \tilde{Q}_{51} & \tilde{Q}_{52} & \tilde{Q}_{56} \\ \tilde{Q}_{61} & \tilde{Q}_{62} & \tilde{Q}_{66} \end{bmatrix} \begin{Bmatrix} \varepsilon_{xx} \\ \varepsilon_{yy} \\ \gamma_{xy} \end{Bmatrix}, \tag{4.5}$$

where $\tilde{Q}_{ij}$ are the *reduced stiffnesses for an inclined facing lamina*, defined as

$$\tilde{Q}_{11} = \frac{\left(\overline{C}_{13}^2 - \overline{C}_{11}\overline{C}_{33}\right)\cos^2\phi}{D},$$

$$\tilde{Q}_{12} = \frac{\left(\left(\overline{C}_{13}\overline{C}_{23} - \overline{C}_{12}\overline{C}_{33}\right)\cos^2\phi + \left(\overline{C}_{12}\overline{C}_{13} - \overline{C}_{11}\overline{C}_{23}\right)\sin^2\phi\right)\cos^2\phi}{D},$$

$$\tilde{Q}_{16} = \frac{\left(\overline{C}_{13}\overline{C}_{36} - \overline{C}_{16}\overline{C}_{33}\right)\cos^3\phi + \left(\overline{C}_{13}\overline{C}_{16} - \overline{C}_{11}\overline{C}_{36}\right)\cos\phi\sin^2\phi}{D},$$

$$\tilde{Q}_{21} = \frac{\overline{C}_{13}\overline{C}_{23} - \overline{C}_{12}\overline{C}_{33}}{D},$$

$$\tilde{Q}_{22} = \frac{\left(\overline{C}_{23}^2 - \overline{C}_{22}\overline{C}_{33}\right)\cos^2\phi + \left(\overline{C}_{13}\overline{C}_{22} - \overline{C}_{12}\overline{C}_{23}\right)\sin^2\phi}{D},$$

$$\tilde{Q}_{26} = \frac{\left(\overline{C}_{23}\overline{C}_{36} - \overline{C}_{26}\overline{C}_{33}\right)\cos^2\phi + \left(\overline{C}_{13}\overline{C}_{26} - \overline{C}_{12}\overline{C}_{36}\right)\sin^2\phi}{D\cos\phi},$$

$$\tilde{Q}_{31} = \frac{\left(\overline{C}_{13}^2 - \overline{C}_{11}\overline{C}_{33}\right)\sin^2\phi}{D},$$

$$\tilde{Q}_{32} = \frac{\left(\left(\overline{C}_{13}\overline{C}_{23} - \overline{C}_{12}\overline{C}_{33}\right)\cos^2\phi + \left(\overline{C}_{12}\overline{C}_{13} - \overline{C}_{11}\overline{C}_{23}\right)\sin^2\phi\right)\sin^2\phi}{D},$$

$$\tilde{Q}_{36} = \frac{\left(\left(\overline{C}_{13}\overline{C}_{23} - \overline{C}_{16}\overline{C}_{33}\right)\cos^2\phi + \left(\overline{C}_{13}\overline{C}_{16} - \overline{C}_{11}\overline{C}_{36}\right)\sin^2\phi\right)\sin^2\phi}{D\cos\phi},$$

$$\tilde{Q}_{41} = \frac{\left(\overline{C}_{16}\overline{C}_{33} - \overline{C}_{13}\overline{C}_{36}\right)\sin\phi}{D},$$

$$\tilde{Q}_{42} = \frac{\left(\overline{C}_{23}\overline{C}_{36} - \overline{C}_{26}\overline{C}_{33}\right)\cos^2\phi\sin\phi + \left(\overline{C}_{13}\overline{C}_{26} - \overline{C}_{16}\overline{C}_{23}\right)\sin^3\phi}{D},$$

$$\tilde{Q}_{46} = \frac{\left(\overline{C}_{36}^2 - \overline{C}_{33}\overline{C}_{66}\right)\cos^2\phi\sin\phi + \left(\overline{C}_{13}\overline{C}_{66} - \overline{C}_{16}\overline{C}_{36}\right)\sin^3\phi}{D\cos\phi},$$

$$\tilde{Q}_{51} = \frac{\left(\overline{C}_{13}^2 - \overline{C}_{11}\overline{C}_{33}\right)\cos\phi\sin\phi}{D},$$

$$\tilde{Q}_{52} = \frac{\left(\overline{C}_{13}\overline{C}_{23} - \overline{C}_{12}\overline{C}_{33}\right)\cos^3\phi\sin\phi + \left(\overline{C}_{12}\overline{C}_{13} - \overline{C}_{11}\overline{C}_{23}\right)\cos\phi\sin^3\phi}{D},$$

$$\tilde{Q}_{56} = \frac{\left(\overline{C}_{13}\overline{C}_{36} - \overline{C}_{16}\overline{C}_{33}\right)\cos^2\phi\sin\phi + \left(\overline{C}_{13}\overline{C}_{16} - \overline{C}_{11}\overline{C}_{36}\right)\sin^3\phi}{D\cos\phi},$$

$$\tilde{Q}_{61} = \frac{\left(\overline{C}_{13}\overline{C}_{36} - \overline{C}_{16}\overline{C}_{33}\right)\cos\phi}{D},$$

$$\tilde{Q}_{62} = \frac{\left(\overline{C}_{23}\overline{C}_{36} - \overline{C}_{26}\overline{C}_{33}\right)\cos^3\phi + \left(\overline{C}_{13}\overline{C}_{26} - \overline{C}_{16}\overline{C}_{23}\right)\cos\phi\sin^2\phi}{D},$$

$$\tilde{Q}_{66} = \frac{\left(\overline{C}_{36}^2 - \overline{C}_{33}\overline{C}_{66}\right)\cos^2\phi + \left(\overline{C}_{13}\overline{C}_{66} - \overline{C}_{16}\overline{C}_{36}\right)\sin^2\phi}{D}. \qquad (4.6)$$

The in-plane stresses σ_{xx}, σ_{yy} and τ_{xy} of the core are assumed to be negligible compared to that in the facings. The transverse shear stresses τ_{xz} and τ_{yz} in the core are assumed to be constant throughout the thickness and they are related to the core shear strains by

$$\begin{aligned} \tau_{xz}^{(C)} &= G_{xz}^{c}\gamma_{xz}^{c}, \\ \tau_{yz}^{(C)} &= G_{yz}^{c}\gamma_{yz}^{c}. \end{aligned} \tag{4.7}$$

The stress resultants are defined as

$$\begin{aligned} [N_x, N_y, N_{xy}] &= \int_{z_1(x)}^{z_{N+1}(x)} [\sigma_{xx}, \sigma_{yy}, \tau_{xy}]\,dz, \\ [M_x, M_y, M_{xy}] &= \int_{z_1(x)}^{z_{N+1}(x)} z[\sigma_{xx}, \sigma_{yy}, \tau_{xy}]\,dz, \\ [Q_x, Q_y] &= \int_{z_1(x)}^{z_{N+1}(x)} [\tau_{xx}, \tau_{yy}]\,dz, \end{aligned} \tag{4.8}$$

where the quantities N_x, N_y and N_{xy} are the in-plane force resultants, Q_x and Q_y are the transverse shear load resultants and M_x, M_y and M_{xy} are the moment resultants, as depicted in Figure 3.2. Substitution of the facing stresses from (4.5) and the core stresses from (4.7) into (4.8) leads to the following matrix equation for the resultant forces and moments in terms of the core shear strains and reference surface strains and curvatures,

$$\begin{Bmatrix} N_x \\ N_y \\ Q_y \\ Q_x \\ N_{xy} \\ M_x \\ M_y \\ M_{xy} \end{Bmatrix} = \begin{bmatrix} A_{11} & A_{12} & 0 & 0 & A_{16} & B_{11} & B_{12} & B_{16} \\ A_{21} & A_{22} & 0 & 0 & A_{26} & B_{21} & B_{22} & B_{26} \\ A_{41} & A_{42} & A_{44} & 0 & A_{46} & B_{41} & B_{42} & B_{46} \\ A_{51} & A_{52} & 0 & A_{55} & A_{56} & B_{51} & B_{52} & B_{56} \\ A_{61} & A_{62} & 0 & 0 & A_{66} & B_{61} & B_{62} & B_{66} \\ B_{11} & B_{12} & 0 & 0 & B_{16} & D_{11} & D_{12} & D_{16} \\ B_{21} & B_{22} & 0 & 0 & B_{26} & D_{21} & D_{22} & D_{26} \\ B_{61} & B_{62} & 0 & 0 & B_{66} & D_{61} & D_{26} & D_{66} \end{bmatrix} \begin{Bmatrix} \varepsilon_{xx}^0 \\ \varepsilon_{yy}^0 \\ \gamma_{yz}^c \\ \gamma_{xz}^c \\ \gamma_{xy}^0 \\ \kappa_{xx}^0 \\ \kappa_{yy}^0 \\ \kappa_{xy}^0 \end{Bmatrix}, \tag{4.9}$$

where A_{ij} are the extensional and shear rigidities, D_{ij} are the bending rigidities and B_{ij} are the bending-extension rigidities defined by

$$\begin{aligned} \left[A_{ij}(x), B_{ij}(x), D_{ij}(x)\right] &= \sum_{\substack{k=1 \\ k \neq C}}^{N} \int_{z_k(x)}^{z_{k+1}(x)} \widetilde{Q}_{ij}^{(k)} \left[1, z, z^2\right] dz; i, j = 1,2,6 \\ \left[A_{44}(x), A_{55}(x)\right] &= \left[G_{yz}^c, G_{xz}^c\right] (z_{C+1}(x) - z_C(x)). \end{aligned} \tag{4.10}$$

The relation (4.9) can be inverted to obtain the following equation, from which the reference strains can be determined if the resultant forces and moments are known:

$$\begin{Bmatrix} \varepsilon_{xx}^0 \\ \varepsilon_{yy}^0 \\ \gamma_{yz}^c \\ \gamma_{xz}^c \\ \gamma_{xy}^0 \\ \kappa_{xx}^0 \\ \kappa_{yy}^0 \\ \kappa_{xy}^0 \end{Bmatrix} = \begin{bmatrix} a_{11} & a_{12} & 0 & 0 & a_{16} & b_{11} & b_{12} & b_{16} \\ a_{21} & a_{22} & 0 & 0 & a_{26} & b_{21} & b_{22} & b_{26} \\ a_{41} & a_{42} & a_{44} & 0 & a_{46} & b_{41} & b_{42} & b_{46} \\ a_{51} & a_{52} & 0 & a_{55} & a_{56} & b_{51} & b_{52} & b_{56} \\ a_{61} & a_{62} & 0 & 0 & a_{66} & b_{61} & b_{62} & b_{66} \\ b_{11} & b_{12} & 0 & 0 & b_{16} & d_{11} & d_{12} & d_{16} \\ b_{21} & b_{22} & 0 & 0 & b_{26} & d_{21} & d_{22} & d_{26} \\ b_{61} & b_{62} & 0 & 0 & b_{66} & d_{61} & d_{62} & d_{66} \end{bmatrix} \begin{Bmatrix} N_x \\ N_y \\ Q_y \\ Q_x \\ N_{xy} \\ M_x \\ M_y \\ M_{xy} \end{Bmatrix}, \tag{4.11}$$

4.3. Beam Bending and Cylindrical Bending

There are also two cases of laminated plates that can be treated as one-dimensional problems: (1) a tapered sandwich beam, and (2) cylindrical bending of a tapered member, as described in Section 3.3.

For a sandwich beam in bending, the transverse load Q_x and bending moment M_x are assumed to be known, whereas the other loads vanish, i.e., $N_x = N_y = Q_y = N_{xy} = M_y = M_{xy} = 0$. By substitution of the resultant force into Equation (4.11), the reference surface strains, curvatures and transverse shear strains are

$$\begin{aligned}
&\varepsilon_{xx}^0 = b_{11}M_x, \varepsilon_{yy}^0 = b_{21}M_x, \\
&\gamma_{yz}^c = b_{41}M_x, \gamma_{xz}^c = a_{55}Q_x + b_{51}M_x, \\
&\kappa_{xx}^0 = d_{11}M_x, \kappa_{yy}^0 = d_{21}M_x, \\
&\gamma_{xy}^0 = b_{61}M_x, \kappa_{xy}^0 = d_{61}M_x.
\end{aligned} \tag{4.12}$$

In the case of cylindrical bending, the transverse shear load Q_x and bending moment M_x are assumed to be know, whereas the strains and curvature in the y-direction and the other resultant forces and moment vanish. That is, $\varepsilon_{yy}^0 = \kappa_{yy}^0 = 0$ and $N_x = Q_y = N_{xy} = M_{xy} = 0$. The force and moment resultants N_y and M_y are obtained in terms of M_x using the second and seventh rows of the matrix equation (4.9) and the strains and curvatures ε_{xx}^0, γ_{yz}^c, γ_{xz}^c, γ_{xy}^0, κ_{xx}^0, κ_{xy}^0 are determined from the remaining six equations in (4.11),

$$
\begin{aligned}
\varepsilon_{xx}^{0} &= \frac{a_{12}(-d_{22}b_{21}+b_{22}d_{21})+b_{11}(a_{22}d_{22}-b_{22}^{2})+b_{12}(b_{22}b_{21}+a_{22}d_{21})}{a_{22}d_{22}-b_{22}^{2}}M_{x},\\
\gamma_{yz}^{c} &= \frac{a_{42}(-d_{22}b_{21}+b_{22}d_{21})+b_{41}(a_{22}d_{22}-b_{22}^{2})+b_{42}(b_{22}b_{21}+a_{22}d_{21})}{a_{22}d_{22}-b_{22}^{2}}M_{x},\\
\gamma_{xz}^{c} &= \frac{a_{52}(-d_{22}b_{21}+b_{22}d_{21})+b_{51}(a_{22}d_{22}-b_{22}^{2})+b_{52}(b_{22}b_{21}+a_{22}d_{21})}{a_{22}d_{22}-b_{22}^{2}}M_{x}+a_{55}Q_{x},\\
\gamma_{xy}^{0} &= \frac{a_{62}(-d_{22}b_{21}+b_{22}d_{21})+b_{61}(a_{22}d_{22}-b_{22}^{2})+b_{62}(b_{22}b_{21}+a_{22}d_{21})}{a_{22}d_{22}-b_{22}^{2}}M_{x},\\
\kappa_{xx}^{0} &= \frac{b_{12}(-d_{22}b_{21}+b_{22}d_{21})+d_{11}(a_{22}d_{22}-b_{22}^{2})+d_{12}(b_{22}b_{21}+a_{22}d_{21})}{a_{22}d_{22}-b_{22}^{2}}M_{x},\\
\kappa_{xy}^{0} &= \frac{b_{62}(-d_{22}b_{21}+b_{22}d_{21})+d_{61}(a_{22}d_{22}-b_{22}^{2})+d_{62}(b_{22}b_{21}+a_{22}d_{21})}{a_{22}d_{22}-b_{22}^{2}}M_{x}.
\end{aligned}
\tag{4.13}
$$

The strain distributions through the thickness of a tapered sandwich section are determined for Equation (3.7) after all the core shear strains and reference surface strains and curvatures have been computed. The stress distributions in the global *x-y-z* coordinate system are obtained using the constitutive relations (4.5) and the stresses and strains in the local *s-y-n* coordinate system are determined using the transformation relations (3.3) and (3.4).

4.4. Elastic Couplings

In chapter three, six important couplings for tapered sandwich members with isotropic facings, namely B_{51}, B_{52}, A_{51}, A_{52}, A_{46} and B_{66}, have been discussed. An examination of Equation (4.9) reveals that there are six additional elastic couplings, namely A_{41}, A_{42}, B_{41}, B_{42}, A_{56} and B_{56}, for tapered sandwich members with anisotropic facings, as shown in Figure 4.2. In this section, we explore the physical interpretation of these additional coupling rigidities. We define two special cases of tapered sandwich members since they are relevant in our discussion of elastic couplings. When the

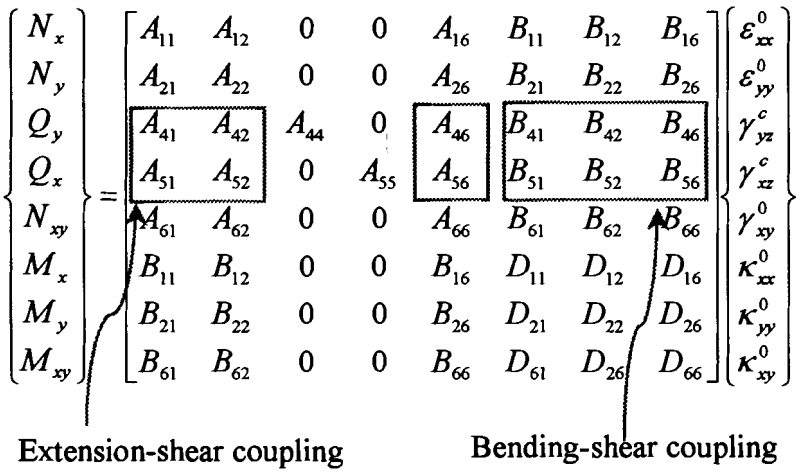

Figure 4.2 Extension-shear and bending-shear coupling in the stiffness matrix

inclination of the facings, laminae thicknesses and laminae fiber-orientations are symmetric about the mid-surface, the laminate is called a *symmetric tapered sandwich member*. However, if the inclination of the facings and laminae thicknesses are symmetric about the mid-surface, but the laminae fiber-orientations are antisymmetric about the mid-surface, it is known as an *antisymmetric tapered sandwich member.*

4.4.1. Extension -Transverse Shear Coupling A_{41}

The elastic rigidity A_{41} in Equation (4.9) causes coupling between the extension strain in the x-direction and transverse shear load Q_y. Consider the situation wherein the strains and curvatures at points on the reference surface of a sandwich member are $\varepsilon^0_{xx} > 0$ and $\varepsilon^0_{yy} = \gamma^0_{xy} = \kappa^0_{xx} = \kappa^0_{yy} = \kappa^0_{xy} = \gamma^c_{yz} = \gamma^c_{xz} = 0$. By substituting the assumed references strains and curvatures into Equation (3.7) and (4.4), transforming the strains from the x-y-z coordinate system to the s-y-n coordinate system using (3.4) and using the constitutive Equation (4.2), we obtain the stresses in the facings σ_{ss}, σ_{nn} and τ_{sy} as shown in Figure 4.3. The shear stress τ_{sy} in the plane of the facings is nonzero because the

principal material directions of the laminae are oriented at an angle to the s-axis; $\tau_{sy} = 0$ for isotropic and cross-ply laminae ($\theta_k = 0^\circ$ or 90°). By transforming shear stresses τ_{sy} to x-y-z coordinate system we obtain a vertical shear stress τ_{yz} that contributes to a shear load Q_y. That is, *a transverse shear force Q_y has to be applied in order to obtain a reference surface strain ε^0_{xx}, although the transverse shear strain of the core in the y-z plane is zero.*

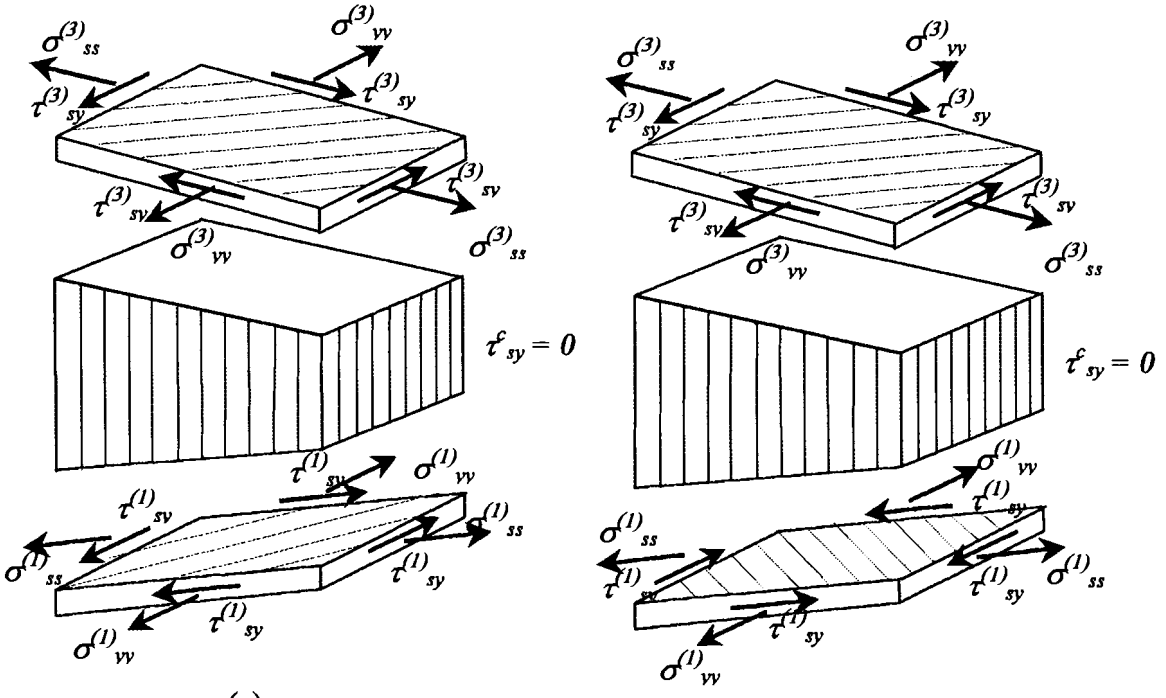

Figure 4.3 Stresses required to produce only ε^0_{xx}
(a) symmetric Case (b) antisymmetric Case

Note that if the tapered sandwich section is symmetric as shown in Figure 4.3a, the shear stress τ_{yz} of top and bottom facings are equal in magnitude and opposite in direction, and therefore $Q_y = 0$. That is, *$A_{41} = 0$ for symmetric sandwich members.* We can also verify that $\tilde{Q}_{41}$ in Equation (4.6) is an odd function of the taper angle ϕ, and therefore the contributions from a lamina in the top facing and the corresponding lamina

in the bottom facing of the symmetric sandwich member cancel out to give $A_{41} = 0$ in Equation (4.10). However, the contributions are additive for the antisymmetric sandwich members shown in Figure 4.3b.

4.4.2. Extension-Transverse Shear Coupling A_{42}

The elastic rigidity A_{42} in Equation (4.9) causes coupling between the extension strain in y-direction and transverse shear load Q_y. Consider the following situation wherein at every point on the reference surface of a sandwich member, $\varepsilon^0_{yy} > 0$ and $\varepsilon^0_{xx} = \gamma^0_{xy} = \kappa^0_{xx} = \kappa^0_{yy} = \kappa^0_{xy} = \gamma^c_{yz} = \gamma^c_{xz} = 0$. From Equation (3.7), the extensional strain ε^0_{yy} on reference surface causes extensional strain ε_{yy} in both facings. We obtain the stresses σ_{ss}, σ_{nn} and τ_{sy} in the facings by using Equation (4.4), the strain transformations Equation $(3.4)_1$ and constitutive equations Equation (4.2). The shear stress τ_{sy} is due to the combination of the Poisson's effect and the anisotropic material properties of the facings. The shear stress τ_{sy} contributes to a shear load Q_y. That is, *a transverse shear force Q_y has to be applied in order to obtain a reference surface strain ε^0_{yy}, although the transverse shear strain of the core in the y-z plane is zero.*

Note that if the tapered sandwich section is symmetric, the shear stress τ_{xz} of top and bottom facings are equal and opposite, as shown in Figure 4.4(a), and therefore $Q_y = 0$, In other words, *$A_{42} = 0$ for symmetric sandwich members.* This can be verified directly from (4.10) since $\tilde{Q}_{42}$ is an odd function of the taper angle ϕ.

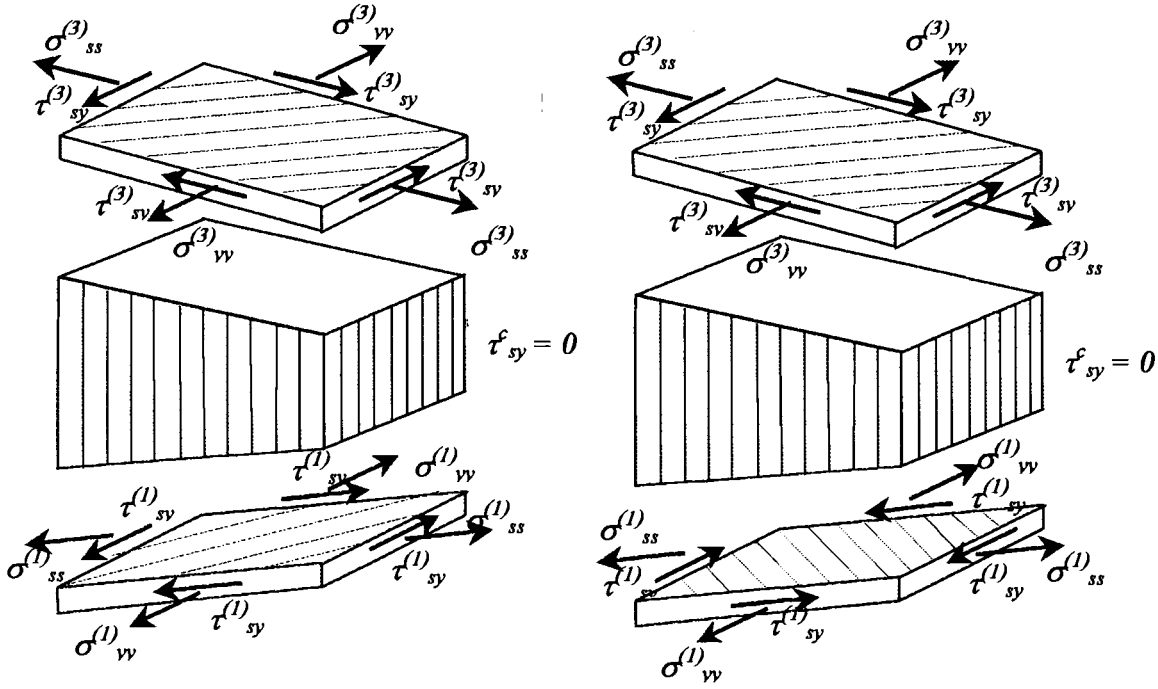

Figure 4.4 Stresses required to produce only ε^{0}_{yy}
(a) symmetric case (b) antisymmetric case

4.4.3. Bending-Transverse Shear Coupling B_{41}

The elastic rigidity B_{41} in Equation (4.9) causes coupling between the bending curvature in the x-direction and transverse shear load Q_y. Consider the following situation wherein at every point on the reference surface of a sandwich members, $\kappa^{0}_{xx} > 0$ and $\varepsilon^{0}_{xx} = \varepsilon^{0}_{yy} = \gamma^{0}_{xy} = \kappa^{0}_{yy} = \kappa^{0}_{xy} = \gamma^{c}_{yz} = \gamma^{c}_{xz} = 0$. Due to reasons explained in Section 4.3.1, we obtain the stress state depicted in Figure 4.5. The shear stress τ_{sy} has a vertical component that contributes to the shear load Q_y. This implies that *a transverse shear force Q_y has to be applied in order to obtain a reference surface curvature κ^{0}_{xx}, although the transverse shear strain of the core in the y-z plane is zero.*

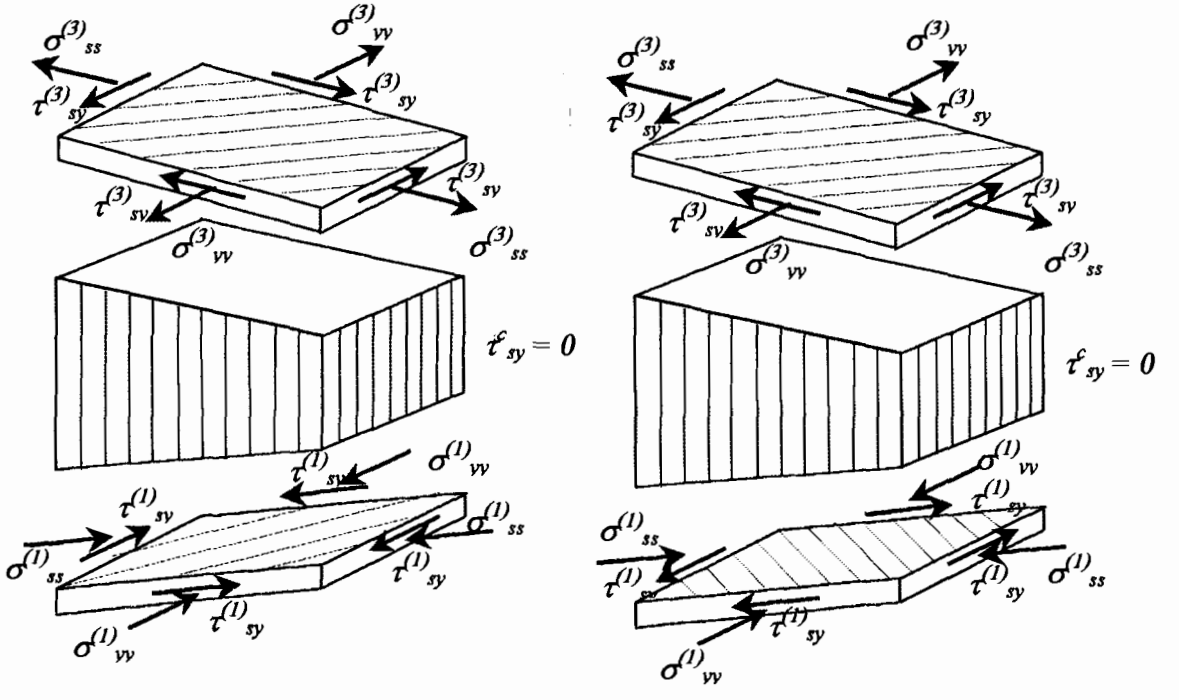

Figure 4.5 Stresses required to produce only κ^{0}_{xx}
(a) symmetric case (b) antisymmetric case

Note that if the tapered sandwich section is antisymmetric, the shear stress τ_{xz} of top and bottom facings are equal and opposite and therefore $Q_y = 0$. That is, $B_{41} = 0$ *for antisymmetric tapered sandwich members.* This can also be directly verified from Equation (4.10) since $\tilde{Q}_{41}$ is an odd function of the taper angle ϕ and material orientation angle θ.

4.4.4. Bending-Transverse Shear Coupling B_{42}

The elastic rigidity B_{42} in Equation (4.9) causes coupling between the bending curvature in y-direction and transverse shear load Q_y. Consider the following situation wherein at a point on the reference surface of a sandwich member, $\kappa^{0}_{yy} > 0$ and $\varepsilon^{0}_{xx} = \varepsilon^{0}_{yy} = \gamma^{0}_{xy} = \kappa^{0}_{xx} = \kappa^{0}_{xy} = \gamma^{c}_{yz} = \gamma^{c}_{xz} = 0$. For reasons explained in Section 4.4.2, the stress state is shown in Figure 4.5. Note that if the tapered sandwich section is antisymmetric, the shear stress τ_{xz}

of top and bottom facings are equal and opposite, therefore $Q_y = 0$. Therefore, $B_{42} = 0$ *for antisymmetric tapered sandwich members.*

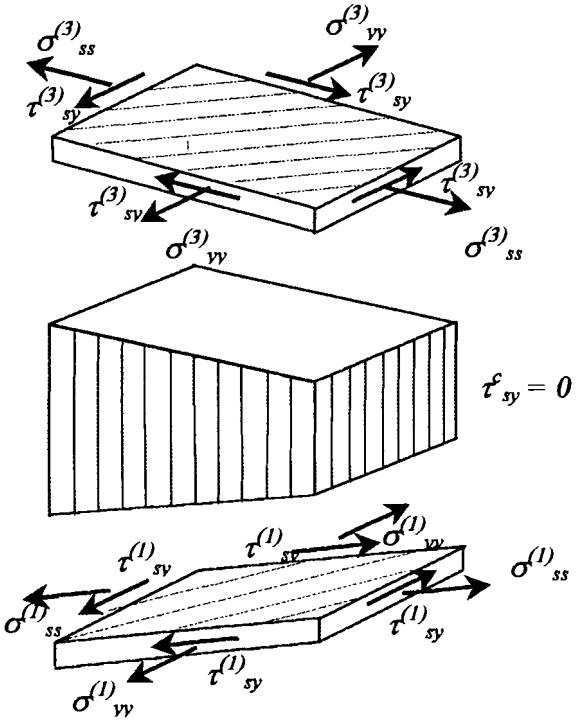

Figure 4.6 Stresses required to produce only γ^0_{xy}

4.4.5. In-plane Shear-Transverse Shear Coupling A_{56}

The elastic rigidity A_{56} in Equation (4.9) causes coupling between in-plane shear strain and transverse shear load Q_x. Consider the following situation wherein at the reference surface strains and curvatures of a sandwich members, $\gamma^0_{xy} > 0$ and $\varepsilon^0_{xx} = \varepsilon^0_{yy} = \kappa^0_{xx} = \kappa^0_{yy} = \kappa^0_{xy} = \gamma^f_{yz} = \gamma^f_{xz} = 0$. The stresses in the facings are shown in Figure 4.6. As before, the stress σ_{ss} has a vertical τ_{xz} component that contributes to Q_x. Note that if the tapered sandwich section is symmetric, the shear stress τ_{xz} of top and bottom facings equal and opposite and therefore $Q_x = 0$. That is, $A_{56} = 0$ *for symmetric sandwich members.* This

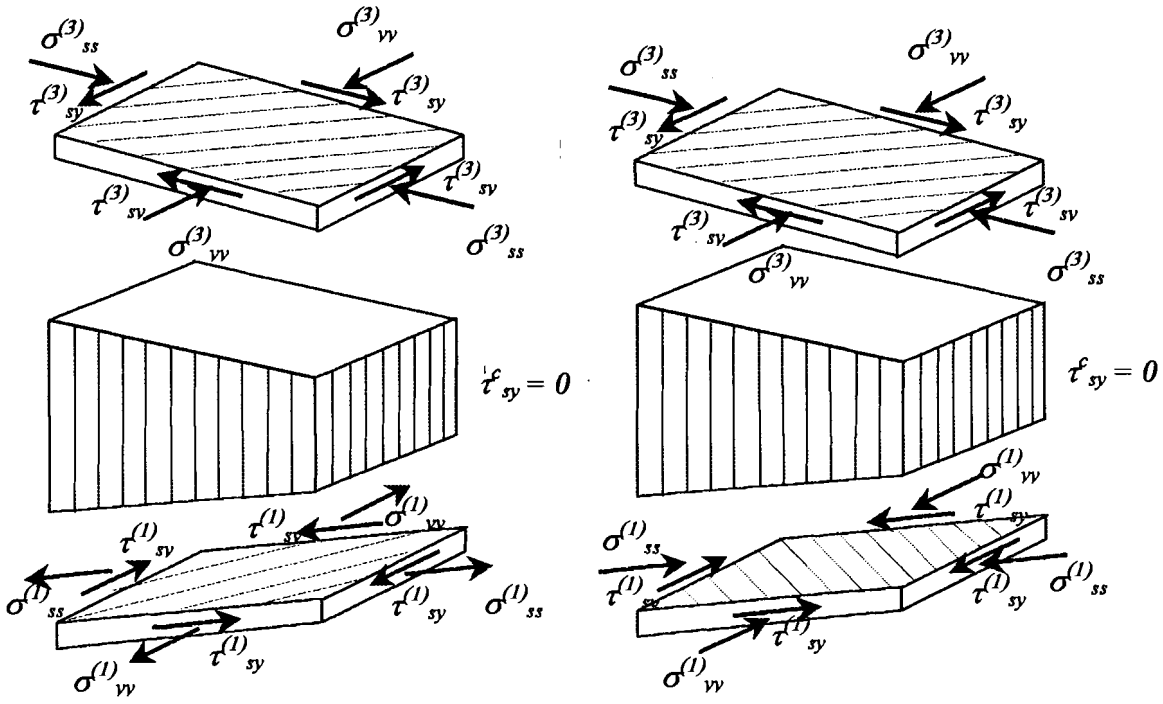

Figure 4.7 Stresses required to produce only κ^{0}_{xy}
(a) symmetric case (b) antisymmetric case

can also be verified directly from Equation (4.10) since $\tilde{Q}_{46}$ is an odd function of the taper angle.

4.4.6. Twisting-Transverse Shear Coupling B_{56}

The elastic rigidity B_{56} in Equation (4.9) causes coupling between the twisting curvature κ^{0}_{xy} and transverse shear load Q_x. Consider the following situation wherein $\kappa^{0}_{xy} > 0$ and $\varepsilon^{0}_{xx} = \varepsilon^{0}_{yy} = \gamma^{0}_{xy} = \kappa^{0}_{xx} = \kappa^{0}_{yy} = \gamma^{f}_{yz} = \gamma^{f}_{xz} = 0$. For this case, the stresses are shown in Figure 4.7. Here too, the vertical component of the shear stress σ_{ss} contributes to Q_x. Note that if the tapered sandwich section is antisymmetric, the shear stress τ_{xz} of the top and bottom facings are equal and opposite. Therefore, $B_{56} = 0$ *for antisymmetric sandwich members.*

Chapter 5

CASE STUDIES AND COMPARISON WITH FINITE ELEMENT ANALYSIS

This section presents the results from the tapered sandwich theory and finite element analysis (FEA). Results for the following three configurations are presented, 1) Aluminum facing symmetric cases, 2) Graphite/epoxy facing symmetric cases and 3) Graphite/epoxy facing unsymmetric cases. It is demonstrated that the tapered sandwich theory developed in the third and fourth chapters accurately represents the response of tapered sandwich sections and gives excellent comparisons with the finite element method. These studies also further expand our understanding of the response of tapered sections to applied loads.

5.1. Finite Element Models

Finite element models of several different configurations were developed to validate the analytical model. For this purpose, linear finite element analyses were run in the ABAQUS/Standard (Hibbitt, Karlsson & Sorensen, Inc., 2002) finite element analysis software package. Although a tapered sandwich composite structure can be modeled as a three-dimensional structure, the number of elements required for the analysis is prohibitively large. This is especially true for sandwich panels with laminated facings with each facing having numerous individual laminae. Since at least three to four elements are required through the thickness of each lamina to accurately compute the stresses, the finite element mesh would be large and impractical for implementation on a

complex structure. Therefore, we have analyzed the tapered sandwich structure using a two-dimensional modeling approach. There are two cases of tapered sandwich structures that can be analyzed using a two-dimensional finite element model,

1) Plane Stress model

The plane stress condition can only be applied when the thickness of the structure along the y-axis is much smaller than the length along the x-axis. The stresses are functions of the planar x- and z-coordinates alone and the out-of-plane normal and shear stress are equal to zero. This case corresponds to the analysis of sandwich beams in our analytical solution.

2) Plane Strain model

The plane strain condition can be applied with the sandwich plate is very long along the y-axis and has a finite dimension along the x-axis. Under these conditions, we can assume that the displacements are functions of x and z coordinates alone. The strains are the functions of planar coordinate alone and the out-of-plane normal and shear strains are equal to zero. This case corresponds to the cylindrical bending of tapered sandwich members.

In order to compare analytical solutions, 2D continuum elements are used for the honeycomb core and facings in the finite element models. In ABAQUS/CAE package, the SOLID SECTION option is used to assign material orientation and thickness of each lamina and several continuum elements are used for each lamina to obtain better accuracy. The elements have two translational degrees of freedom in the x and z-directions. The laminate consists of several laminae that are perfectly bonded together.

Each lamina has four elements through its thickness. The honeycomb core is modeled as homogenous. The microstructure of the honeycomb is neglected and it is modeled as a homogeneous orthotropic continuum. This is a reasonable approach since we are interested in the macroscopic behavior of the tapered sandwich member and we are not concerned about the deformation and stresses in the individual cells of the honeycomb. This simplified modeling technique is widely used for sandwich composite structures since it reduces the computational cost tremendously. When defining the properties of the honeycomb core, we assume that the in-plane Young's moduli are negligible, i.e., E_x and E_y are very small. We do not set them equal to zero, but instead assign very small values to avoid a singularity. In addition, the in-plane shear modulus G_{xy} and Poisson's ratios ν_{xy}, ν_{xz} and ν_{yz} are negligible.

Consider tapered sandwich structures that are simply supported at the edges, such

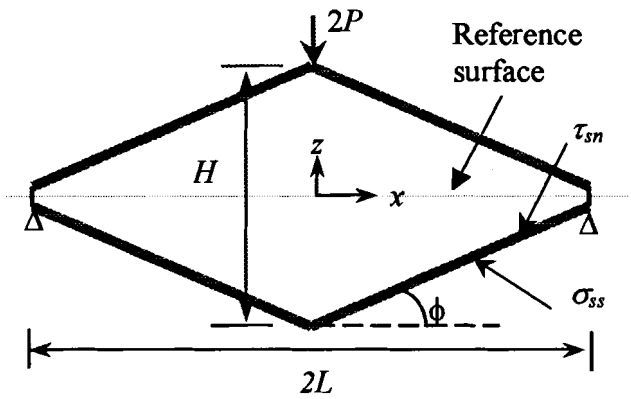

Figure 5.1 Schematic representation of symmetric tapered sandwich beam

as the tapered member depicted in Figure 5.1. Note that the boundary condition is simply supported along the height at the right end. A concentrated load of magnitude $2P$ is applied on the top surface of the top facing at the mid span. All of the tapered members that we analyzed are symmetric about the centerline $x = 0$. Due to the symmetry about the

centerline, only the right half of the member is modeled using FEA and symmetry boundary conditions about the centerline is used. Eight-noded biquadratic plane strain full integration quadrilateral elements (CPE8) are used to obtain accurate FEA results. Several models with the increasing mesh densities were studied to establish convergence. Our studies show that the displacements and stresses gradually converge. We have used sufficient number of elements to obtain satisfactory results.

5.2. Tapered Sandwich Members with Aluminum Facings in Cylindrical Bending

In the cases studied, the facings of the sandwich composite are made of 7075 aluminum of 0.8 mm thickness, whose elastic modulus is 70 GPa, and Poisson's ratio is 0.33. The core is made of aluminum (Hexcel HexWeb^{TM} 5052 4.5-1/8-10) with physical properties given in Table 5.1.

Table 5.1 Honeycomb core properties

Hexcel HexWeb^{TM} 5052 4.5-1/8-10		
	Modulus (MPa)	483
L-direction Plate Shear (G_{xz})	Strength (MPa)	2.3
	Modulus (MPa)	214
W-direction Plate Shear (G_{yz})	Strength (MPa)	1.5

The tapered sandwich member is symmetric about the horizontal mid-surface as shown in Figure 5.1. The facings are of equal thickness and the angle of inclination of the top and bottom facings with respect to the horizontal axis are the same, i.e., $\phi_b = -\phi_t$. The mid-surface is chosen as the reference surface $z = 0$.

Due to the symmetry of the sandwich composite structure about the reference surface, the magnitude of the in-plane normal stress σ_{ss} in the bottom facing is the same as that in the upper facing. Experiments on tapered members have shown that in many cases, the facings delaminate from the core. Therefore we pay close attention to stresses at the interface between the facings and the core. We will compare the following three

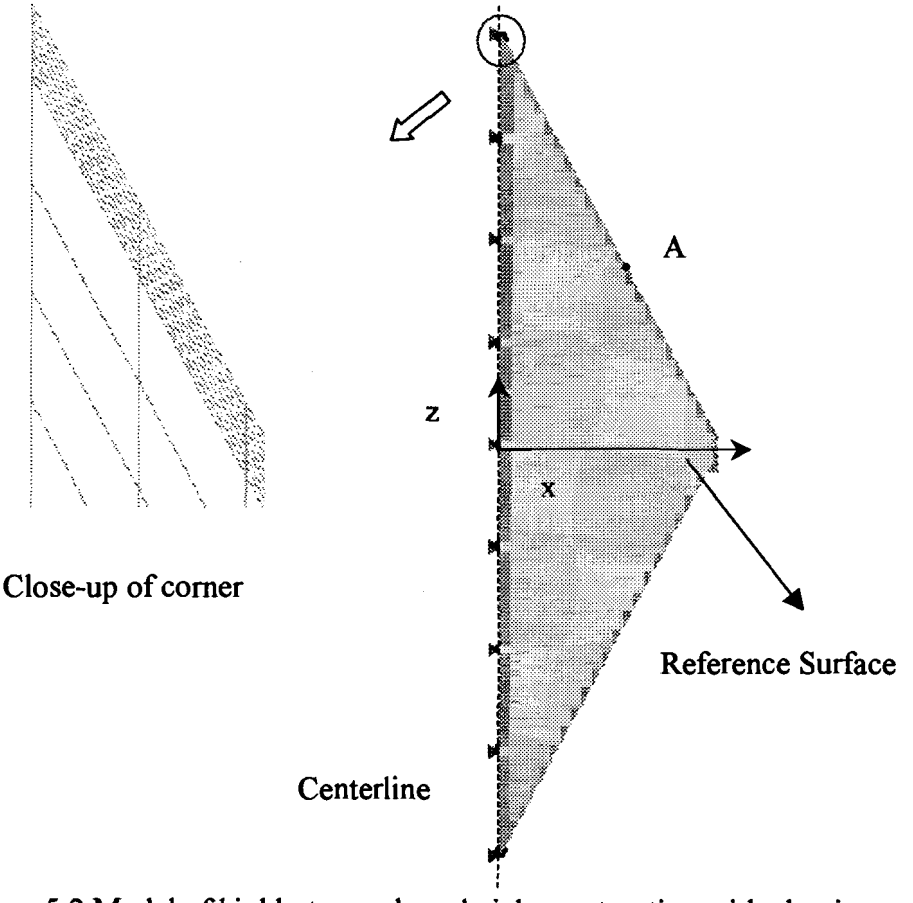

Figure 5.2 Model of highly tapered sandwich construction with aluminum facing (H =1800mm, L = 500 mm, t = 0.8 mm and $\phi = 60^0$)

stress components between the analytical and finite element solutions: 1) extensional stresses on the bottom-most surface of the bottom facing σ_{ss}, 2) transverse shear stress at the interface between the bottom facing and core τ_{sn}, and 3) peeling stresses at the interface between the bottom facing and core σ_{nn}.

5.2.1. Highly Tapered Sandwich Members

In order to validate the analytical model for highly tapered sandwich beams with negative bending rigidity and to understand the influence of the bending-shear elastic coupling on the deformation, we present results for a tapered sandwich construction with taper angle $\phi = 60^0$ which is greater than the critical tapered angle $\phi_{cr} = 54.93^0$. The core is 1800 mm thick at the centerline and the span $2L$ = 1000 mm. The tapered member is simply supported at both ends. A downward concentrated load of $2P$ = 20 KN is placed at a point that is located on the upper surface of the top facing at mid-span.

A finite element mesh consisting of 33,500 8-noded quadratic elements is used to model the tapered member. The stresses of analytical and FEA results are compared at point A which is located at the top surface of the upper facing at $x = L/2$, as illustrated in Figure 5.2. The Deflection is compared at the original of the x-y-z coordinate system. The numerical comparison in Table 5.2 shows that results of our analytical model are in very good agreement with finite element analysis.

Table 5.2 Comparison of the analytical results with FEA at point A (H =1800mm, L = 500 mm, t = 0.8 mm and $\phi = 60^0$)

Variable	Analytical	FEA	Error
σ_{xx}	-1.673 MPa	-1.671 MPa	0.12%
σ_{zz}	-5.019 MPa	-5.026 MPa	0.14%
τ_{xz}	2.898 MPa	2.897 MPa	0.03%
σ_{ss}	-2.208 MPa	-2.210 MPa	0.09%
σ_{ss}	-6.692 MPa	-6.697 MPa	0.07%
ε_{xx}	10.172	10.235	0.62%
ε_{ss}	-85.187	-85.25	0.07%
$U_z(0,0)$	-8.548(10^{-5}) m	-8.509(10^{-5}) m	0.46%

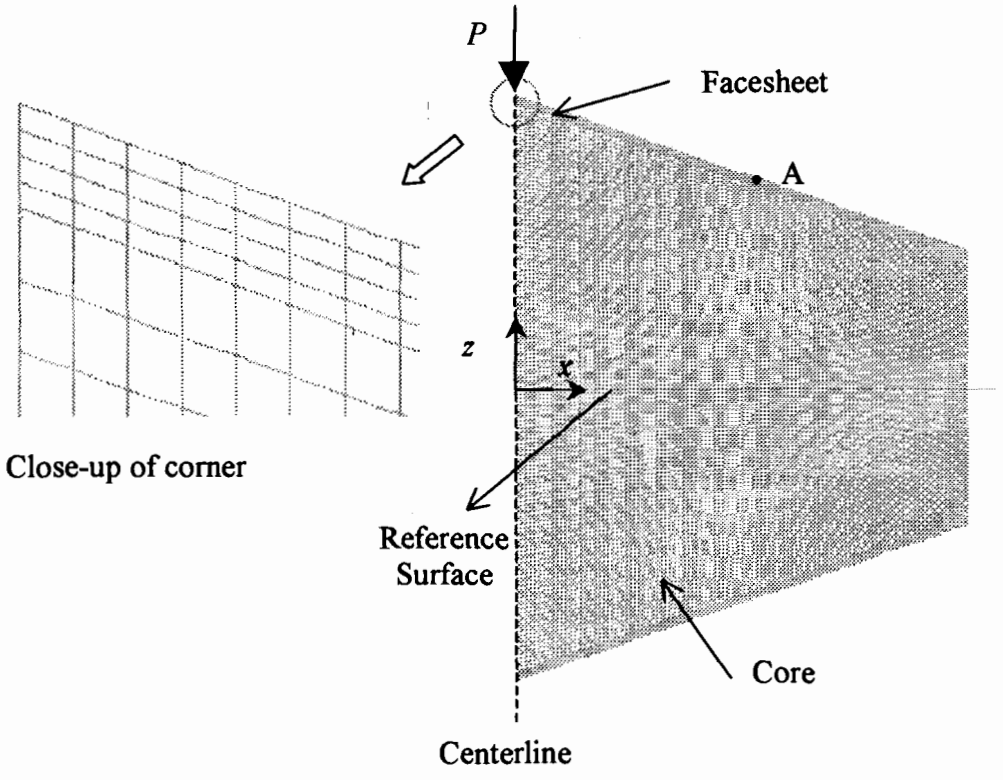

Figure 5.3 Model of tapered sandwich construction with aluminum facings
(H = 60 mm, L = 45 mm, t = 0.8 mm and $\phi = 20^0$)

According to our tapered sandwich theory, the extensional and bending rigidities at x = $L/2$ are A_{11} = -530MPa and D_{11} = -120MPa. The strain ε_{xx} at point A is positive, although the bending moment M_x at that location is negative. As previously discussed in Section 3.7, this behavior is due to the negative bending rigidity D_{11}. However the strain ε_{ss} in the top facing at point A is negative as expected since the bending moment causes a compressive in-plane strain in the upper facing. The normal stress σ_{xx} at point A is also negative as expected although the strain ε_{xx} at point A is positive.

5.2.2. Results for Various Taper Angles

In order to understand the influence of the tapered angles on the deflection and stresses, the tapered angle is varied from 0, 5, 10, 15, 20, 25, 30 and 33.5 degrees while other geometry configurations was kept the same. The span of the tapered member is $2L$

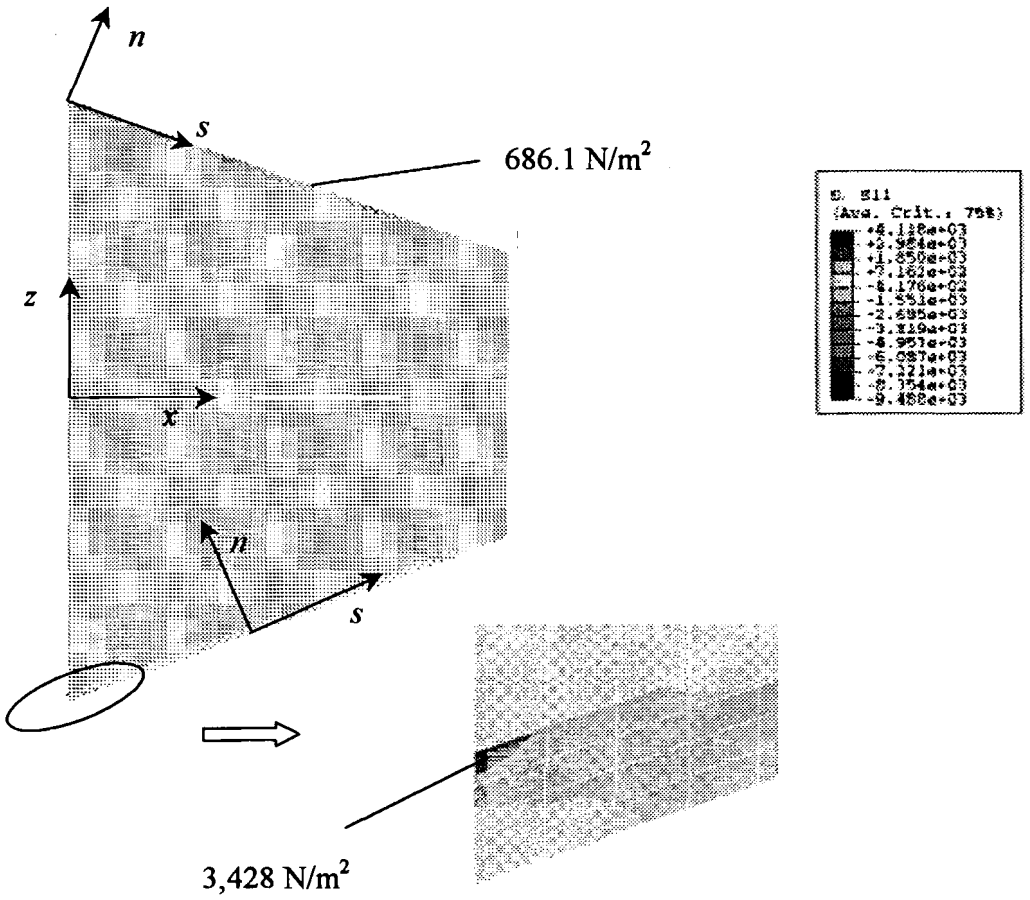

Figure 5.4 Stress distributions of σ_{ss} (H = 60 mm, L = 45 mm, t = 0.8 and $\phi = 20^0$)

=180 mm and the core is 60 mm thick at mid-span. The core thickness at the two ends would depend on the taper angle. The finite element model used in this case is presented in Figure 5.3. The edges are simply supported and a downward concentrated load of $2P$=2 N is placed on the top of the upper facing at mid-span. Totally 10,800 8-noded quadratic elements are used in this model. There are four elements through the thickness of each aluminum facing.

5.2.2.1. Stresses

Extensional stresses on the bottom surface of the bottom facing and transverse shear stresses on the bottom interface between facing and core will be studied in this section. All the stresses are presented in the local *s-y-n* coordinate system. Figure 5.4 shows a contour plot of normal stress in *s*-direction, σ_{ss}. It should be noted that stress σ_{ss}

is in the local coordinate system. For the core, the local coordinate system is the *x-y-z* coordinate system. The peak tensile stress of 4,118 N/m^2, occurs at the mid-span in interface between the upper facing and the core. This stress concentration is due to two factors. The first one is that the concentrated force will stress concentration. Secondly, the abrupt change in the orientation of the facings at mid-span also cause stress variation and it cannot be captured by our simple tapered sandwich theory.

The comparison between the finite element and analytical models is shown in the Figure 5.5 (a,b) for $\phi = 0^0$. In this figure, σ_{ss} is the normal stresses at the bottom surface of the lower facing, and the τ_{sn} is the shear stress at the interface between the bottom facing and core. It clearly demonstrates that analytical and FEA normal stresses are in very good comparison at most points, except at the mid-span. The FEA normal stress σ_{ss} reaches a peak of 1,300 Pa near $x = 0.05L$, probably due to a singularity in the stress field due to the abrupt change in taper angle at mid-span. As to the analytical transverse shear stress τ_{sn} on the interface between the core and bottom facing, it remains constant at 17 Pa along the entire length. There is considerable deviation between the analytical and FEA values of τ_{sn} near the mid-span due to the abrupt change in taper angle.

The axial variation of the longitudinal stress σ_{ss} at the bottom-most surface of the lower facing is depicted in Figure 5.5(c) for $\phi = 15^\circ$. The maximum value of the tensile stress σ_{ss} from the analytical solution is 970 Pa, whereas the finite element solution reaches a peak of 1,400 Pa slightly to the right of mid-span. The transverse shear stresses increases from 11 Pa at $x = 0$ to 20 Pa at $x = L$.

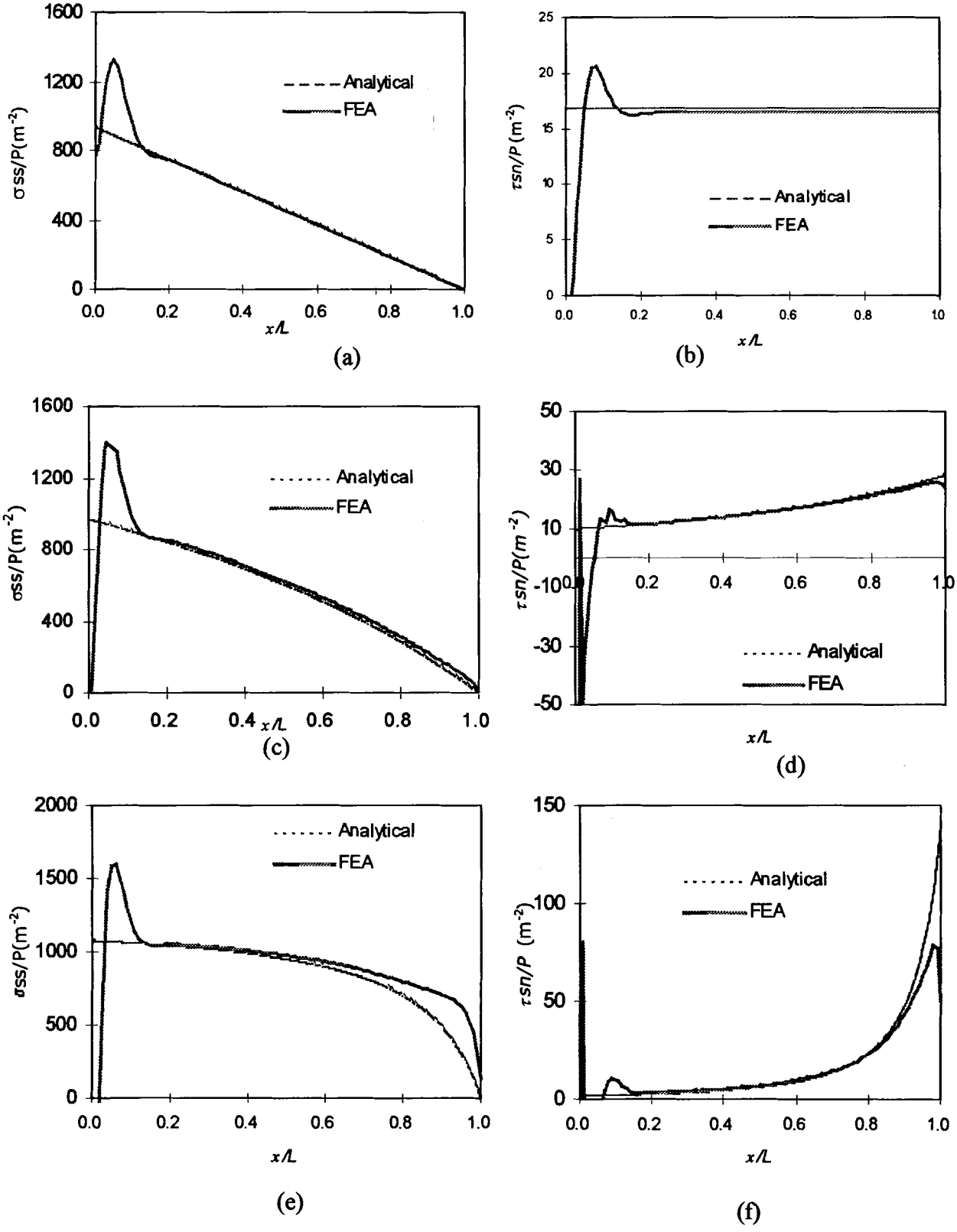

Figure 5.5 Comparison of analytical and FEA (H = 60 mm, L = 45 mm) normal stress at bottom surface of the lower facing, σ_{ss} and shear stress at the interface between bottom facing and core, τ_{sn}, (a,b) $\phi = 0^0$, (c,d) $\phi = 15^0$ and (e,f) $\phi = 30^0$.

For $\phi = 30°$, the core thickness at the right edge is only 8.06 mm compared to 60 mm at the mid-span. Results for this taper angle are given in Figure 5.5 (e) and (f). The normal stress σ_{ss} at the bottom surface remains nearly uniform, except near the right edge where it exhibits a large gradient. The analytical solution deviates from the FEA solution near the right edge for large taper angles. As the taper angle increases, the core thickness at the right edge decreases and the transverse shear stress τ_{sn} increases. Therefore, the plane stress condition $\tau_{sn} = 0$ is a poor assumption for the facings near the right edge for large ϕ. The large shear stress could cause delamination to begin at the interface between the core and facing at the right edge for large taper angles and lead to the debonding of the facings. The delamination of the facings has been observed experimentally by Kuczma and Vizzini (1999).

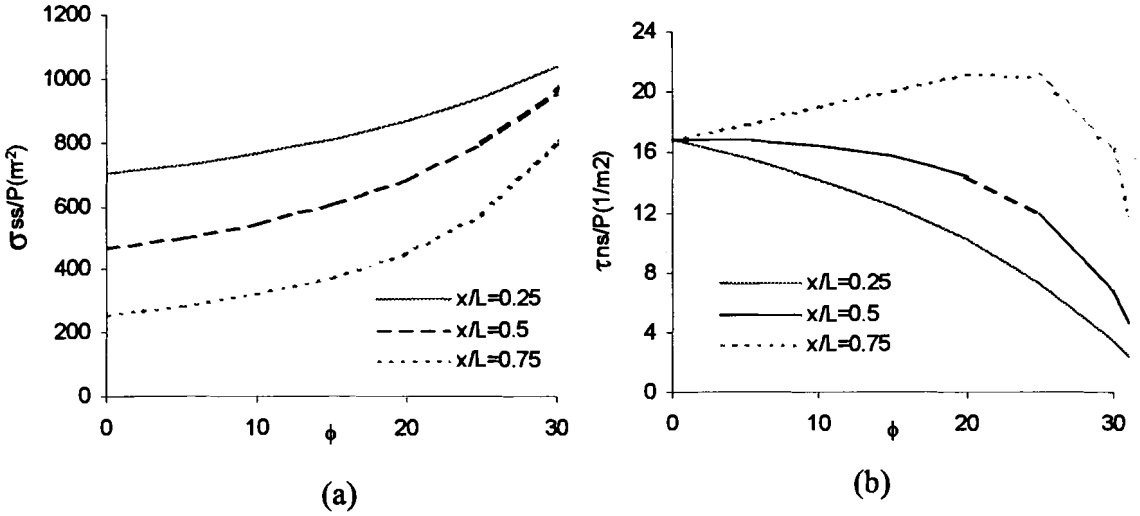

Figure 5.6 Analytical solution of case with (H = 60 mm, L = 45 mm, t = 0.8 mm) a) normal stresses at the bottom surface of the lower facing, σ_{ss} and b) shear stress at the interface between the bottom facing and core, τ_{sn} versus taper angles at three locations

The normal stress σ_{ss} at three different locations on the bottom surface versus the taper angle is depicted in Figure 5.6a. It shows that the normal stress monotonically increases as the taper angle becomes larger. This is because of the decreasing core thickness and increasing participation of the facings in resisting the transverse shear force. The shear stress between the core and bottom facing versus tapered angles is depicted in Figure 5.6b. Interestingly, the interface shear stresses τ_{sn} at $x/L = 0.25$ and 0.5 decreases as the taper angle increases. However τ_{sn} at $x/L = 0.75$ initially increases and reaches a maximum at $\phi = 25^0$ before decreasing.

5.2.2.2. Deflection

The mid-span deflections are investigated as the tapered angle varies from 0^0 to 30^0, as shown in Figure 5.7. It helps us to understand how the taper angle affects the overall stiffness of the structure. It should be noted that the core depth at the mid-span is kept constant as the taper angle is increased. The deflection predicted by the tapered sandwich theory is roughly 5% larger than the FEA solution for small taper angles. Numerical results for the deflection from the analytical solution and FEA are given in Table 5.3. As the taper angle increases, the deflection initially decreases despite the fact that the core depth has decreased at locations other than the mid-span. It should be noted that the defection of a sandwich structure is the sum of the flexural deformation in the facings and the shear deformation in the core. In a tapered sandwich member, the facings participate in resisting the transverse shear force, thereby reducing the transverse shear load in the core. This results in an overall reduction in the transverse shear deformation of the core. The decrease in shear deformation for small taper angles is larger than the

associated increase in flexural deformation. For the parameters used in this study, an

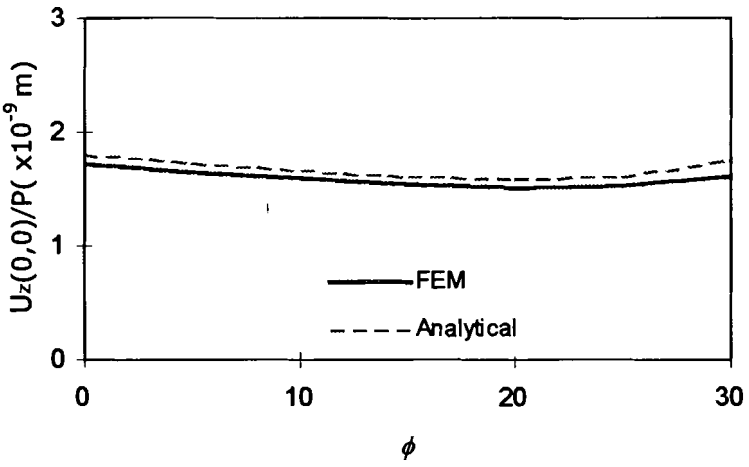

Figure 5.7 Comparison of analytical and FEA deflection for various taper angles ϕ (H = 60 mm, L = 45 mm and t = 0.8mm)

optimum taper angle of approximately 20° exists where the deflections become a minimum. Beyond this taper angle, the deflection starts to increase as a result of the dramatic increase in flexural deformation caused by the significant reduction in the vertical distance between the facings.

Table 5.3 Deflections of mid-span $u_z(0,0)/P$ (10^{-9} m/N)

Angle	Analytical	FEM	Error
0^0	-1.81	-1.72	4.93%
5^0	-1.74	-1.65	4.86%
10^0	-1.67	-1.59	4.78%
15^0	-1.62	-1.54	4.73%
20^0	-1.59	-1.51	4.78%
25^0	-1.61	-1.52	5.26%
30^0	-1.75	-1.61	8.03%

5.3. Symmetric Sandwich Members with Laminated Anisotropic Facings

In the case studied next, the facings of sandwich composite are made of 6 layers graphite/epoxy fiber-reinforced laminae. The sandwich member is symmetric about the mid-surface and the orientation of the fibers in the top and bottom facings are $[0_2/90_2/0_2]$. The material properties of each lamina in the principal material coordinates are shown in Table 5.4. The orthotropic elastic constants shown in Table 5.5 are used to define the material properties in ABAQUS for the 0^0 and 90^0 laminae, respectively. Here D_{ijkl} are the components of the fourth-order elastic tensor. The thickness of each lamina is 0.15 mm and the thickness of the laminated facing is 0.9 mm. The core is made of Hexcel HRP-3/16-5.5 Fiberglass/Phenolic honeycomb core with the elastic properties shown in Table 5.6.

Table 5.4 Facing lamina properties

E1 *(GPa)*	*E2 = E3* *(GPa)*	ν_{23}	$\nu_{13} = \nu_{12}$	G_{23} (GPa)	$G_{12} = G_{31}$ (GPa)	*t* (mm)
155	12.1	0.458	0.248	3.2	4.4	0.15

Table 5.5 Orthotropic material properties by the terms in the elastic stiffness matrix

	D_{1111} (GPa)	D_{1122} (GPa)	D_{2222} (GPa)	D_{1133} (GPa)	D_{2233} (Gpa)	D_{3333} (GPa)	D_{1212} (GPa)	D_{1313} (GPa)	D_{2323} (GPa)
Ply 0	157.8	5.636	15.51	5.636	7.214	15.51	4.4	4.4	3.2
Ply 90	15.51	7.214	15.51	5.636	5.636	157.8	3.2	4.4	4.4

Table 5.6 Honeycomb core properties

Hexcel HRP-3/16-5.5		
L-direction Plate Shear	Modulus (MPa)	131
	Strength (MPa)	3.38
W-direction Plate Shear	Modulus (MPa)	76
	Strength (MPa)	1.83

The geometric configuration of the symmetric tapered sandwich composite beam is depicted in Figure 5.1. The taper angle is varied from 0 to 20 degree. The tapered member is simply supported at both edges, the span is $2L$ = 160 mm, the core depth at mid-span is H = 60 mm and the magnitude of the concentrated load is $2P$ = 2 N. The

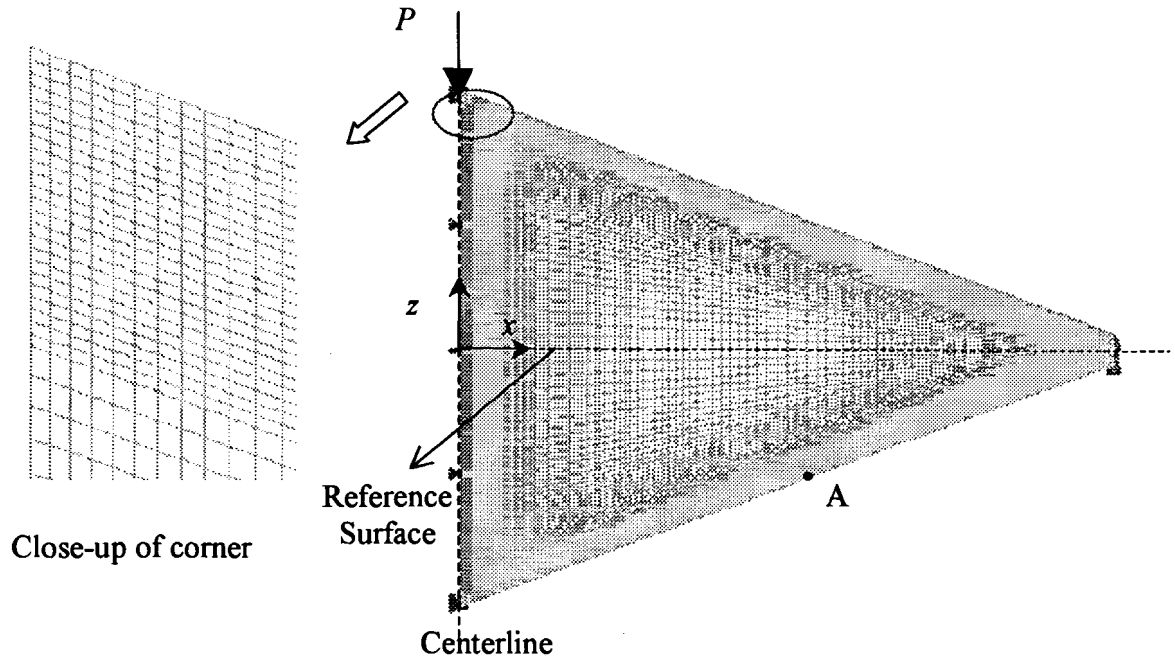

Figure 5.8 Model of tapered sandwich construction with Gr/Ep facings
(H = 60 mm, L = 80 mm, t = 0.9 mm and $\phi = 20^0$)

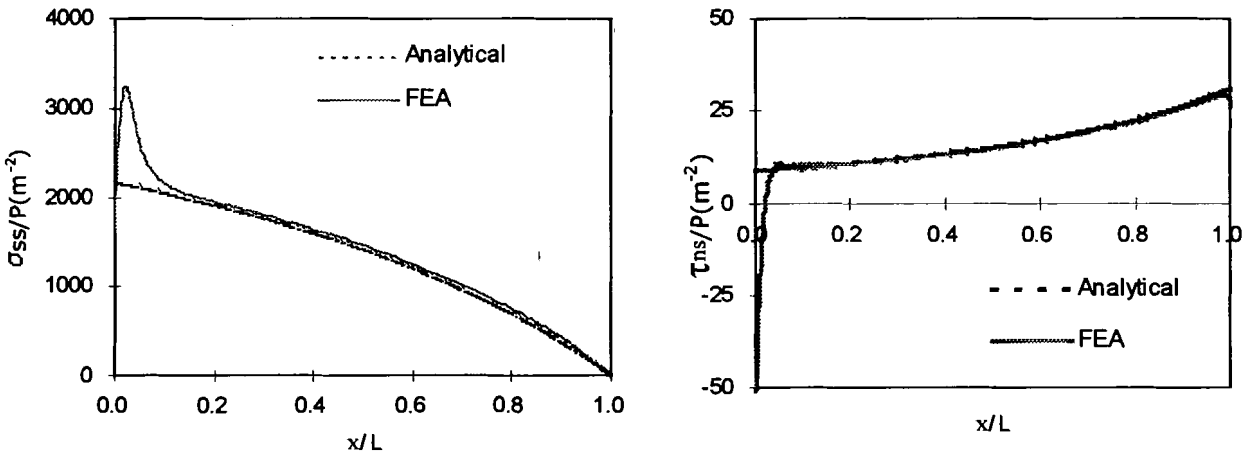

Figure 5.9 Comparison of analytical and FEA (H = 60mm, L = 80mm, t = 0.9mm, ϕ = 10^0) a) normal stresses at the bottom surface of the lower facing, σ_{ss}
b) shear stress at the interface between the bottom facing and core, τ_{sn}.

finite element model contains 29,600 8-noded quadratic elements. The finite element mesh used in this case is presented in Figure 5.8. A total of 24 elements are used through the thickness of each facing, with four elements through the thickness of each lamina.

5.3.1. Stresses

When the tapered angle $\phi = 10^0$, the axial variation of the longitudinal stress σ_{ss} in the facing at the bottom-most surface is depicted in Figure 5.9(a) and the interface shear stress τ_{sn} between the core and bottom facing versus normalized distance is shown in Figure 5.9(b). The maximum value the normal stress σ_{ss} predicted by the analytical solution is approximately 2,200 Pa at the mid-span, while the FE solution reaches a peak value of over 3,000 Pa at $x = 0.1L$.

The analytical value of the transverse shear stresses at the interface between the core and the bottom facing increase from approximately 10 Pa at $x = 0$ to over 30 Pa at $x = L$.

However, the FEA solution exhibits a very large negative shear stresses at $x = 0$, which can be attributed to the discontinuity in the taper angle at mid-span.

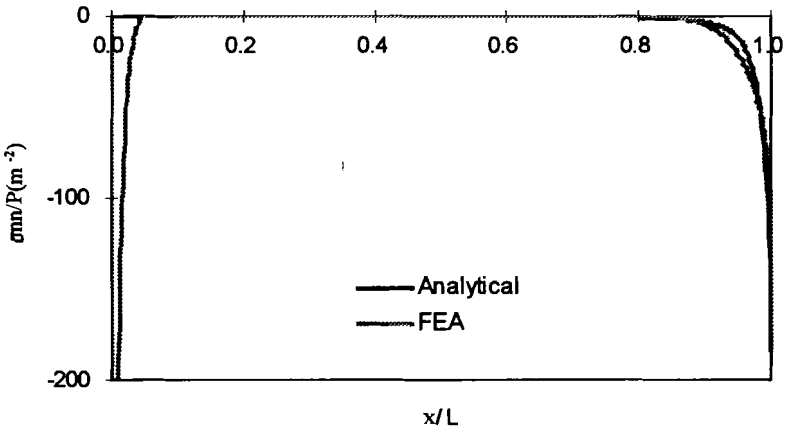

Figure 5.10 Comparison of analytical and FEA: normal stresses at the interface between the bottom facing and core, σ_{nn}. (H = 60mm, L = 80mm, $\phi = 20^0$)

The transverse normal stress at the interface between the bottom facing and core, σ_{nn}, versus normalized distance is depicted in Figure 5.10. It shows that the transverse normal stress is localized at the edges and it is negligible everywhere else. The large transverse normal stress near the edge could cause the facing to peel off from the core, especially at the interface between the top facing and the core, where it is tensile.

The axial variations of the longitudinal stress σ_{ss} and the shear stress τ_{sn} are depicted in Figure 5.11 (a) and (b), respectively for taper angle $\phi = 20^0$. Note that core depth at $x = L$ is only 8.06 mm. The normal stress σ_{ss} is approximately 2,200 Pa at $x = 0$ and remains constant along the span except near the edges. It drops dramatically at $x = 0.8\,L$ to 0 Pa at the right edge. There is considerable deviation between the analytical and FEA values of the normal stress σ_{ss} near the edges. A reason for the discrepancy is that the plane stress assumption for the facing laminae is not valid near the right edge due to

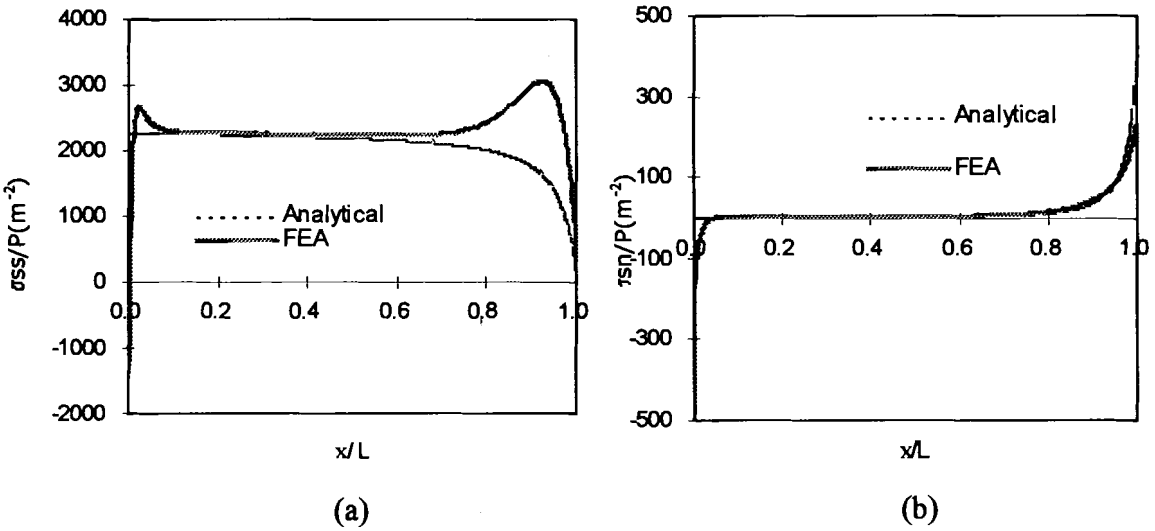

Figure 5.11 Comparison of analytical and FEA(H = 60mm, L = 80mm, $\phi = 20^0$)
a) normal stresses at the bottom surface of the lower facing, σ_{ss}
b) shear stress at the interface between the bottom facing and core, τ_{sn}.

the large interfacial shear stress τ_{sn}. The interface shear stress remains very small for points between $x = 0$ to $x = 0.8\ L$, and increases dramatically after that to reach 500 Pa at the right edge. Comparing Figure 5.9b and Fig 5.11b, we see that the transverse shear stress at the interface for $\phi = 20^\circ$ is more than an order of magnitude larger than that for $\phi = 10^\circ$.

5.3.2. Deflection

The mid-span deflection versus the taper angle is shown in Figure 5.12 as the taper angle varies from 0^0 to 20^0. As the taper angle increases from 0^0 to 20^0, the analytical solution predicts that the deflection decreases due to the participation of the facings in resisting transverse shear load. However, the FEA predicts that beyond 20^0, the reduction in cross-sectional height leads to a dramatic increase in the deflection. The inability of the analytical solution to capture the increase in deformation can be attributed to the complex state of stress near the ends where the core depth is very small. Overall,

deflection from the analytical solution is about 5 % lower than the FEA solution for small taper angles.

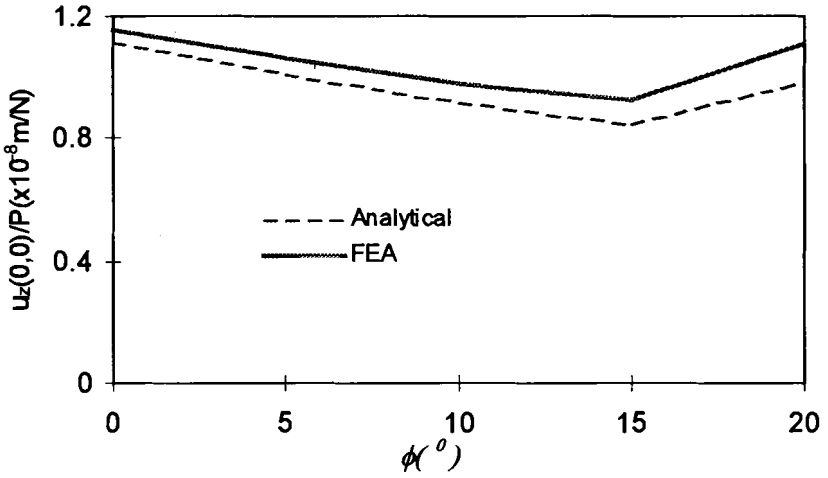

Figure 5.12 Comparison of analytical and FEA deflection for various taper angles ϕ (H = 60 mm, L = 80 mm and t = 0.9 mm)

5.4. Graphite/Epoxy Facing Unsymmetric Cases

5.4.1. Various Taper Angles

In practical applications, the unsymmetric tapered sandwich members are more often used than symmetric ones, such as the case shown in Figure 5.13. In order to understand the behavior of tapered unsymmetric cases, the inclination of the bottom facing $\phi = \phi_b$ is varied from 0, 15, 30 and 45 degree while the top facing is kept horizontal. The top surface of the honeycomb core is chosen as the reference surface z = 0. The facings are composed of 6 layers of graphite/epoxy laminate fiber-reinforced composite with fiber orientations $[0_2/90_2/0_2]$. The elastic properties of the 0^0 and 90^0

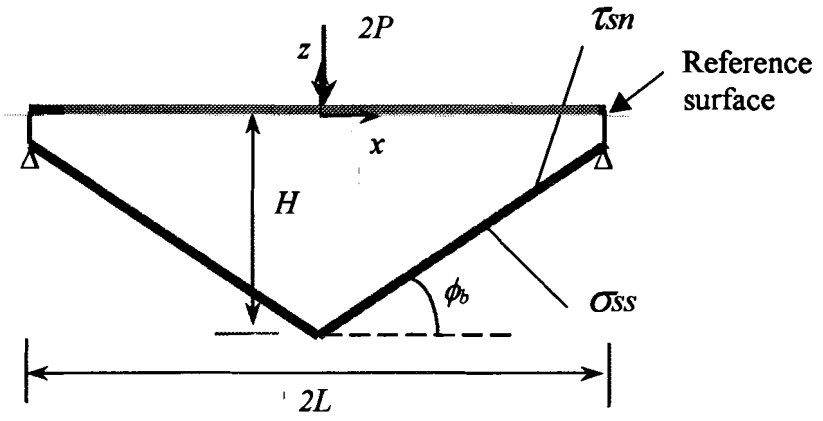

Figure 5.13 Schematic representation of unsymmetric tapered sandwich beam

laminae are given in Table 5.5. The thickness of each lamina is 0.15 mm and the core is made of Hexcel HRP-3/16-5.5 Fiberglass/Phenolic honeycomb core with elastic properties shown in Table 5.6. The span is $2L$ = 160 mm long and the core depth at mid-span is H = 85 mm. The finite element model used in this case is presented in Figure 5.14. The finite element mesh consists of 29,600 8-noded quadratic elements with four elements through the thickness of each lamina.

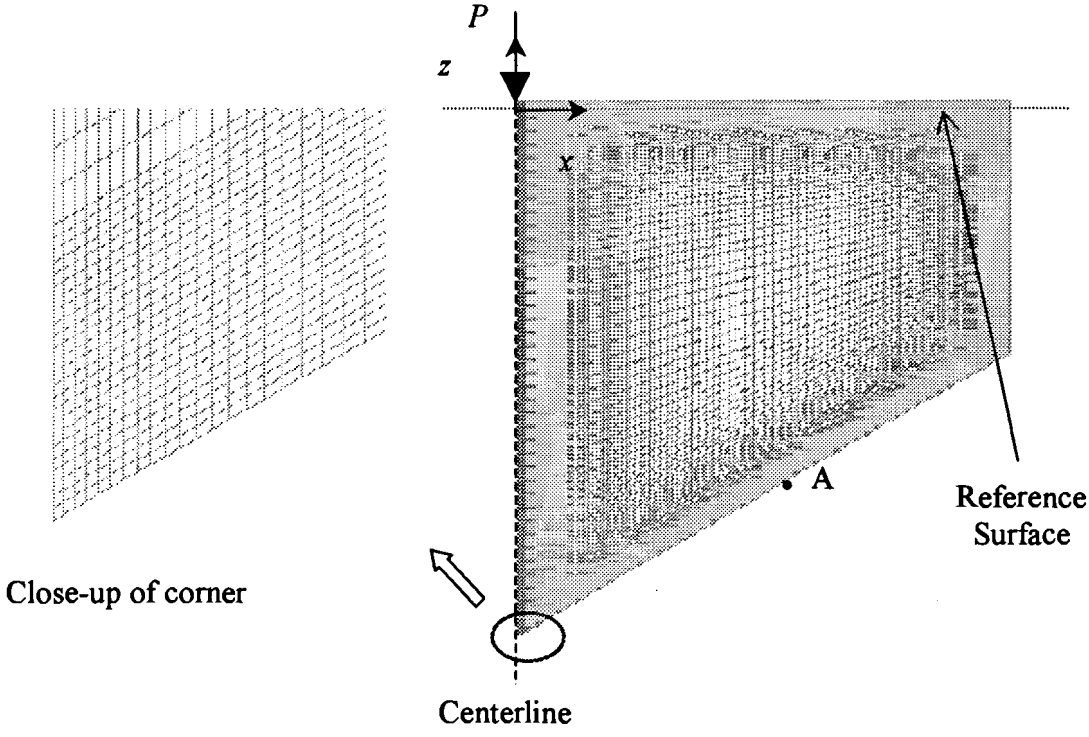

Figure 5.14 Model of tapered sandwich construction with aluminum facings ,
(H = 85 mm, L = 80 mm, t = 0.9 mm, P = 1N and $\phi = 30^0$)

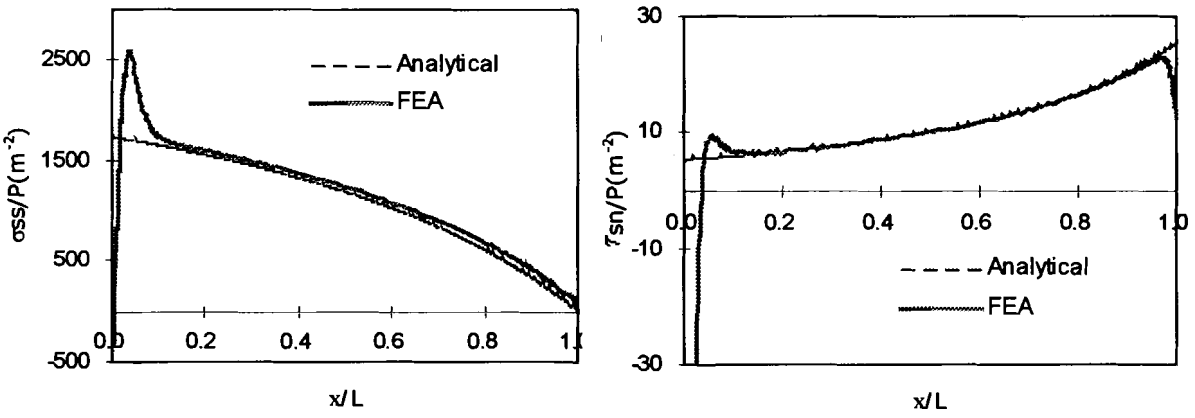

(a) (b)

Figure 5.15 Comparison of analytical and FEA a) normal stresses at the bottom surface of the lower facing, σ_{ss} b) shear stress at the interface between the bottom facing and core, τ_{sn}. ($H = 85$ mm, $L = 80$ mm, $P = 1$N and $\phi = 30^0$)

Extensional stresses on the bottom surface and transverse shear stresses on the interface between the bottom facing and core are reported in this section. Note that all the stresses are presented in the local *s-y-n* coordinate system. The axial variations of the stresses are depicted in Figure 5.15 for $\phi_b = 30^0$. The trends are qualitatively similar to the symmetric tapered sandwich members discussed earlier.

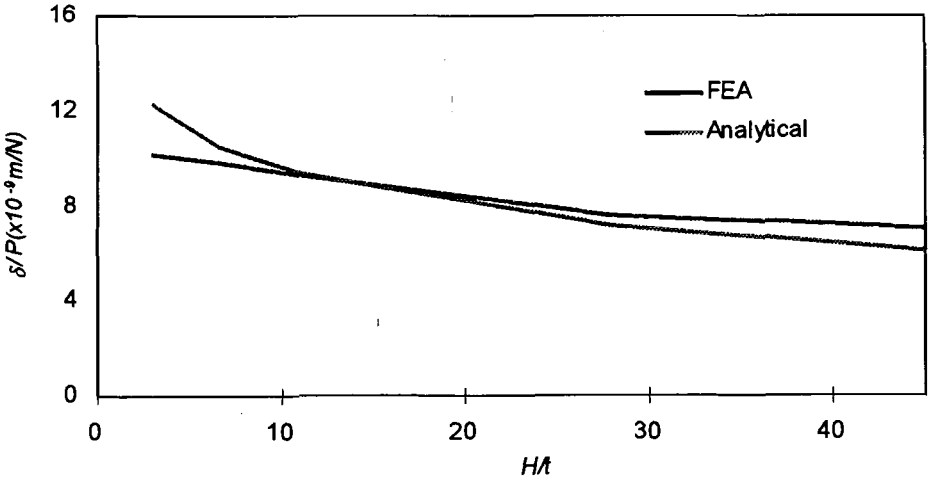

Figure 5.16 Comparison of analytical and FEA deflection for core thickness (L = 80 mm, t = 0.9 mm, and $\phi = 30^0$ mm)

5.4.2. Core Thickness

In order to understand effects of the core thickness, cases with L = 80 mm and $\phi = 30^0$ are studied. The ratio of thickness of core at the right end to facing thickness is varied from 3 to 50.

The deflection comparison of FEA and analytical solution is shown in Figure 5.16. The deflection decreases dramatically as the core becomes thicker. The analytical solution overestimates the deflection when the core is very thin.

The analytical solutions predict that when the core depth at the right end is small, the shear stress and peeling stress between the core and facing are large, as shown in Figure 5.17. As the core becomes thicker, the shear stress and peeling stress drop dramatically. This is also the reason why the failures always happen to the cross section where the core is very thin. Note that the numbers in the legend in Figure 5.17 represent the ratio of thickness of core at the right end to facing thickness.

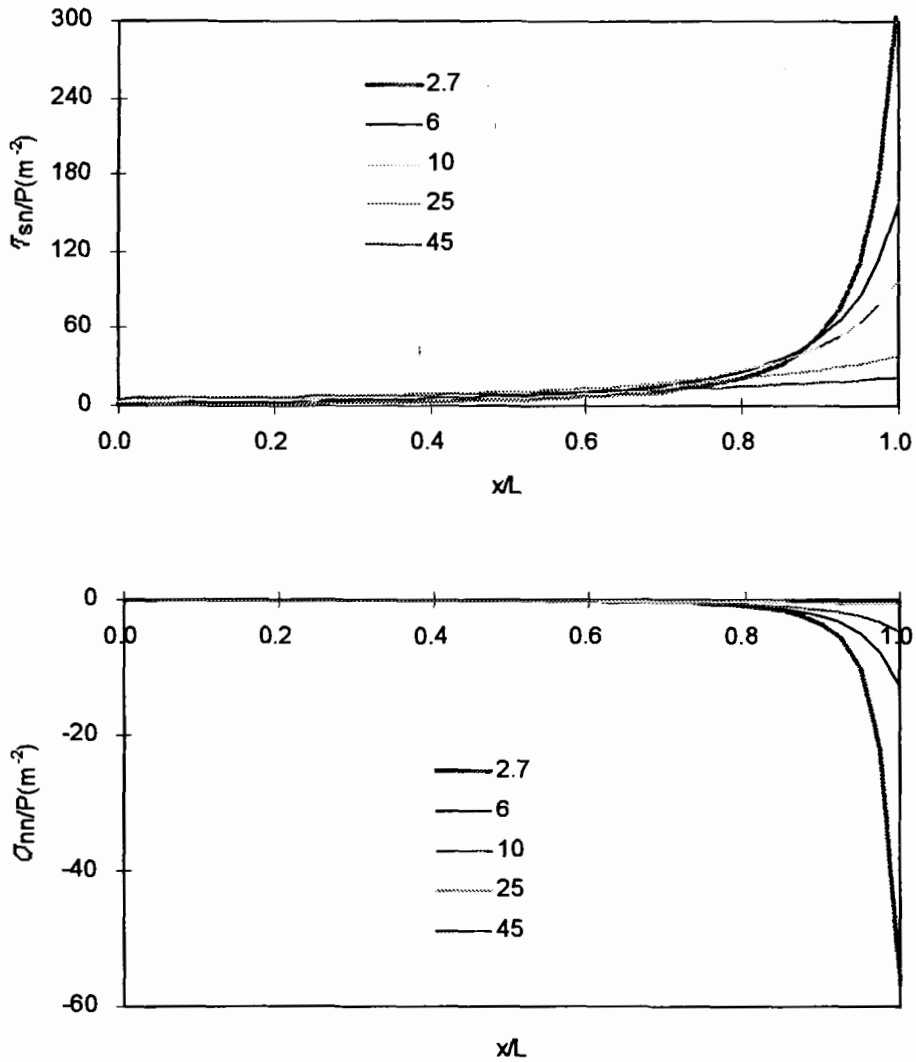

Figure 5.17 Shear stress and peeling Stress between core and facing
(H = 85 mm, L = 80 mm and $\phi = 30^0$)

5.4.3. Core Materials

In order to understand effects of the core material, cases with H = 85 mm, L = 80 mm and $\phi = 30^0$ are studied. Various core materials are selected, as shown in Table 5.7.

The deflection decreases as the shear stiffness of the cores increases, as shown in Figure 5.18. Comparison between FEA and analytical solution is very good.

Table 5.7 Core material properties

	Compression		Plate shear			
			L direction		W direction	
	ksi	MPa	ksi	MPa	ksi	MPa
HRP – 3/8 – 2.2	13	90	6	41	3	21
HRP – 3/8 – 3.2	38	262	11	76	5	34
HRP – 3/16 – 4.0	57	393	13	90	6.5	45
HRP – 3/16 – 5.5	95	655	19	131	11	76
HRP – 3/16 – 7.0	136	938	30	207	14	97
HRP – 3/16 – 12.0	260	1793	44	303	28	193

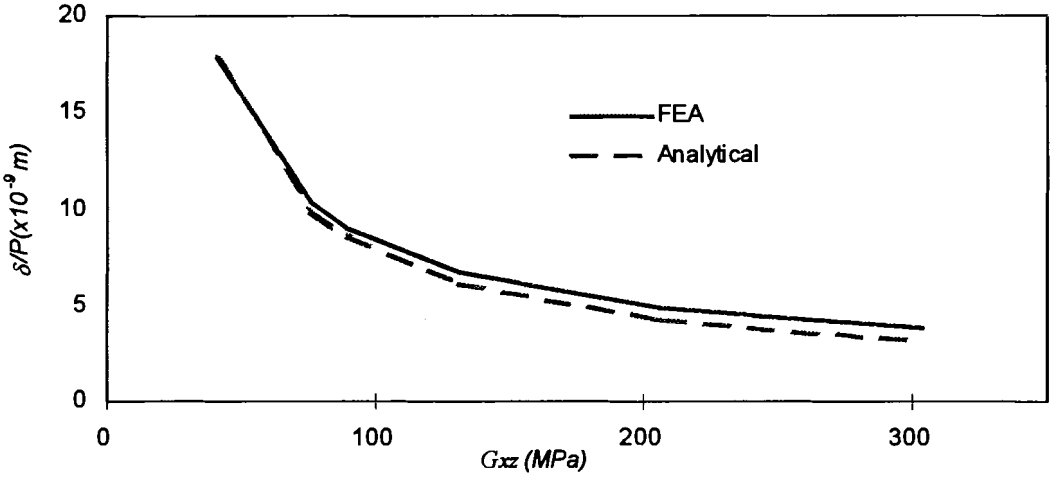

Figure 5.18 Comparison of analytical and FEA deflection for various core materials (H = 60 mm, L = 80 mm and $\phi = 30^0$ mm)

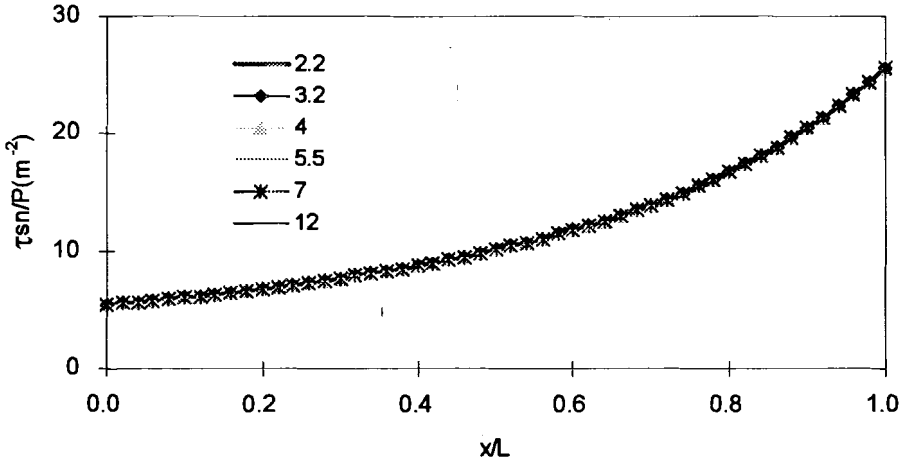

Figure 5.19 Analytical solution of shear stress for various core materials (H = 60 mm, L = 80 mm and ϕ = 30^0 mm)

The shear stress between the core and facing is shown in Figure 5.19. The shear stresses are the same for different core shear stiffnesses. Therefore, the core material has no influence on the shear stress at the interface between the core and facing.

5.4.4. Three-dimensional Continuum Finite Element Model

In order to verify stress distribution of the sandwich construction with the angle-ply laminate in a state of plane stress condition in the y-direction, a three-dimensional model was built, as shown in Figure 5.20. The top and bottom facings are made of six-layer [45^0/-45^0/30^0/-30^0/45^0/-45^0] and [-45^0/45^0/-30^0/30^0/-45^0/45^0] Gr/Ep laminates, respectively. The top and bottom facings are symmetric. The FE model contains 28,160 20-node quadratic hexahedral elements, which reaches the maximum capability of the workstation used for the analysis. Since the sandwich construction is relatively thin, a state of plane stress in y-direction is assumed for the analytical model. The stressed at location A and B would be compared with analytical solutions, as denoted in Table 5.8. Note that point A lies at the bottom surface on the lower facing and point B lies at the interface between the bottom facing and core when $x = L/2$.

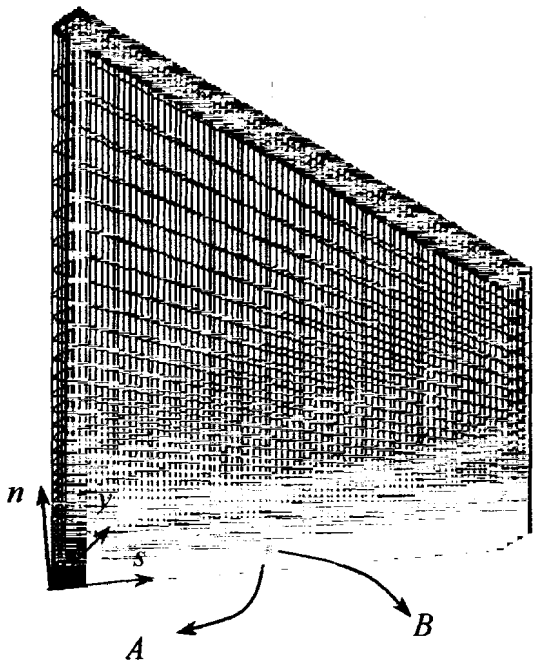

Figure 5.20 3D Continuum model of tapered sandwich construction with angle ply laminate facings ($H = 85$ mm, $L = 80$ mm, $W = 5$ mm and $\phi = 30^0$)

Table 5.8 Comparison of FEA and analytical solutions

	Location A			Location B		
	FEA	Analytical	Error	FEA	Analytical	Error
σ_{ss}	366.0	340.0	7.1%	304.7	326.5	7.2%
σ_{yy}	-145.0	-143.9	0.8%	-166.2	-141.3	15.0%
τ_{sy}	85.2	80.3	5.8%	-54.3	-77.1	42.1%

Results demonstrated in Table 5.8 show that the FEA and analytical solutions match fairly well at the Point A. However there is some error for the shear stress τ_{sy} at the point B. There are two reasons which can contribute to this error. First, the FE model is three-dimensional whereas the analytical model is one-dimensional. Secondly, the three-

dimensional FE model needs meshes along the y direction, therefore the mesh density on x-z plane is much sparser than the two-dimensional FE models discussed earlier.

Chapter 6

SUMMARY AND CONCLUSIONS

In this thesis, we have developed a tapered sandwich theory in which the force and moment resultants are related to the reference surface strains and curvatures through the familiar [A], [B] and [D] matrices. Since the analysis of tapered sandwich panels could be cast in this standard notation by our formulation, computer codes that have been developed for the analysis and design of composite structures can be modified to incorporate our taper sandwich theory. Our formulation reduces the dimensionality of the analysis and therefore simplifies the analysis of complex sandwich structures.

We also have systematically derived a total of 12 elastic stiffnesses that couple the force and moment resultants to the transverse shear deformation. Six of the twelve elastic couplings are due to the tapered sandwich construction itself, irrespective of whether the facings are isotropic or anisotropic, whereas the remaining six elastic couplings are present only for anisotropic laminated facings. Their influence on the behavior of tapered sandwich beams of the stiffnesses is investigated. It is shown that the extension and bending stiffness could be negative at large taper angles.

The deflection of a symmetric simply supported member initially decreases for the increasing taper angle and there is an optimum taper angle where the deflection is a minimum. This decrease in deformation with increasing taper angle is due to the participation of the facings in resisting transverse shear loads.

Results from the tapered sandwich theory show good comparison with finite element models for several case studies. The deflections are overestimated by the theory.

This is because the facing transverse shear stiffnesses G_{13} and G_{23} have been neglected. The error could also be caused by the concentrated point load which leads to thickness distention of the sandwich structure. While we have compared the analytical deflection to the transverse displacement at the center of the structure, better results could have been obtained for other locations.

REFERENCES

ABAQUS Online Documents, 2002.

Allen, H. G., 1969, *Analysis and Design of Structural Sandwich Panels*, Pergamon Press, Oxford.

Bijlaard, P. P., 1951, Analysis of Elastic and Plastic Stability of Sandwich Plates by Method of Split Rigidities, *Journal of the Aeronautical Sciences.*

Bitzer, T. N., 1992, Recent Honeycomb Core Developments, *Proceedings of the Second International Conference on Sandwich Construction,* Editors, D. Weissman Berman and K-A. Olsson, EMAS Publications, Unite Kingdom, pp. 555-563.

Burton, W. S., and Noor, A. K., 1995, Assessment of Computational Models for Sandwich Panels and Shells, *Computer Methods in Applied Mechanics and Engineering*, Vol. 124, pp. 125-151.

Caccese, V., and Gauthier, R., 1998a, Strength and Stability of Composite Sandwich Panels for the NASA X-38, *Report to MSTF-NASA Space Grant under Grant No. MSTF 96-48*, Department of Mechanical Engineering, University of Maine, Orono, ME 04469, 132 pp.

Caccese, V., and Gauthier, R., 1998b, Strength of the X-38 Crew Return Vehicle Aeroshell Composite Panels, *Report to NASA JSC under Grant No. NGT 9-7*, Department of Mechanical Engineering, University of Maine, Orono, ME 04469, 73 pp.

Caccese, V., and Malm, C., 1999, Flexure, Compression and Tension Testing of Bolted Composite Sandwich Panels in Support of LMMSS X-38 V201 Panel #13 Subcomponent test Program, *Report to Lockheed Martin Michoud Space Systems Report No. C-9901*, Department of Mechanical Engineering, University of Maine, Orono, ME 04469, 129 pp.

Davies, J. M., 1997, Design Criteria for Sandwich Panels for Building Construction, *Proceedings of the ASME Aerospace Division, Structures and Materials Committee,* ASME-AD-Vol. 55, New York, pp. 273-284.

Erickson, W. S., 1956, Supplement of Effects of Shear Deformation in the Core of a Flat Rectangular Sandwich Panel, *Forest Products Laboratory Report 1583-c.*

Eringen, A. C., 1952, Bending and Buckling of Rectangular Sandwich Plates, *Proceedings of the First U.S. National Congress of Applied Mechanics,* ASME, pp. 381-390.

Feichtinger, K. A., 1988, Test Methods and Performance of Structural Core Materials – 1 Static Properties, *4th Annual ASM International/Engineering Society of Detroit – Advanced Composites Conference/Exposition.*

Flugge, W., 1952, The Optimum Problem of Sandwich Plate, *Journal of Applied Mechanics,* Vol. 19, No. 1, pp. 104-108.

Gibson, R. F., 1994, *Principles of Composite Material Mechanics,* McGraw-Hill, New York.

Ha, K. H., 1989, Finite Element and Sandwich Construction: A Critical Review, *Sandwich Constructions– Proceedings of the First International Conference on Sandwich Construction,* Stockholm, Sweden, Editors, K-A. Olsson and R.P. Richard, EMAS Publications, United Kingdom, pp. 69-84.

Herakovich, C. T., 1997, *Mechanics of Fibrous Composites,* John Wiley & Sons, New York.

Hoff, N. J., 1950, Bending and Buckling of Rectangular Sandwich Plates, *NACA Technical Note 2225.*

Huang, S. N., and Alspaugh, D. W., 1974, Minimum Weight Sandwich Beam Design, *AIAA Journal,* Vol.12, pp. 1617-1618.

Hyer, M. W., 1998, *Stress Analysis of Fiber-Reinforced Composite Materials*, McGraw-Hill, New York.

Jones, R. M., 1998, *Mechanics of Composite Materials*, 2 ed., Taylor & Francis Inc., Philadelphia, PA.

Karbhari, V. M., 1997, Application of Composite Materials to the Renewal of Twenty-first Century Infrastructure, *Proceedings of the Eleventh International Conference on Composite Materials*, Gold Cost, Australian Composite Structures Society, Melbourne, Australia.

Kuczma, S. K., and Vizzini, A. J., 1999, Failure of Sandwich to Laminate Tapered Composite Structures, *AIAA Journal*, Vol. 37, pp. 227-231.

Libove, C., and Batdorf, S. B., 1948, A General Small Deflection Theory for Sandwich Plates, *NACA Report 899*, Washington, D.C.

Libove, C., and Lu, C. H., 1989, Beam-like Bending of Variable-Thickness Sandwich Plates, *AIAA Journal*, Vol. 27, pp. 500-507.

Llorente, S., 1990, Honeycomb Sandwich Primary Structure Applications on the Boeing Model 360 Helicopter, *Proceedings of the 22nd International SAMPE Technical Conference*, Vol. 22, Boston, MA, pp. 1051-1069.

Lu, C. H., 1994, Bending of Anisotropic Sandwich Beams of Variable Thickness, *Journal of Thermoplastic Composite Materials*, Vol. 7, pp. 364-374.

Lu, C. H., and Libove, C., 1991, Beamlike Harmonic Vibration of Variable-Thickness Sandwich Plates, *AIAA Journal*, Vol. 29, pp. 299-305.

Marguerre, K., 1944, *The Optimum Buckling Load of Flexibly Supported Plate Composed of Two Sheets Joined by a Light Weight Filler, When Under Longitudinal Compression*, Deutsche Vierteljahrsschrist fur Literalurwissenschaft und Giests Geschiechte, D.V.L, p.5.

Noor, A. K., Burton, W. S., and Bert, C. W., 1996, Computational Models for Sandwich Panels and Shells, *Applied Mechanics Reviews*, Vol. 49, No.3, pp. 155-199.

Paydar, N., and Libove, C., 1986, Stress Analysis of Sandwich Plates with Unidirectional Thickness Variation, *Journal of Applied Mechanics*, Vol. 53, pp. 609-613.

Paydar, N., and Libove, C., 1988, Bending of Sandwich Plates of Variable Thickness, *Journal of Applied Mechanics*, Vol. 55, pp. 419-424.

Peled, D., and Frostig, Y., 1994, High-Order Bending of Sandwich Beams with Transverse Flexible Core and Nonparallel Skins, *ASCE Journal of Engineering Mechanics*, Vol. 120, pp. 1255-1269.

Plantema, F. J., 1966, *Sandwich Construction: The Bending and Buckling of Sandwich Beams, Plates and Shells*, John Wiley & Sons, New York.

Reddy, J. N., 1997, *Mechanics of Laminated Composite Plates*, CRC Press, Boca Raton, FL.

Vinson, J. R., 1999, *The Behavior of Sandwich Structures of Isotropic and Composite Materials*, Technomic Publishing Company, Lancaster, PA.

Whitney, J. M., 1987, *Structural Analysis of Laminated Anisotropic Plates*, Technomic Publishing Company, Lancaster, PA.

APPENDIX

MATHCAD Program

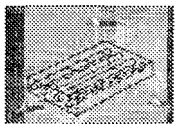

Simplified Formulation

Number of layers Nb at the bottom of Core

$Nb := 6$

Number of layers Nt on the top of Core

$Nt := 6$

Tapered angle of bottom facesheet

$\phi b := 10 \cdot deg$

Tapered angle of top facesheet

$\phi t := -\phi b$

Thickness of each layer

$h := 0.15 \cdot 10^{-3}$

Thickness of the Core

$hc := 60 \cdot 10^{-3}$

Length of the composite beam

$L := 80 \cdot 10^{-3}$

Material properties of each layer

$E1 := 155 \cdot 10^{9}$ $E2 := 12.1 \cdot 10^{9}$ $E3 := E2$

$\nu 23 := 0.458$ $\nu 12 := 0.248$ $\nu 13 := \nu 12$

$G12 := 4.4 \cdot 10^{9}$ $G23 := 3.2 \cdot 10^{9}$ $G31 := 4.4 \cdot 10^{9}$

Material properties of the core

$Gc13 := 131 \cdot 10^{6}$ $Gc23 := 76 \cdot 10^{6}$

Lamina fiber orientations in degrees from bottom to top,

$\theta := (0 \ 0 \ 90 \ 90 \ 0 \ 0 \ 0 \ 0 \ 0 \ 0 \ 90 \ 90 \ 0 \ 0)^{T} \cdot deg$

Location of the top and bottom surfaces of the core at the left edge

$tcTop := 30 \cdot 10^{-3}$

$tcBottom := 30 \cdot 10^{-3}$

The applied loads for plane strain case

$P := 1$ $Mx(x) := -P \cdot (L - x)$

$$Qx(x) := \frac{d}{dx} Mx(x)$$

$Nxy(x) := 0$ $\quad Qy(x) := 0$ $\quad \kappa 0y(x) := 0$

Pre-processing

Reorder the Lamina fiber orientation in degree

$\theta := \text{augment}(0, \theta^T)^T$ $\quad \theta^T =$

	0	1	2	3	4	5	6	7	8	9
0	0	0	0	0	0	0	0	0	0	0

deg

Total Number of layers

$N := Nb + Nt + 1$

$Nc := Nb + 1$ $\quad N = 13$ $\quad Nc = 7$

Location of the top surface, the interfaces between adjoining layers and the bottom surface

$$H := \frac{h \cdot Nb}{\cos(\phi b)} + hc + \frac{h \cdot Nt}{\cos(\phi t)} \qquad H = 0.0618$$

Total thickness on the left end

$$Z(n,x) := \begin{cases} \left[-tcBottom - \frac{h \cdot (Nt - n)}{\cos(\phi b)} + x \cdot \tan(\phi b) \right] & \text{if } n < Nc \\ \left[tcTop + \frac{h \cdot (n - Nc)}{\cos(\phi t)} + x \cdot \tan(\phi t) \right] & \text{if } n \geq Nc \end{cases}$$

z-coordinates of the interfaces and the top surface

Height of the core at the right end

$Hc\_right := Z(Nc, L) - Z(Nb, L)$ $\quad Hc\_right = 0.0317877$ $\quad Z(Nb, L) = -0.0159$

Define the tapered angle for the different layers

$k := 0..N$

$$\phi_k := \begin{cases} \phi b & \text{if } k < Nc \\ 0 & \text{if } k = Nc \\ \phi t & \text{if } k > Nc \end{cases}$$

$\phi^T =$

	0	1	2	3	4	5	6	7	8	9
0	0	0	0	0	0	0	0	0	0	0

deg

The compliant and stiffness matrix in the local system, 1.2.3 system

$$S := \begin{pmatrix} \frac{1}{E1} & \frac{-\nu 12}{E1} & \frac{-\nu 13}{E1} & 0 & 0 & 0 \\ \frac{-\nu 12}{E1} & \frac{1}{E2} & \frac{-\nu 23}{E2} & 0 & 0 & 0 \\ \frac{-\nu 13}{E1} & \frac{-\nu 23}{E2} & \frac{1}{E3} & 0 & 0 & 0 \\ 0 & 0 & 0 & \frac{1}{G23} & 0 & 0 \\ 0 & 0 & 0 & 0 & \frac{1}{G31} & 0 \\ 0 & 0 & 0 & 0 & 0 & \frac{1}{G12} \end{pmatrix}$$

$C123 := S^{-1}$

The stiffness matrix in the local s-y-n system

$m := \cos(\theta)$ $\quad n := \sin(\theta)$

$k := 1 .. N$ k is a range variable from 1 to N

$$T_k := \begin{bmatrix} (m_k)^2 & (n_k)^2 & 0 & 0 & 0 & -2\,m_k \cdot n_k \\ (n_k)^2 & (m_k)^2 & 0 & 0 & 0 & 2\,m_k \cdot n_k \\ 0 & 0 & 1 & 0 & 0 & 0 \\ 0 & 0 & 0 & m_k & n_k & 0 \\ 0 & 0 & 0 & -n_k & m_k & 0 \\ m_k \cdot n_k & -m_k \cdot n_k & 0 & 0 & 0 & (m_k)^2 - (n_k)^2 \end{bmatrix}$$

$C_k := T_k \cdot C123 \cdot T_k^{T}$ $\quad C_0 := C_1$

$k := 0 .. N$

$C11_k := (C_k)_{0,0}$ $\quad C12_k := (C_k)_{0,1}$ $\quad C13_k := (C_k)_{0,2}$ $\quad C16_k := (C_k)_{0,5}$

$$C22_k := (C_k)_{1,1} \qquad C23_k := (C_k)_{1,2} \qquad C26_k := (C_k)_{1,5}$$

$$C33_k := (C_k)_{2,2} \qquad C36_k := (C_k)_{2,5} \qquad C44_k := (C_k)_{3,3} \qquad C45_k := (C_k)_{3,4}$$

$$C55_k := (C_k)_{4,4} \qquad C66_k := (C_k)_{5,5}$$

Reduced stiffnesses for a taped facesheet lamina

$k := 1..N$

$$Db_k := C13_k \cdot \sin(\phi_k)^2 - C33_k \cdot \cos(\phi_k)^2 \qquad Db_0 := Db_1$$

$$Q11b_k := \left[(C13_k)^2 - C11_k C33_k\right] \cdot \frac{\cos(\phi_k)^2}{Db_k}$$

$$Q12b_k := \frac{\left[(C13_k C23_k - C12_k C33_k) \cdot \cos(\phi_k)^2 + (C12_k C13_k - C11_k C23_k) \cdot \sin(\phi_k)^2\right] \cdot \cos(\phi_k)^2}{Db_k}$$

$$Q16b_k := \frac{\left[(C13_k C36_k - C16_k C33_k) \cdot \cos(\phi_k)^2 + (C13_k C16_k - C11_k C36_k) \cdot \sin(\phi_k)^2\right] \cdot \cos(\phi_k)}{Db_k}$$

$$Q21b_k := \frac{(C13_k \cdot C23_k - C12_k C33_k)}{Db_k}$$

$$Q22b_k := \frac{\left[(C23_k)^2 - C22_k C33_k\right] \cdot \cos(\phi_k)^2 + (C13_k C22_k - C12_k C23_k) \cdot \sin(\phi_k)^2}{Db_k}$$

$$Q26b_k := \frac{(C23_k \cdot C36_k - C26_k C33_k) \cdot \cos(\phi_k)^2 + (C13_k C26_k - C12_k C36_k) \cdot \sin(\phi_k)^2}{Db_k \cdot \cos(\phi_k)}$$

$$Q31b_k := \left[(C13_k)^2 - C11_k C33_k\right] \cdot \frac{\sin(\phi_k)^2}{Db_k}$$

$$Q32b_k := \frac{\left[(C13_k \cdot C23_k - C12_k \cdot C33_k) \cdot \cos(\phi_k)^2 + (C12_k \cdot C13_k - C11_k \cdot C23_k) \cdot \sin(\phi_k)^2\right] \cdot \sin(\phi_k)^2}{Db_k}$$

$$Q36b_k := \frac{\left[(C13_k \cdot C36_k - C16_k \cdot C33_k) \cdot \cos(\phi_k)^2 + (C13_k \cdot C16_k - C11_k \cdot C36_k) \cdot \sin(\phi_k)^2\right] \cdot \sin(\phi_k)^2}{Db_k \cdot \cos(\phi_k)}$$

$$Q41b_k := \frac{(C16_k \cdot C33_k - C13_k C36_k) \cdot \sin(\phi_k)}{Db_k}$$

$$Q42b_k := \frac{(C23_k \cdot C36_k - C26_k C33_k) \cdot \cos(\phi_k)^2 \cdot \sin(\phi_k) + (C13_k C26_k - C16_k C23_k) \cdot \sin(\phi_k)^3}{Db_k}$$

$$Q46b_k := \frac{\left[(C36_k)^2 - C33_k C66_k\right] \cdot \cos(\phi_k)^2 \cdot \sin(\phi_k) + (C13_k C66_k - C16_k C36_k) \cdot \sin(\phi_k)^3}{Db_k \cdot \cos(\phi_k)}$$

$$Q51b_k := \frac{\left[(C13_k)^2 - C11_k C33_k\right] \cdot \cos(\phi_k) \cdot \sin(\phi_k)}{Db_k}$$

$$Q52b_k := \frac{(C13_k \cdot C23_k - C12_k C33_k) \cdot \cos(\phi_k)^3 \cdot \sin(\phi_k) + (C12_k C13_k - C11_k C23_k) \cdot \sin(\phi_k)^3 \cdot \cos(\phi_k)}{Db_k}$$

$$Q56b_k := \frac{(C13_k \cdot C36_k - C16_k C33_k) \cdot \cos(\phi_k)^2 \cdot \sin(\phi_k) + (C13_k C16_k - C11_k C36_k) \cdot \sin(\phi_k)^3}{Db_k}$$

$$Q61b_k := \frac{(C13_k \cdot C36_k - C16_k C33_k) \cdot \cos(\phi_k)}{Db_k}$$

$$Q62b_k := \frac{(C23_k \cdot C36_k - C26_k C33_k) \cdot \cos(\phi_k)^3 + (C13_k C26_k - C16_k C23_k) \cdot \sin(\phi_k)^2 \cdot \cos(\phi_k)}{Db_k}$$

$$Q66b_k := \frac{\left[(C36_k)^2 - C33_k C66_k\right] \cdot \cos(\phi_k)^2 + (C13_k C66_k - C16_k C36_k) \cdot \sin(\phi_k)^2}{Db_k}$$

$Q11b_{Nc} := 0$ $Q21b_{Nc} := 0$ $Q41b_{Nc} := 0$ $Q51b_{Nc} := 0$ $Q61b_{Nc} := 0$

$Q12b_{Nc} := 0$ $Q22b_{Nc} := 0$ $Q42b_{Nc} := 0$ $Q52b_{Nc} := 0$ $Q62b_{Nc} := 0$

$Q16b_{Nc} := 0$ $Q26b_{Nc} := 0$ $Q46b_{Nc} := 0$ $Q56b_{Nc} := 0$ $Q66b_{Nc} := 0$

$$A11(x) := \sum_{n=1}^{N} Q11b_n(Z(n,x) - Z(n-1,x)) \qquad A21(x) := \sum_{n=1}^{N} Q21b_n(Z(n,x) - Z(n-1,x))$$

$$A12(x) := \sum_{n=1}^{N} Q12b_n(Z(n,x) - Z(n-1,x)) \qquad A22(x) := \sum_{n=1}^{N} Q22b_n(Z(n,x) - Z(n-1,x))$$

$$A16(x) := \sum_{n=1}^{N} Q16b_n(Z(n,x) - Z(n-1,x)) \qquad A26(x) := \sum_{n=1}^{N} Q26b_n(Z(n,x) - Z(n-1,x))$$

$$A41(x) := \sum_{n=1}^{N} Q41b_n(Z(n,x) - Z(n-1,x))$$

$$A42(x) := \sum_{n=1}^{N} Q42b_n(Z(n,x) - Z(n-1,x))$$

$$A46(x) := \sum_{n=1}^{N} Q46b_n(Z(n,x) - Z(n-1,x))$$

$$A61(x) := \sum_{n=1}^{N} Q61b_n(Z(n,x) - Z(n-1,x))$$

$$A62(x) := \sum_{n=1}^{N} Q62b_n(Z(n,x) - Z(n-1,x))$$

$$A51(x) := \sum_{n=1}^{N} Q51b_n(Z(n,x) - Z(n-1,x))$$

$$A52(x) := \sum_{n=1}^{N} Q52b_n(Z(n,x) - Z(n-1,x))$$

$$A56(x) := \sum_{n=1}^{N} Q56b_n(Z(n,x) - Z(n-1,x))$$

$$A44(x) := Gc23(Z(Nc,x) - Z(Nb,x))$$

$$A55(x) := Gc13(Z(Nb+1,x) - Z(Nb,x))$$

$$A66(x) := \sum_{n=1}^{N} Q66b_n(Z(n,x) - Z(n-1,x))$$

$$B11(x) := \frac{1}{2}\sum_{n=1}^{N} Q11b_n\left(Z(n,x)^2 - Z(n-1,x)^2\right)$$

$$B12(x) := \frac{1}{2}\sum_{n=1}^{N} Q12b_n\left(Z(n,x)^2 - Z(n-1,x)^2\right)$$

$$B16(x) := \frac{1}{2}\sum_{n=1}^{N} Q16b_n\left(Z(n,x)^2 - Z(n-1,x)^2\right)$$

$$B41(x) := \frac{1}{2}\sum_{n=1}^{N} Q41b_n\left(Z(n,x)^2 - Z(n-1,x)^2\right)$$

$$B42(x) := \frac{1}{2}\sum_{n=1}^{N} Q42b_n\left(Z(n,x)^2 - Z(n-1,x)^2\right)$$

$$B46(x) := \frac{1}{2}\sum_{n=1}^{N} Q46b_n\left(Z(n,x)^2 - Z(n-1,x)^2\right)$$

$$B61(x) := \frac{1}{2}\sum_{n=1}^{N} Q61b_n\left(Z(n,x)^2 - Z(n-1,x)^2\right)$$

$$B21(x) := \frac{1}{2}\sum_{n=1}^{N} Q21b_n\left(Z(n,x)^2 - Z(n-1,x)^2\right)$$

$$B22(x) := \frac{1}{2}\sum_{n=1}^{N} Q22b_n\left(Z(n,x)^2 - Z(n-1,x)^2\right)$$

$$B26(x) := \frac{1}{2}\sum_{n=1}^{N} Q26b_n\left(Z(n,x)^2 - Z(n-1,x)^2\right)$$

$$B51(x) := \frac{1}{2}\sum_{n=1}^{N} Q51b_n\left(Z(n,x)^2 - Z(n-1,x)^2\right)$$

$$B52(x) := \frac{1}{2}\sum_{n=1}^{N} Q52b_n\left(Z(n,x)^2 - Z(n-1,x)^2\right)$$

$$B56(x) := \frac{1}{2}\sum_{n=1}^{N} Q56b_n\left(Z(n,x)^2 - Z(n-1,x)^2\right)$$

$$B66(x) := \frac{1}{2}\sum_{n=1}^{N} Q66b_n\left(Z(n,x)^2 - Z(n-1,x)^2\right)$$

$$B62(x) := \frac{1}{2}\sum_{n=1}^{N} Q62b_n\left(Z(n,x)^2 - Z(n-1,x)^2\right)$$

$$D11(x) := \frac{1}{3}\sum_{n=1}^{N} Q11b_n\left(Z(n,x)^3 - Z(n-1,x)^3\right) \qquad D21(x) := \frac{1}{3}\sum_{n=1}^{N} Q21b_n\left(Z(n,x)^3 - Z(n-1,x)^3\right)$$

$$D12(x) := \frac{1}{3}\sum_{n=1}^{N} Q12b_n\left(Z(n,x)^3 - Z(n-1,x)^3\right) \qquad D22(x) := \frac{1}{3}\sum_{n=1}^{N} Q22b_n\left(Z(n,x)^3 - Z(n-1,x)^3\right)$$

$$D16(x) := \frac{1}{3}\sum_{n=1}^{N} Q16b_n\left(Z(n,x)^3 - Z(n-1,x)^3\right) \qquad D26(x) := \frac{1}{3}\sum_{n=1}^{N} Q26b_n\left(Z(n,x)^3 - Z(n-1,x)^3\right)$$

$$D61(x) := \frac{1}{3}\sum_{n=1}^{N} Q61b_n\left(Z(n,x)^3 - Z(n-1,x)^3\right) \qquad D62(x) := \frac{1}{3}\sum_{n=1}^{N} Q62b_n\left(Z(n,x)^3 - Z(n-1,x)^3\right)$$

$$D66(x) := \frac{1}{3}\sum_{n=1}^{N} Q66b_n\left(Z(n,x)^3 - Z(n-1,x)^3\right)$$

ABD matrices

$$ABD(x) := \begin{pmatrix} A11(x) & A12(x) & 0 & 0 & A16(x) & B11(x) & B12(x) & B16(x) \\ A21(x) & A22(x) & 0 & 0 & A26(x) & B21(x) & B22(x) & B26(x) \\ A41(x) & A42(x) & A44(x) & 0 & A46(x) & B41(x) & B42(x) & B46(x) \\ A51(x) & A52(x) & 0 & A55(x) & A56(x) & B51(x) & B52(x) & B56(x) \\ A61(x) & A62(x) & 0 & 0 & A66(x) & B61(x) & B62(x) & B66(x) \\ B11(x) & B12(x) & 0 & 0 & B16(x) & D11(x) & D12(x) & D16(x) \\ B21(x) & B22(x) & 0 & 0 & B26(x) & D21(x) & D22(x) & D26(x) \\ B61(x) & B62(x) & 0 & 0 & B66(x) & D61(x) & D62(x) & D66(x) \end{pmatrix}$$

The midsurface strains and curvatures

$$ABDinverse(x) := ABD(x)^{-1}$$

Soluve this equation blocks for Qy(x) and My(x)

$$QMy(x) := -\begin{pmatrix} ABDinverse(x)_{1,1} & ABDinverse(x)_{1,6} \\ ABDinverse(x)_{1,6} & ABDinverse(x)_{6,6} \end{pmatrix}^{-1} \cdot \begin{pmatrix} ABDinverse(x)_{6,0} \\ ABDinverse(x)_{6,5} \end{pmatrix} \cdot Mx(x)$$

$Ny(x) := QMy(x)_0$

$My(x) := QMy(x)_1$

$Strain\_mid(x) := ABDinverse(x) \cdot (Nx(x)\ \ Ny(x)\ \ Qy(x)\ \ Qx(x)\ \ Nxy(x)\ \ Mx(x)\ \ My(x)\ \ Mxy(x))^T$

$\varepsilon 0x(x) := Strain\_mid(x)_0$ $\quad \varepsilon 0y(x) := Strain\_mid(x)_1$ $\quad \gamma cyz(x) := Strain\_mid(x)_2$

$\gamma cxz(x) := Strain\_mid(x)_3$ $\quad \gamma 0xy(x) := Strain\_mid(x)_4$

$\kappa 0x(x) := Strain\_mid(x)_5$ $\quad \kappa 0y(x) := Strain\_mid(x)_6$ $\quad \kappa 0xy(x) := Strain\_mid(x)_7$

The strains

$\varepsilon x(x,z) := \varepsilon 0x(x) + z \cdot \kappa 0x(x)$

$\varepsilon y(x,z) := \varepsilon 0y(x) + z \cdot \kappa 0y(x)$ Kirchhoff Hypothesis

$\gamma xy(x,z) := \gamma 0xy(x) + z \cdot \kappa 0xy(x)$

The strains on the top and bottom surfaces

$I\_\varepsilon xx(n,x) := \varepsilon x(x, Z(n,x))$ $\quad I\_\varepsilon yy(n,x) := \varepsilon y(x, Z(n,x))$ $\quad I\_\gamma xy(n,x) := \gamma xy(x, Z(n,x))$

$$I\_\varepsilon zz(n,x) := \frac{C13_n \cdot \cos(\phi_n)^2 - C33_n \cdot \sin(\phi_n)^2}{Db_n} \cdot I\_\varepsilon xx(n,x) + \frac{C23_n \cdot \left(\cos(\phi_n)^2 - \sin(\phi_n)^2\right)}{Db_n} \cdot I\_\varepsilon yy(n,x)$$

$$I\_\varepsilon zz(n,x) := I\_\varepsilon zz(n,x) + \frac{C36_n \cdot \left(\cos(\phi_n)^2 - \sin(\phi_n)^2\right)}{Db_n \cdot \cos(\phi_n)} \cdot I\_\gamma xy(n,x)$$

$$I\_\gamma xz(n,x) := \frac{-2 \cdot (C13_n + C33_n) \cdot \cos(\phi_n) \cdot \sin(\phi_n)}{Db_n} \cdot I\_\varepsilon xx(n,x) - \frac{2(C23_n) \cdot \cos(\phi_n) \cdot \sin(\phi_n)}{Db_n} \cdot I\_\varepsilon yy(n,x)$$

$$I\_\gamma xz(n,x) := I\_\gamma xz(n,x) - \frac{2(C36_n) \cdot \sin(\phi_n)}{Db_n} \cdot I\_\gamma xy(n,x)$$

$$I\_\gamma yz(n,x) := \tan(\phi_n)\, I\_\gamma xy(n,x)$$

$$R(\alpha) := \begin{pmatrix} \cos(\alpha)^2 & 0 & \sin(\alpha)^2 & 0 & 2\cos(\alpha)\cdot\sin(\alpha) & 0 \\ 0 & 1 & 0 & 0 & 0 & 0 \\ \sin(\alpha)^2 & 0 & \cos(\alpha)^2 & 0 & -2\cos(\alpha)\cdot\sin(\alpha) & 0 \\ 0 & 0 & 0 & \cos(\alpha) & 0 & -\sin(\alpha) \\ -\cos(\alpha)\cdot\sin(\alpha) & 0 & \cos(\alpha)\cdot\sin(\alpha) & 0 & \cos(\alpha)^2 - \sin(\alpha)^2 & 0 \\ 0 & 0 & 0 & \sin(\alpha) & 0 & \cos(\alpha) \end{pmatrix}$$

$$T(\alpha) := \begin{pmatrix} \cos(\alpha)^2 & 0 & \sin(\alpha)^2 & 0 & -2\cos(\alpha)\cdot\sin(\alpha) & 0 \\ 0 & 1 & 0 & 0 & 0 & 0 \\ \sin(\alpha)^2 & 0 & \cos(\alpha)^2 & 0 & 2\cos(\alpha)\cdot\sin(\alpha) & 0 \\ 0 & 0 & 0 & \cos(\alpha) & 0 & \sin(\alpha) \\ \cos(\alpha)\cdot\sin(\alpha) & 0 & -\cos(\alpha)\cdot\sin(\alpha) & 0 & \cos(\alpha)^2 - \sin(\alpha)^2 & 0 \\ 0 & 0 & 0 & -\sin(\alpha) & 0 & \cos(\alpha) \end{pmatrix}$$

$$I\_\varepsilon syn(n,x) := T(\phi_n)^T \cdot (I\_\varepsilon xx(n,x)\ \ I\_\varepsilon yy(n,x)\ \ I\_\varepsilon zz(n,x)\ \ I\_\gamma yz(n,x)\ \ I\_\gamma xz(n,x)\ \ I\_\gamma xy(n,x))^T$$

$$I\_\varepsilon xyz(n,x) := (I\_\varepsilon xx(n,x)\ \ I\_\varepsilon yy(n,x)\ \ I\_\varepsilon zz(n,x)\ \ I\_\gamma yz(n,x)\ \ I\_\gamma xz(n,x)\ \ I\_\gamma xy(n,x))^T$$

$$I\_\varepsilon ss(n,x) := I\_\varepsilon syn(n,x)_0$$

$$I\_\varepsilon yy(n,x) := I\_\varepsilon syn(n,x)_1$$

$$I\_\varepsilon nn(n,x) := I\_\varepsilon syn(n,x)_2$$

The stresses in layer number k

$$Q_k := \begin{pmatrix} Q11b_k & Q12b_k & Q16b_k \\ Q21b_k & Q22b_k & Q26b_k \\ Q31b_k & Q32b_k & Q36b_k \\ Q41b_k & Q42b_k & Q46b_k \\ Q51b_k & Q52b_k & Q56b_k \\ Q61b_k & Q62b_k & Q66b_k \end{pmatrix} \qquad Q_0 := Q_1$$

$$Sxyz(n,x) := Q_n \cdot \begin{pmatrix} I\_\varepsilon xx(n,x) \\ I\_\varepsilon yy(n,x) \\ I\_\gamma xy(n,x) \end{pmatrix}$$

Stresses in the global coordinate system

$I\_\sigma xx(n,x) := Sxyz(n,x)_0$ $I\_\sigma yy(n,x) := Sxyz(n,x)_1$ $I\_\sigma zz(n,x) := Sxyz(n,x)_2$

$I\_\tau yz(n,x) := Sxyz(n,x)_3$ $I\_\tau xz(n,x) := Sxyz(n,x)_4$ $I\_\tau xy(n,x) := Sxyz(n,x)_5$

$Ssyn(k,x) := R(\phi_k) \cdot Sxyz(k,x)$

Stresses in the local coordinate system

$I\_\sigma ss(n,x) := Ssyn(n,x)_0$

Normalized strains and stresses at the specific points

$I\_\varepsilon xx\left(0,\frac{L}{2}\right) = 8.7343 \times 10^{-9}$ $I\_\varepsilon xx\left(N,\frac{L}{2}\right) = -8.7343 \times 10^{-9}$

$I\_\varepsilon ss\left(0,\frac{L}{2}\right) = 9.1087 \times 10^{-9}$ $I\_\varepsilon ss\left(N,\frac{L}{2}\right) = -9.1087 \times 10^{-9}$

$I\_\sigma xx\left(0,\frac{L}{2}\right) = 1.3759 \times 10^{3}$ $I\_\sigma xx\left(N,\frac{L}{2}\right) = -1.3759 \times 10^{3}$

$I\_\sigma ss\left(0,\frac{L}{2}\right) = 1.4187 \times 10^{3}$ $I\_\sigma ss\left(N,\frac{L}{2}\right) = -1.4187 \times 10^{3}$

$I\_\sigma zz\left(0,\frac{L}{2}\right) = 42.7779$ $I\_\sigma zz\left(N,\frac{L}{2}\right) = -42.7779$

$I\_\tau xz\left(0,\frac{L}{2}\right) = 242.6055$ $I\_\tau xz\left(N,\frac{L}{2}\right) = 242.6055$

$I\_\sigma yy\left(0,\frac{L}{2}\right) = 27.4653$ $I\_\sigma yy\left(N,\frac{L}{2}\right) = -27.4653$

$Gc13 \cdot \gamma cxz\left(\frac{L}{2}\right) = 15.224$

Energy Method

$$Ubot(x) := \sum_{k=1}^{Nb} \int_{Z(k-1,x)}^{Z(k,x)} \left(I\_\sigma xx(k,x) \cdot I\_\varepsilon xx(k,x) + I\_\sigma yy(k,x) \cdot I\_\varepsilon yy(k,x) + I\_\tau xy(k,x) \cdot I\_\gamma xy(k,x)\right) dx$$

$$Utop(x) := \sum_{k=Nc+1}^{N} \int_{Z(k-1,x)}^{Z(k,x)} \left(I\_\sigma xx(k,x) \cdot I\_\varepsilon xx(k,x) + I\_\sigma yy(k,x) \cdot I\_\varepsilon yy(k,x) + I\_\tau xy(k,x) \cdot I\_\gamma xy(k,x)\right) dx$$

$$Ucore(x) := \int_{Z(Nc-1,x)}^{Z(Nc,x)} Gc13 \cdot \gamma cxz(x)^2 + Gc23 \cdot \gamma cyz(x)^2 \, dx$$

$$Nubot := \int_0^L Ubot(x)\, dx \qquad Nutop := \int_0^L Utop(x)\, dx \qquad Nucore := \int_0^L Ucore(x)\, dx$$

$Utotal := Nubot + Nutop + Nucore$

$$Deflection := \frac{Utotal}{P}$$

Deflection =

BIOGRAPHY OF THE AUTHOR

Huyue Zhao was born in Dongyang, Zhejiang, in P.R. China, on September 16, 1974. He was raised in Weishang, Zhejiang and graduated from Weishang High School in 1992. He attended the Huazhong University of Science and Technology (HUST) and graduated in 1996 with a Bachelor's degree in Mechanical Engineering. In 1996, he worked for Baoma Micro-Electrical Motor Corp. for a year. Then he returned to HUST and entered the Mechanical Engineering graduate program in the fall of 1997. After receiving his Master's degree in HUST, he entered the Mechanical Engineering graduate program at The University of Maine in the fall of 2000.

After receiving his degree, Huyue will be joining Northwestern University to begin his pursuit of a Ph.D. degree in the field of Mechanical Engineering. Huyue is a candidate for the Master of Science degree in Mechanical Engineering from The University of Maine in December, 2002